

A LABVIEW INTERFACE TO INTEGRATE MAGNETIC RESONANCE
IMAGING (MRI) SIMULATOR WITH SYSTEM CONTROL AND ITS
APPLICATION TO REGIONAL MAGNETIC RESONANCE ELECTRICAL
IMPEDANCE TOMOGRAPHY (MREIT) RECONSTRUCTION

A THESIS SUBMITTED TO
THE GRADUATE SCHOOL OF NATURAL AND APPLIED SCIENCES
OF
MIDDLE EAST TECHNICAL UNIVERSITY

BY

TANKUT TOPAL

IN PARTIAL FULFILLMENT OF THE REQUIREMENTS
FOR
THE DEGREE OF MASTER OF SCIENCE
IN
ELECTRICAL AND ELECTRONICS ENGINEERING

JULY 2010

Approval of the Thesis:

**A LABVIEW INTERFACE TO INTEGRATE MAGNETIC RESONANCE
IMAGING (MRI) SIMULATOR WITH SYSTEM CONTROL AND ITS
APPLICATION TO REGIONAL MAGNETIC RESONANCE ELECTRICAL
IMPEDANCE TOMOGRAPHY (MREIT) RECONSTRUCTION**

submitted by **TANKUT TOPAL** in partial fulfillment of the requirements for the degree of **Master of Science in Electrical and Electronics Engineering Department, Middle East Technical University** by,

Prof. Dr. Canan Özgen
Dean, Graduate School of **Natural and Applied Sciences** _____

Prof. Dr. İsmet Erkmen
Head of Department, **Electrical and Electronics Engineering** _____

Prof. Dr. B. Murat Eyüboğlu
Supervisor, **Electrical and Electronics Engineering Dept., METU** _____

Examining Committee Members

Prof. Dr. Nevzat Güneri Gençer
Electrical and Electronics Engineering Dept., METU _____

Prof. Dr. B. Murat Eyüboğlu
Electrical and Electronics Engineering Dept., METU _____

Assist. Prof. Dr. Yeşim Serinağaoğlu Doğrusöz
Electrical and Electronics Engineering Dept., METU _____

Prof. Dr. Yusuf Ziya İder
Electrical and Electronics Engineering Dept., Bilkent University _____

Prof. Dr. Adnan Köksal
Electrical and Electronics Engineering Dept., Hacettepe University _____

Date: 23/07/2010

I hereby declare that all information in this document has been obtained and presented in accordance with academic rules and ethical conduct. I also declare that, as required by these rules and conduct, I have fully cited and referenced all material and results that are not original to this work.

Name, Last name: Tankut TOPAL

Signature:

ABSTRACT

A LABVIEW INTERFACE TO INTEGRATE MAGNETIC RESONANCE IMAGING (MRI) SIMULATOR WITH SYSTEM CONTROL AND ITS APPLICATION TO REGIONAL MAGNETIC RESONANCE ELECTRICAL IMPEDANCE TOMOGRAPHY (MREIT) RECONSTRUCTION

Topal, Tankut

M.Sc., Department of Electrical and Electronics Engineering

Supervisor: Prof. Dr. B. Murat Eyübođlu

July 2010, 91 pages

Magnetic resonance imaging (MRI) is a high resolution medical imaging technique based on distinguishing tissues according to their nuclear magnetic properties. Magnetic resonance electrical impedance tomography (MREIT) is a conductivity imaging technique which reconstructs images of electrical properties, based on their effect on induced magnetic flux density due to externally applied current flow. Both of these techniques are of interest for novel research and development. Simulators help researchers observe the accuracy and the results of the study. In this study a user friendly complete MRI/MREIT simulator is designed. This simulator is the

combination of improved version of MRI simulator (implemented by V. E. Arpinar, H. Yigitler), a forward solver, to observe the current injection effect, the improved version of user interface that is designed on LabVIEW graphical programming environment (designed by M. Ozsut), and equi-potential projection (EPP) reconstruction algorithm (proposed by M. S. Ozdemir, M. Eyuboglu, O. Ozbek). All of these individual parts are improved and gathered in LabVIEW environment in order to work in synchrony. In addition to that, regional image reconstruction technique (proposed by H. Altunel, M. Eyuboglu) is also included in the simulator.

The simulator is run for various inputs and system specifications. It is observed that the simulation results are consistent with the expected results for MRI, MREIT and conventional/regional MREIT reconstruction. Four different models are designed and results are obtained using these models. The accuracy of the results usually differs with the input parameters and model geometry. Validating numerically the accuracy of the forward solution part using Biot-Savart and Ampere's laws, the consistency of the forward problem solution part is obtained at a percentage of 95%. In the MREIT part, magnetic flux density distribution taken from forward solver part is added to the main magnetic flux density used in the MRI part. Consistency of the magnetic flux density distribution given to the simulator as input and the output taken from the MREIT part of the simulator is found as 99%.

In addition to conventional EPP algorithm, regional MREIT reconstruction algorithm is applied for various noise levels. It is observed that, as the noise level increases, regional MREIT reconstruction algorithm gives relatively much better results compared to conventional MREIT reconstruction algorithm. Errors obtained by applying conventional reconstruction and regional reconstruction are compared for each inhomogeneity individually. Therefore, accuracies of the different current patterns depending on the inhomogeneities are observed as well.

Keywords: electrical impedance tomography, magnetic resonance imaging, simulator, regional reconstruction

ÖZ

MANYETİK REZONANS GÖRÜNTÜLEME SİMÜLATÖRÜNÜ SİSTEM DENETİMİ İLE BİRLEŞTİREN LABVIEW ARAYÜZÜ VE BÖLGESEL MANYETİK REZONANS ELEKTRİKSEL EMPEDANS TOMOGRAFİ (MREET) GERİÇATIMINA UYGULANMASI

Topal, Tankut

Yüksek Lisans, Elektrik ve Elektronik Mühendisliği Bölümü

Tez Yöneticisi: Prof. Dr. B. Murat Eyüboğlu

Temmuz 2010, 91 sayfa

Manyetik rezonans görüntüleme (MRG), dokuları nükleer manyetik özelliklerine göre ayırt eden yüksek çözünürlüklü tıbbi görüntüleme tekniğidir. Manyetik rezonans elektriksel empedans tomografi (MREET) ise dokuların elektriksel özelliklerinin, harici akımdan kaynaklanan manyetik akı yoğunluğu dağılımları ölçülerek geriçatılması esasına dayanır. Her iki teknik de, araştırmaya ve geliştirmeye açık yeni tekniklerdir. Simülatörler, araştırmacılara çalışmanın doğruluğunu ve alınacak sonuçları gözlemlene açısından yardımcı olur. Bu çalışmada kullanıcıya kolaylık sağlayan tüm bir MRG/MREET simülatörü

gerçekleştirilmiştir. Simülatör, V. E. Arpınar, H. Yiğitler tarafından tasarlanmış olan MRG simülatörünün geliştirilmiş halinin, akım etkisini gözlemlemek amacıyla geliştirilen bir ileri problem çözücünün, M. Ozsut tarafından tasarlanmış olan ODTÜ MR sistemi arayüzünün ve M. S. Özdemir, M. Eyüboğlu, O. Özbek tarafından önerilen eş-potansiyel izdüşümü (EPP) algoritmasının birleşiminden oluşmaktadır. Bütün bu bağımsız parçalar geliştirilerek LabVIEW görsel programlama ortamı altında bir araya getirilmiş ve birbirleriyle uyumlu bir şekilde çalışmalarını sağlamıştır. Bunlara ek olarak, H. Altunel ve M. Eyüboğlu tarafından önerilen bölgesel görüntü oluşturma tekniği de bu simülatöre eklenmiştir.

Simülatör çeşitli girdiler ve sistem özellikleri için çalıştırılmış ve elde edilen sonuçların MRG, MREET ve klasik/bölgesel geriçatım için beklenenle tutarlılık gösterdiği gözlemlenmiştir. Simülatör için dört farklı model hazırlanmış ve sonuçlar bu modeller üzerinden elde edilmiştir. Sonuçların doğruluğu genellikle girdilere ve model geometrilerine bağlı olarak değişebilmektedir. Simülatörden elde edilen ileri problem sonuçları Amper Biot-Savart yasaları ile doğrulanmış, sonuçlar %95 tutarlı elde edilmiştir. MREET bölümünde, ileri problem çözümünden çıktı olarak alınan manyetik akı yoğunluğu dağılımı, MRG bölümünde ana manyetik akı yoğunluğu dağılımına eklenir. MREET bölümüne girdi olarak verilen bu bölümden çıktı olarak alınan manyetik akı yoğunluğu dağılımlarının tutarlılığı, MREET bölümünün doğruluğunu gösterir. Sonuçlar, bu bölümün girdileri ve çıktı olan manyetik akı yoğunluklarının 99% tutarlı olduğunu göstermiştir.

Klasik EPP algoritmasının yanında, bölgesel geriçatım tekniği de farklı gürültü değerleri için uygulanmıştır. Bunun sonucunda gürültü miktarı arttıkça bölgesel geriçatım tekniğinin klasik geriçatım tekniğine kıyasla daha iyi sonuç verdiği görülmüştür. Klasik geriçatım tekniği ile bölgesel geriçatım tekniği farklı inhomojenlikler için karşılaştırılmış hatalar hesaplanmıştır. Böylelikle farklı akım yollarının doğrulukları da geometriye bağlı olarak gözlemlenmiştir.

Anahtar Kelimeler: elektriksel empedans tomografi, manyetik rezonans görüntüleme, simülatör, bölgesel geriçatım

ACKNOWLEDGEMENTS

Firstly, I would like to express my sincere gratitude to my supervisor Prof. Dr. Murat Eyübođlu for his guidance and support throughout this study.

I would like to thank to TUBITAK-BIDEB for their supports for my thesis study.

I would like to thank my laboratory mates and friends Ali, Gökhan, Rasim, Soner, Alireza, Ümit, Ceren, Ersin, Balkar, Berna, Azadeh, Feza, Koray, Emre, Evren and others for their sincere friendship and chats. It was a great pleasure to complete this study when you were with me. I shared many things with you, and I finished my study with unforgettable memories.

I especially thank to Emre and Evren. Emre, you changed my point of view towards the life. I learnt many many things from you. You are a great friend and a great engineer. You solved lots of my problems in my hopeless times. It was almost impossible to complete my thesis without your help and patience. I am sure that I will need your advices, help, friendship and chats in my life. Evren, thank you very much for your friendship and support throughout my study. You helped me even your rush was at peak. There is no doubt that we will keep in touch for a long time.

Special thanks to Sila for her support in my studies. You were always with me in any difficulty. Life is easy to live with you. Your love makes me warm, strong and durable. You are my biggest luck.

More than all, I would like to thank my family for their support and confidence. They are always with me in my tough times. The reason that I can succeed it today is their guidance starting from my babyhood.

TABLE OF CONTENTS

ABSTRACT	iv
ÖZ	vi
ACKNOWLEDGEMENTS	viii
TABLE OF CONTENTS	ix
LIST OF FIGURES	xii
LIST OF TABLES	xvii
CHAPTERS	
1. INTRODUCTION	1
1.2 Introduction to Magnetic Resonance Imaging	1
1.3 Basic Principle of Magnetic Resonance Imaging	2
1.4 Magnetic Resonance Electrical Impedance Tomography	2
1.5 METU Magnetic Resonance Imaging System	3
1.6 Objectives of This Study	3
1.7 Outline of the Thesis	5
2. THEORY	7
2.1 Magnetic Resonance Imaging Background	7
2.2 Magnetic Resonance Electrical Impedance Tomography Background	20
2.3 Regional Image Reconstruction Using Optimum Currents	24
3. MRI / MREIT SIMULATOR	27
3.1 Forward Problem Solving	27
3.1.1 Idea and Implementation of Forward Problem Solving	27

3.1.2	Forward Problem Solving Part on User Interface	31
3.2	MRI Simulator Development	32
3.3	MREIT Simulator Development	35
3.4	Image Reconstruction.....	36
3.4.1	Conventional Image Reconstruction.....	36
3.4.2	Regional Image Reconstruction.....	37
3.5	User Interface Design Using LabVIEW	42
3.5.1	Introduction to LabVIEW	42
3.5.2	LabVIEW Part of the MRI/MREIT Simulator.....	43
3.5.2.1	Data Acquisition Panel	43
3.5.2.2	Image Reconstruction Panel	49
3.6	Models Designed For the Simulator	57
3.6.1	Square - Circle Model.....	57
3.6.2	Diagonal Squares Model.....	58
3.6.3	Impulsive Squares Model.....	59
3.6.4	Shepp - Logan Model.....	60
3.6.5	Electrode Configurations of the Models	62
4.	RESULTS	64
4.1	Forward Problem Solution Results	64
4.1.1	Models Created by the Simulator.....	64
4.1.2	Potential, Current Density and Magnetic Flux Density Results.....	65
4.2	Magnetic Resonance Imaging Results	70
4.3	Magnetic Resonance Electrical Impedance Tomography Results	72
4.4	MREIT Reconstruction Results	74
4.5	Regional Magnetic Resonance Electrical Impedance Tomography Reconstruction.....	77
5.	CONCLUSIONS AND FUTURE WORK	85

5.1 Conclusions	85
5.2 Future Works.....	87
REFERENCES.....	88
APPENDIX.....	91

LIST OF FIGURES

FIGURES

Figure 2.1- Spin-echo pulse sequence with phase-encoding is along the y -direction and frequency-encoding is along the x -direction.	15
Figure 2.2 - K-space coverage of the spin-echo pulse shown in Figure 2.1. (a) k-space trajectory of a single echo, (b) k-space trajectory of a set of spin-echo cycles [6].	16
Figure 2.3 - Axial MRI images of a patient with relapsing-remitting MS. a) T_2 weighted spin echo axial MRI image. b) T_1 weighted spin echo axial MRI image [16].	20
Figure 2.4 - The process block-diagram of obtaining J components from MRI signals.	23
Figure 2.5- An illustration of phase images before and after unwrapping. a) wrapped MRI phase image b) unwrapped phase image.	24
Figure 2.6 - Square model with two conductivity perturbations. Current patterns are shown with arrows numbered from A1 to A4.	25
Figure 2.7 - Current injection patterns and regions of FOV	26
Figure 3.1 - An experimental phantom model showing electrode localization and current injection.	28
Figure 3.2 - Example simulation model showing surface current injection electrodes.	29
Figure 3.3 - General view of the mesh mode for square-circle model.	30

Figure 3.4 - Block diagram showing the steps of forward problem solution.....	32
Figure 3.5 - Current injection patterns and region divisions for regional image reconstruction.....	38
Figure 3.6 - Current injection and sink electrode placements for each current injection pattern.....	40
Figure 3.7 - The regions of FOV for RIR using Shepp-Logan phantom.	41
Figure 3.8 - Screenshot of the data acquisition front panel while spin echo pulse sequence is being applied.....	44
Figure 3.9 - New vision of the data acquisition window after the additional parts ...	45
Figure 3.10 - "Acquisition Parameters" tab.	46
Figure 3.11 - "Model Parameters" tab.....	47
Figure 3.12 - "Create Current Distribution" tab.....	48
Figure 3.13 - "Create Shepp - Logan Phantom" tab.....	49
Figure 3.14 - Old version of the image reconstruction panel.....	50
Figure 3.15 - New version of the image reconstruction panel.	51
Figure 3.16 - "Simulator B Comp. Reconstruction" tab.	52
Figure 3.17 - "Reconstruct B and J" tab.....	54
Figure 3.18 - "Reconstruct Conductivity (EPP)" tab.	55
Figure 3.19 - "Optimum Currents" tab.....	57
Figure 3.20 - Square -circle model.....	58

Figure 3.21 - Diagonal squares model	59
Figure 3.22 - Impulsive squares model.....	60
Figure 3.23 - Shepp-Logan model.	61
Figure 3.24 - Electrode configuration with their names and sizes.....	63
Figure 4.1 - Models used in the simulator. (a) Square - circle model, (b) diagonal squares model, (c) impulsive squares model, (d) Shepp-Logan model.	65
Figure 4.2 -Conductivity, potential and current density distributions of square circle model for 20mA current injection in horizontal axis and noise free case (a) conductivity distribution (S/m), (b) potential distribution (V), (c) x-component of J (J_x) (A/m^2), (d) y-component of J (J_y) (A/m^2).....	66
Figure 4.3 - x, y, z components of the magnetic flux density distribution for square circle model and noise free case. (a) B_x (T), (b) B_y (T), (c) B_z (T).	67
Figure 4.4 - Derivatives of B components shown in Figure 4.3 with respect to their orthogonal directions for square circle model and noise free case. (a) dB_x/d_y , (T/m), (b) dB_x/d_z (T/m), (c) dB_y/d_x (T/m), (d) dB_y/d_z (T/m), (e) dB_z/d_x (T/m), (f) dB_z/d_y (T/m).	68
Figure 4.5 - Comparison of J components for square circle model obtained using equation (3.3), (3.4) and (3.6) for noise free case. (a) J_x (A/m^2) distribution obtained by using equation (3.3), (b) J_x (A/m^2) distribution obtained by using equation (3.6), (c) J_y (A/m^2) distribution obtained by using equation (3.4), (d) J_y (A/m^2) distribution obtained by using equation (3.6), (e) J_z (A/m^2) distribution which is equal to zero, (f) J_z (A/m^2) distribution obtained by using equation (3.6).	69
Figure 4.6 - Spin density distribution for square circle model (S/m).....	70
Figure 4.7 - Magnitude and phase images of acquired k-space data and reconstructed data for the model given in Figure 4.6. (a) Magnitude image of k-space data (cycles/m), (b) phase image of k-space data (rad), (c) magnitude image of the reconstructed data, (d) unwrapped phase image of the reconstructed image (rad)....	71

Figure 4.8 - Phase images for model in Figure 4.6 obtained using and without using 20 mA horizontal current injection. (a) Phase image for current-free case, (b) phase image with current application..... 72

Figure 4.9 - Magnetic flux density obtained by forward solver and obtained by subtracting and scaling phase images with and without current. (a) Magnetic flux density (T) which is given as input to MREIT simulator, (b) magnetic flux density (T) taken as output of the MREIT simulator..... 73

Figure 4.10 - Potential, J_x and J_y distributions given into reconstruction part of the simulator as input for horizontal current injection having the amplitude of 20mA. (a) Potential distribution (V), (b) J_x distribution (A/m^2), (c), J_y distribution (A/m^2). 74

Figure 4.11 - True conductivity and reconstructed conductivity using EPP algorithm for horizontal current injection pattern. (a) True conductivity (S/m), (b) reconstructed conductivity (S/m) using EPP algorithm..... 75

Figure 4.12 - Reconstruction results obtained using horizontal current injection pattern for SNR 30 and SNR 13. (a) Conductivity distribution (S/m) for SNR 30, (b) conductivity distribution for SNR 13 (S/m)..... 75

Figure 4.13 - Reconstructed conductivity results for various current injection patterns having the amplitude of 20mA and for noise free case. (a) Reconstructed conductivity (S/m) distribution for horizontal current injection pattern, (b) reconstructed conductivity (S/m) distribution for vertical current injection pattern, (c) reconstructed conductivity (S/m) distribution for diagonal (from top-left to bottom-right) current injection pattern, (d) reconstructed conductivity (S/m) distribution for diagonal (from top-right to bottom-left) current injection pattern. 76

Figure 4.14 - Conductivity distributions for regional MREIT reconstruction part obtained by applying individual current patterns shown in Figure 3.5, where conductivities of square, circle and background are 0.1 S/m, 0.4 S/m, and 0.2 S/m respectively. (a) Reconstructed conductivity distribution (S/m) for Vertical 1 (V1) current pattern, (b) reconstructed conductivity distribution (S/m) for Horizontal 1 (H1) current pattern, (c) reconstructed conductivity distribution (S/m) for Vertical 2 (V2) current pattern, (d) reconstructed conductivity distribution (S/m) for Horizontal 2 (H2) current pattern, (e) reconstructed conductivity distribution (S/m) for Vertical 3 (V3) current pattern, (f) reconstructed conductivity distribution (S/m) for Horizontal 3 (H3) current pattern, (g) reconstructed conductivity distribution (S/m) for Diagonal 1 (D1) current pattern, (h) reconstructed conductivity distribution (S/m) for Diagonal 2 (D2) current pattern. 78

Figure 4.15 - Conductivity distribution obtained by regional MREIT reconstruction where conductivities of square, circle and background are 0.1 S/m, 0.4 S/m, and 0.2 S/m respectively. 79

Figure 4.16 - Shepp - Logan model used for comparison of regional reconstruction and conventional reconstruction techniques. 82

Figure 4.17 - Conductivity distributions for regional MREIT reconstruction part obtained by applying individual current patterns shown in Figure 3.5, where conductivity distribution of the model is as shown in Figure 4.16. (a) Reconstructed conductivity distribution (S/m) for Vertical 1 (V1) current pattern, (b) reconstructed conductivity distribution (S/m) for Horizontal 1 (H1) current pattern, (c) reconstructed conductivity distribution (S/m) for Vertical 2 (V2) current pattern, (d) reconstructed conductivity distribution (S/m) for Horizontal 2 (H2) current pattern, (e) reconstructed conductivity distribution (S/m) for Vertical 3 (V3) current pattern, (f) reconstructed conductivity distribution (S/m) for Horizontal 3 (H3) current pattern, (g) reconstructed conductivity distribution (S/m) for Diagonal 1 (D1) current pattern, (h) reconstructed conductivity distribution (S/m) for Diagonal 2 (D2) current pattern..... 83

Figure 4.18 - Conductivity distribution obtained by regional MREIT reconstruction where conductivity distribution of the Shepp - Logan phantom is as shown in Figure 4.16..... 84

LIST OF TABLES

TABLES

Table 2.1 - Contrast table for saturation-recovery spin-echo sequence with respect to T_E and T_R values.	19
Table 3.1 - Injection patterns utilized for each sub-regions.....	39
Table 3.2 - Sub-regions of Shepp-Logan phantom and corresponding current injection patterns utilized for each region.....	41
Table 3.3 - Conductivity values created using the conductivity vector shown in equation (3.7)	62
Table 4.1 - Reconstruction errors calculated using various current injection pattern combinations shown in Figure 3.5 for square circle model and noise-free case.....	80
Table 4.2 - Reconstruction errors calculated using various current injection pattern combinations shown in Figure 3.5 for square circle model and SNR 30.....	80
Table 4.3 - Reconstruction errors calculated using various current injection pattern combinations shown in Figure 3.5 for square circle model and SNR 13.....	80
Table 4.4 - Reconstruction errors calculated using various current injection pattern combinations shown in Figure 3.5 for Shepp - Logan model.....	84

CHAPTER 1

INTRODUCTION

1.2 Introduction to Magnetic Resonance Imaging

Magnetic Resonance Imaging (MRI) is a medical imaging technique which is based on imaging radiofrequency response of spinning nuclei to magnetic field [1].

Nuclear magnetic resonance (NMR) phenomenon, that inspired researchers to develop MRI, was first discovered by Purcell *et al* [2], [3], and Bloch *et al* [4] independently in 1946. This phenomenon led to identification of different nuclei with chemical properties by observing the chemical shifts occurred in nuclei. The idea and the developments in this field are then related with imaging spin in MRI technique.

MRI is a relatively new imaging technique, in such a manner that the first MRI image was published in 1977 [5]. This leading research triggered many developments in fast and high resolution tissue imaging modalities. Moreover, MRI systems became the most popular medical imaging systems which provide high resolution soft tissue contrast, and created an industry of multi-billion dollars.

1.3 Basic Principle of Magnetic Resonance Imaging

Objects are composed of many atoms which have nuclei spinning in a random direction and speed. However, each nucleus has different spinning characteristics due to its type. When magnetic resonance active nuclei are exposed of high magnetic field, they tend to align in some definite directions, and keep on spinning in the space. This procedure is realized by magnets. Different atoms have different spinning speeds depending when the main magnetic field is applied. In most of the clinical MRI applications hydrogen atoms are imaged, since excessive amount of water exists in human body.

In addition to a main magnet creating the high static magnetic field, gradient coils are designed to generate time-varying magnetic fields. These coils are utilized to control spatial non-uniformity, which is crucial for signal localization. The lower limit of gradient strength should be stronger than the main magnetic field inhomogeneity [6].

The other fundamental component of an MRI system is RF coil, which consists of both transmitter and receiver coils. The transmitter coil generates a rotating magnetic field for spin excitation. The receiver coil detects the magnetic precession of the spins generated by the transmitted RF signal and converts into electrical signal. Instead of using two separate coils for signal transmission and reception, a single coil can be used as both RF transmitter and receiver [6].

1.4 Magnetic Resonance Electrical Impedance Tomography

Electrical conductivities of tissues vary due to their physiological and pathological properties. Conventional electrical impedance tomography (EIT) reconstructs conductivity and permittivity images using current or voltage data which are acquired by the electrodes on the surface. First, current is applied between electrodes, and then voltage generated by the injected current is detected on different surface electrodes. However, the data measured at the surface are limited by the number of

surface electrodes and highly affected by surface geometry, and electrode position. The data is contaminated by systemic artifacts and numerous noise sources. Due to these facts, EIT reconstructed images have relatively low resolution and accuracy [7].

The main idea of magnetic resonance electrical impedance tomography (MREIT) is based on detecting magnetic flux density generated by the induced currents via MRI system. Induced currents affect the precession of nuclei and create a phase shift. The effect of phase shift can be seen clearly when the MR images with applied current and without applied current are subtracted and scaled. This modality was proposed to overcome technical difficulties of EIT in early 1990's. Three independent trials were attempted initially by Zhang (1992) [8], Woo *et al* (1994) [9], Ider and Birgul (1995) [10].

1.5 METU Magnetic Resonance Imaging System

MRI research at Middle East Technical University (METU) is performed at METU Magnetic Resonance Imaging Research Laboratory (METU - MRIRL) of Electrical and Electronics Engineering department which involves an MRI system with a main magnetic field of 0.15 T. This system was set up in early 90's by researchers in METU-EEE department. M. Ozsut has constructed software including graphical interface to control the MRI system in this MSc thesis study [1]. LabVIEW was used as the software programming environment and National Instruments A/D, D/A TMS-DSP cards are integrated to control the signals. Using this graphical interface, required parameters are controlled and changed as needed easily.

1.6 Objectives of This Study

MRI and MR-EIT are relatively new imaging techniques, thus, these fields are open for novel research such as system optimization, algorithm construction, new imaging

technique development. This kind of novel research is generally created and tested by simulators and system modeling techniques. That is, before testing a system experimentally, new techniques are applied on simulators, in order to observe the results and expectations on virtual environment. For most cases in MREIT research area, this procedure is followed for testing reconstruction algorithms, checking the accuracy of mathematical background, observing noise effects and many parameters which affect the system. As a result, simulation studies help researchers to investigate consistency of expected and obtained results of proposed techniques.

Previously, V.E. Arpinar and H. Yigitler have developed an MRI simulator as a part of their PhD. and M.S. thesis respectively [11], [12]. This simulator has been implemented to perform simulations on MR imaging with inhomogeneous main magnetic fields. Although it is a well-designed simulator, its application is specific, it does not include a graphical user interface, and parameters to be changed are not easy to be reached. Since there is no graphical interface, users change the inputs by typing directly into the software codes. To overcome these difficulties, a graphical user interface is designed in LabVIEW 7.0 as a part of this thesis. The interface is embedded into the MRI system software which was designed by M. Ozsut as M.S. thesis [1].

MREIT can be examined as solution of two problems; those are forward problem and inverse problem. Forward problem of MREIT is the problem of calculating magnetic flux density and current density distributions in the object caused by externally injected currents. The additive magnetic flux density is measured in MREIT system and it is desired to find out the magnetic flux density and current density distributions of injected currents. To obtain this information, forward solver software having the capability of calculating the given distributions is designed. The software allows user to define the model geometry, conductivity values, electrode locations, and injected current.

There are generally two types of reconstruction approaches used in MREIT. These are current density based (J based) and magnetic flux density based (B based)

algorithms. These reconstruction techniques require different inputs depending on type of the algorithm. In the forward solver part of the simulator, these data, such as, spatial derivatives of B fields, x-y-z components of J , are also calculated to be used as inputs of the reconstruction algorithms in the further studies.

In addition to conventional MREIT procedure, there are some different approaches to enhance the image quality. Optimization of current injection patterns is one of these approaches. A PhD study on this subject was performed by H. Altunel at METU in 2008 [13]. To briefly explain the phenomena, spatial sensitivity of magnetic flux density with respect to conductivity distribution differs due to localization of current paths. The inhomogeneities closer to the current paths are more accurately calculated. Inversely, if the current passing through the inhomogeneity is relatively weak, then the accuracy of the measurement in that area will not be high. Therefore, current optimization approach is based on applying multiple current injection patterns and using the proper current injection patterns maximizing the amount of current passing through the region of interest. Although a similar way is followed with H. Altunel [13], this software is newly designed to be compatible with the simulator created. The regional reconstruction algorithm, proposed by M. Eyuboglu and H. Altunel [14], is also implemented and included in the software. Equipotential projection algorithm is utilized for regional reconstruction [15].

To conclude, an MR / MREIT simulator was designed and embedded into METU MRI system.

1.7 Outline of the Thesis

In chapter 2, theory of MRI and MREIT is briefly explained. The equations utilized in the thesis and derivations of some equations are shown. Signal acquisition approaches are investigated, and the effects of input to the simulating system are explained by equations. Next, the theory of regional image reconstruction method and the main approach of the method are shown with illustrations. In chapter 3, the sections of the simulator are introduced. Inputs, outputs and functions of each section are explained. User interface design is explained. Models which are used in the

study are given and their specifications are shown. In chapter 4, results obtained by the simulator changing proper variables are given. Different functions of the simulator are used. Finally in chapter 5, the results and the performance of the simulator are discussed. In addition to that, conclusions and future work are given.

CHAPTER 2

THEORY

2.1 Magnetic Resonance Imaging Background

Although sub-atomic particles behave quantum mechanically, principles of MRI can be described using vector models, since MRI deals with collective effects of nuclei. Nuclei with odd atomic number or weight, such as hydrogen atom, have an angular momentum called *nuclear spin*. An ensemble of the same nuclei in an object is known as a nuclear spin system. For example ^1H atoms form a spin system, while ^{31}P atoms form another one. The physical basis of MRI deals with nuclear magnetism which is created by placing nuclei in an external magnetic field [6].

Like any spinning charged object, nucleus creates a microscopic magnetic field around itself while spinning. It is called *magnetic moment* ($\vec{\mu}$) [6]. Angular momentum and magnetic moment vectors are related as follows:

$$\vec{\mu} = \gamma \vec{J} \quad (2.1)$$

where,

\vec{J} : Angular momentum,

γ : Gyro magnetic constant.

The precession frequency of $\vec{\mu}$ under a B_0 magnetic field is given by,

$$\omega_0 = \gamma B_0 \quad (2.2)$$

ω_0 : *Larmour frequency* (angular frequency of nuclear precession)

B_0 : External magnetic field strength

The bulk magnetization vector for 1/2 spin system aligns exactly along positive z-direction (main magnetic field direction) at equilibrium [6]. The magnitude of bulk magnetization vector is,

$$|\overline{M}| = M_z^0 = \frac{\gamma^2 \hbar B_0 N_s}{4KT_s} \quad (2.3)$$

where,

B_0 : External magnetic field strength,

\hbar : Planck's constant divided by 2π ,

N_s : Total number of spins,

T_s : Temperature,

K : Boltzmann constant.

For a spin system, the external energy comes from an oscillating magnetic field obtained by an RF signal, which is denoted as $\overline{B}_1(t)$.

The resonance conditions occurs when $\overline{B}_1(t)$ rotates in the same manner with precess of the spins.

$$\omega_f = \omega_0 \quad (2.4)$$

Equation (2.4) is known as resonance condition.

General $\vec{B}_1(t)$ equation is in the following form,

$$\vec{B}_1(t) = 2B_1^e(t) \cos(\omega_f t + \varphi) \vec{i} \quad (2.5)$$

where,

$B_1^e(t)$: Pulse envelope function

ω_f : Excitation carrier frequency

φ : Initial phase angle

The envelope function in equation (2.5) can be either a *rectangular pulse* or a *sinc pulse*.

Equation of a rectangular envelope pulse is,

$$B_1^e(t) = B_1 \Pi\left(\frac{t - \tau_p / 2}{\tau_p}\right) = \begin{cases} B_1 & 0 \leq t \leq \tau_p \\ 0 & \text{otherwise} \end{cases} \quad (2.6)$$

where τ_p is the pulse width.

Similarly a sinc envelope pulse equation is:

$$B_1^e(t) = \begin{cases} B_1 \text{sinc}[\pi f_w (t - \tau_p / 2)] & 0 \leq t \leq \tau_p \\ 0 & \text{otherwise} \end{cases} \quad (2.7)$$

Time dependent characteristics of \vec{M} , when a $\vec{B}_1(t)$ magnetic field applied, is described by *Bloch equation*. The Bloch equation takes general form of,

$$\frac{d\vec{M}}{dt} = \gamma \vec{M} \times \vec{B} - \frac{M_x \vec{i} + M_y \vec{j}}{T_1} - \frac{(M_z - M_z^0) \vec{k}}{T_1} \quad (2.8)$$

where,

M_x : x component of bulk magnetization vector,

M_y : y component of bulk magnetization vector,

M_z : z component of bulk magnetization vector,

M_z^0 : Thermal equilibrium for \vec{M} in the presence of \vec{B}_0 only

T_1, T_2 : Time constants which characterize the relaxation process of a bulk magnetization vector after it has been excited.

According to the laws of thermodynamics, after a spin system being perturbed by an RF pulse, it will return to its thermal equilibrium state if the force is removed and sufficient time is given for relaxation. This process is called *free precession*. The z-component of magnetization vector (M_z) recovery is called *longitudinal relaxation* and recovery of transverse magnetization vector (M_{xy}) is called *transverse relaxation*.

The total effect of free precession can be found using equation (2.9) and (2.10).

$$M_z(t) = M_z^0(1 - e^{-t/T_1}) + M_z(0_+)e^{-t/T_1} \quad (2.9)$$

$$M_z(t) = M_z^0(1 - e^{-t/T_1}) + M_z(0_+)e^{-t/T_1} \quad (2.10)$$

The signals arising from the action of a single pulse on nuclear spin system is called *free induction decay* (FID). FID signals are basic form of transient signals gained after the excitation pulse. Mathematical form of an FID signal generated after α pulse is as follows:

$$S(t) = \sin \alpha \int_{-\infty}^{+\infty} \rho(\omega) e^{-t/T_2(\omega)} e^{-i\omega t} d\omega \quad t \geq 0 \quad (2.11)$$

where,

$\rho(\omega)$: Spectral density function

Simpler than equation (2.11), the FID signal of a single spectrum component which has a resonating frequency of ω_0 can be expressed as:

$$S(t) = M_z^0 \sin \alpha e^{-t/T_2} e^{-i\omega_0 t} \quad t \geq 0 \quad (2.12)$$

Another form of an MR signal is called *echo* signal. Echo signal is two-sided signal and necessary for symmetric frequency mapping. It can be obtained by either reversing gradient magnetic field or transmitting multiple RF pulses which are called *gradient echoes* and *RF echoes* respectively.

For RF echo generation, at least two RF pulses must be applied. One of the most common usages of this procedure is started by a 90° pulse and followed by a 180° pulse with a delay of τ . The signal generated by this approach is called *spin echo* (SE) signal.

The objects that are being imaged are heterogeneous, thus it is necessary to differentiate local signals with respect to different parts of the object.

Two of the most basic methods for spatial localization are *selective excitation* and *spatial encoding*. Modern MRI systems involve three orthogonal gradients of different shapes and forms.

Specifically, the received frequency - encoded FID signal is generally in the following form:

$$S(t) = \int_{object} \rho(\mathbf{r}) e^{-i\gamma \mathbf{g}_{fe} \cdot \mathbf{r}t} d\mathbf{r} \quad (2.13)$$

where,

$\mathbf{g}_{fe} = (g_x, g_y, g_z)$ is defined as the frequency - encoding gradient.

Phase encoding can also be done along an arbitrary direction for multi-dimensional object by turning on g_x, g_y, g_z during the phase-encoding period simultaneously.

The initial phase angle can be written as:

$$\varphi(\mathbf{r}) = -\gamma \mathbf{g}_{pe} \cdot \mathbf{r} T_{pe} \quad (2.14)$$

In the equation (2.14), T_{pe} denotes the interval of phase encoding.

The received signal can be expressed as the sum of all local phase encoded signals, which is given in equation (2.15).

$$S(t) = \left[\int_{object} \rho(\mathbf{r}) e^{-i\gamma \mathbf{g}_{pe} \cdot \mathbf{r} T_{pe}} d\mathbf{r} \right] e^{-i\omega_0 t} \quad (2.15)$$

After demodulation, the carrier signal $e^{-i\omega_0 t}$ will be removed from the signal.

An important connection between Fourier transform and spatial encoding (phase and frequency encoding) is established by the *k-space interpretation*. Using this method, complex imaging schemes can be described in k-space notation.

The relation between k and t is as follows when frequency encoding is done by multiple gradients:

$$\mathbf{k} = \begin{cases} \frac{\gamma}{2\pi} \mathbf{g}_{fe} t & \text{FID signals} \\ \frac{\gamma}{2\pi} \mathbf{g}_{fe} (t - T_E) & \text{echo signals} \end{cases} \quad (2.16)$$

For an FID signal, if the gradient fields are functions of time, the relation between k-space and gradient fields can be written as:

$$\mathbf{k}(t) = \frac{\gamma}{2\pi} \int_0^t \mathbf{g}_{fe}(\tau) d\tau \quad (2.17)$$

The corresponding k-space signal to equation (2.13) is

$$S(\mathbf{k}) = \int_{object} \rho(\mathbf{r}) e^{-i2\pi \mathbf{k} \cdot \mathbf{r}} d\mathbf{r} \quad (2.18)$$

As it can be seen on the equation above, the transformation is very similar to Fourier transform. However, $S(\mathbf{k})$ is available only for limited number of points in k-space.

Basic k-space mapping for two-dimensional imaging is,

$$S(k_x, k_y) = \int_{\text{object}} I(x, y) e^{-i2\pi(k_x x + k_y y)} dx dy \quad (2.19)$$

where $I(x, y)$ is the desired image function and formulized as follows:

$$I(x, y) = \int_{z_0 + \Delta z/2}^{z_0 + \Delta z/2} \rho(x, y, z) dz \quad (2.20)$$

An example for spin-echo pulse sequence is given in Figure 2.1. In this two dimensional imaging sequence, phase-encoding is applied along y-direction and frequency encoding is done in x-direction.

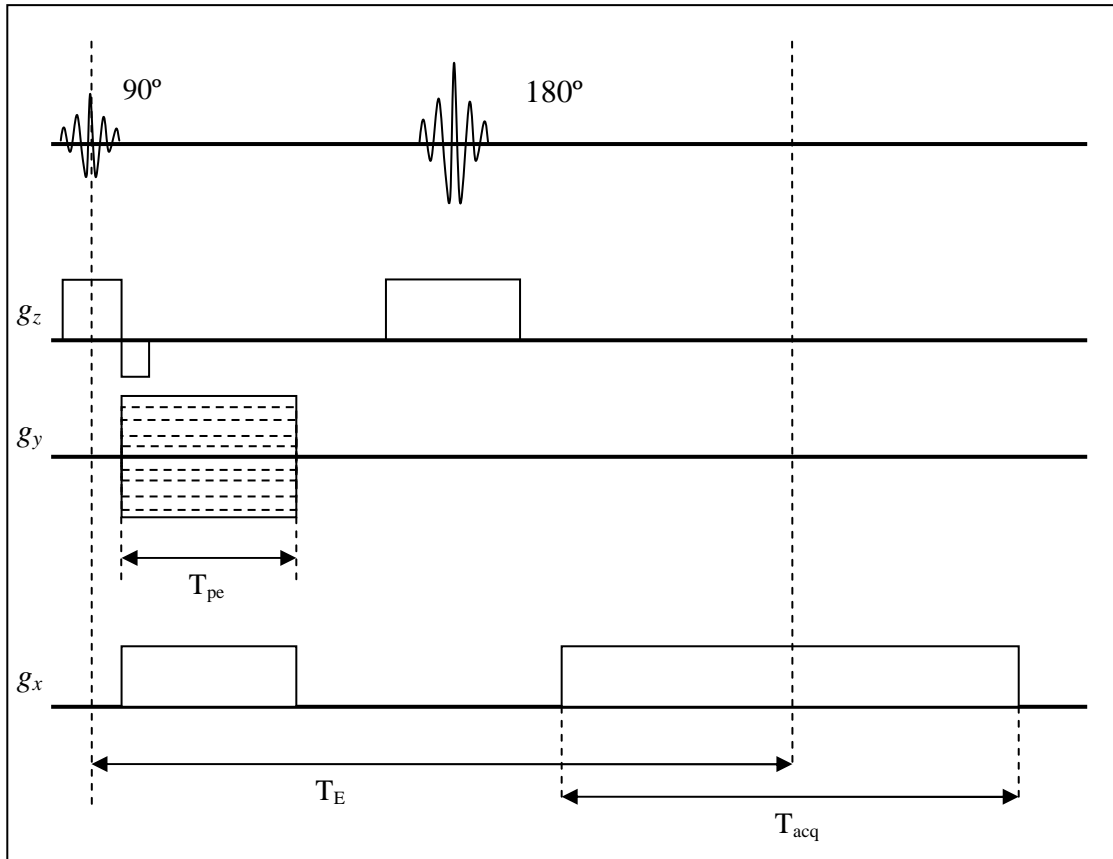


Figure 2.1- Spin-echo pulse sequence with phase-encoding is along the y -direction and frequency-encoding is along the x -direction.

This is known as *phase-encoding method*, k_x and k_y values are calculated as shown in equation (2.21).

$$\begin{aligned}
 k_x &= \frac{\gamma}{2\pi} g_x (t - T_E) & |t - T_E| < T_{acq} / 2 \\
 k_y &= \frac{\gamma}{2\pi} n \Delta g_y T_{pe}
 \end{aligned}
 \tag{2.21}$$

The k -space coverage of the pulse sequence given in Figure 2.1 is shown in Figure 2.2.

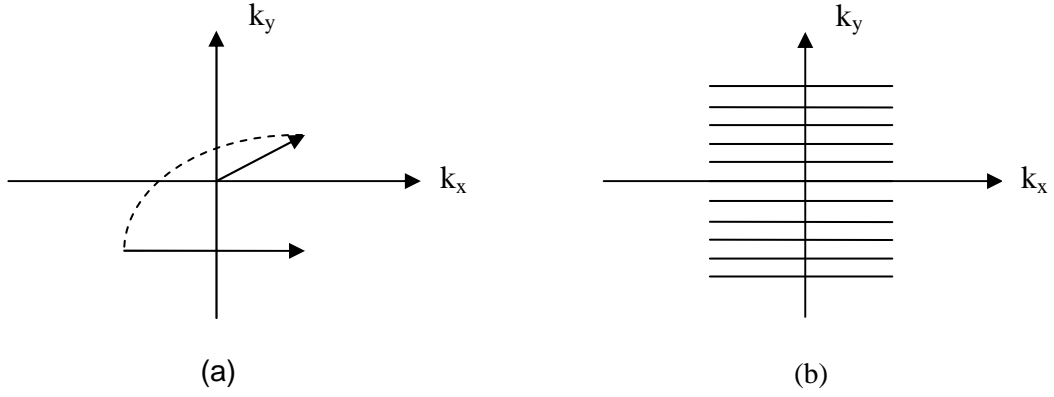


Figure 2.2 - K-space coverage of the spin-echo pulse shown in Figure 2.1. (a) k-space trajectory of a single echo, (b) k-space trajectory of a set of spin-echo cycles [6].

Sampling of k-space is an important issue to be examined. For rectilinear mapping, if the object is bounded by a rectangle having a width of W_x and W_y , the sampling theorem is as follows:

$$\Delta k_x \leq \frac{1}{W_x} \quad \text{and} \quad \Delta k_y \leq \frac{1}{W_y} \quad (2.22)$$

If the hybrid case is of interest, for which frequency encoding is applied along x -direction and phase encoding is applied along y -direction, the step sizes on k-space are calculated as shown in equation (2.23).

$$\begin{cases} \Delta k_x = \frac{\gamma}{2\pi} |g_x| \Delta t \\ \Delta k_y = \frac{\gamma}{2\pi} \Delta g_y T_{pe} \end{cases} \quad (2.23)$$

where,

g_x : Frequency encoding gradient

Δt : Readout sampling time interval

Δg_y : Phase encoding gradient step size

T_{pe} : Phase encoding gradient interval

By substituting equation (2.23) into (2.22) we obtain,

$$\begin{cases} \Delta t \leq \frac{2\pi}{\gamma |g_x| W_x} \\ \Delta g_y \leq \frac{2\pi}{\gamma T_{pe} W_y} \end{cases} \quad (2.24)$$

There are various methods for sampling k-space. Since the hybrid case is used in the designed simulator, other approaches are not examined in theory part of the thesis.

While explaining k-space mapping, it is shown in equation (2.18) and equation (2.19) that the transformation from spatial domain into frequency domain is realized by an approach which is very similar to Fourier transformation. In addition to that, for image reconstruction the inverse case is on. In other words, the method is similar to inverse Fourier transform.

According to Nyquist criterion, the largest pixel size acceptable is,

$$\Delta x = \frac{1}{N\Delta k} \quad (2.25)$$

which is known as *Fourier pixel size*. For the given pixel size in equation (2.25), there are exactly N pixels within the field of view (FOV).

$$\frac{\text{FOV}}{\Delta x} = \frac{1 / \Delta k}{1 / N \Delta k} = N \quad (2.26)$$

These pixels are determined by (equation 2.27) which is known as *direct DFT / FFT reconstruction*.

$$I[m] = \Delta k \sum_{n=-N/2}^{N/2-1} S[n] e^{i2\pi nm/N} \quad -N/2 \leq m < N/2 \quad (2.27)$$

In the simulator, saturation recovery spin-echo sequence, shown in Figure 2.1, is implemented.

For the saturation recovery spin-echo sequence, the amplitude of the spin echo signal is as follows:

$$A_E = M_z^0 (1 - 2e^{-(T_R - T_E/2)/T_1} + e^{-T_R/T_1}) e^{-T_E/T_2} \quad (2.28)$$

where,

T_R : Pulse repetition time

T_E : Echo time

T_1 : Longitudinal relaxation time for bulk magnetization vector

T_2 : Transverse relaxation time for bulk magnetization vector

In practice, T_E is much smaller than T_R . Therefore, equation (2.28) can be simplified as,

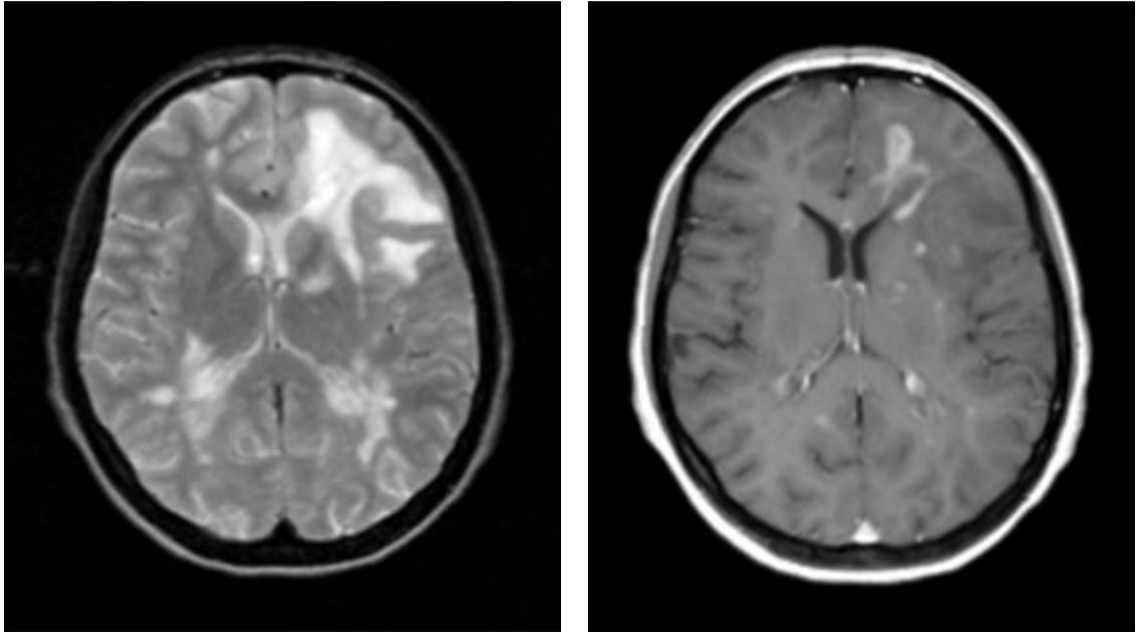
$$A_E = M_z^0(1 - e^{-T_R/T_1})e^{-T_E/T_2} \quad (2.29)$$

The signal expressed in equation (2.29) indicates that, the image intensity is dependent on *spin density-weight*, T_1 -weight, and T_2 -weight. As a result of this, one can adjust contrast parameters by choosing T_1 and T_2 appropriately. According to equation (2.29), contrast table of a saturation-recovery spin-echo sequence can be constructed as shown in Table 2.1.

Table 2.1 - Contrast table for saturation-recovery spin-echo sequence with respect to T_E and T_R values.

Contrast	T_E	T_R
T_1 -weighting	short	appropriate
T_2 -weighting	appropriate	long
ρ -weighting	short	long

An example of T_1 and T_2 weighted images obtained using saturation recovery spin echo pulse sequence are illustrated in Figure 2.3.



(a)

(b)

Figure 2.3 - Axial MRI images of a patient with relapsing-remitting MS. a) T_2 weighted spin echo axial MRI image. b) T_1 weighted spin echo axial MRI image [16].

2.2 Magnetic Resonance Electrical Impedance Tomography Background

Electrical conductivities of tissues vary depending on pathological or physiological properties of different tissue types. Electrical impedance tomography (EIT) is developed in order to distinguish tissues according to their electrical properties [17]. The resolution and accuracy of EIT technique is poor and its sensitivity is space dependent. These disadvantages limit the usage of conventional EIT when high resolution and accuracy is required.

Magnetic resonance current density imaging (MRCDI) technique was proposed within the last decade (Scott *et al* 1991, Eyuboglu *et al* 1998). This new modality is based on imaging magnetic flux density caused by applied current using MRI. Using this technique, magnetic flux density is imaged in the same resolution with MRI resolution and current density is imaged providing the half of MRI resolution.

Magnetic resonance electrical impedance tomography (MREIT) technique reconstructs conductivity distribution using both potential measurements obtained by surface electrodes and current density obtained by MRCDI.

Electric current injected to a conductor generates a magnetic flux density. The component of this magnetic flux density, which is in the same direction with main magnetic field, creates a phase shift on the signal:

$$S = \int_x \int_y M(x, y) \exp\left\{j\left[\gamma(g_x x t + g_y y t_y) + \gamma B_j T_c\right]\right\} dx dy \quad (2.30)$$

where,

$M(x, y)$: Transverse magnetization

$g_x x$: Gradient magnetic field applied along x-direction

$g_y y$: Gradient magnetic field applied along y-direction

B_j : Component of current based magnetic field parallel to main magnetic field

T_c : Duration of current pulse

t, t_y : Duration of x and y gradients respectively

Phase accumulation generated by the current pulse is expressed in equation (2.31).

$$\phi_{jn} = \gamma B_j(x, y) T_c \quad (2.31)$$

In the procedure, first MR signal is obtained without current injection. Then, the phase term of this signal is calculated. The same process is also done for the case which current is applied. Finally, difference between these two phase terms is calculated and additive phase term is found. Using the equation (2.31), magnetic flux density caused by the applied current can be obtained.

The current density depending on calculated magnetic flux density is found using Ampere's law:

$$\vec{J} = \mu_0^{-1}(\nabla \times \vec{B}) \quad (2.32)$$

And conversely, magnetic flux density also can be calculated using Biot-Savart law shown in equation (2.33), if the current density distribution is known.

$$\vec{B} = \int \frac{\mu_0}{4\pi} \frac{(\vec{J}dV) \times \vec{r}}{r^3} \quad (2.33)$$

In order to calculate one component of current density distribution, two components of magnetic flux density distributions which are perpendicular to the desired current density component are required. This process is illustrated in Figure 2.4.

There are several approaches for MREIT reconstruction. Basically two methods are used, these are J-based reconstruction algorithms and B-based reconstruction algorithms [18], [19]. In this thesis, equipotential projection (EPP) algorithm, which is a J-based reconstruction algorithm, is used for reconstruction [20]. This method requires J components and surface potential as input and gives true conductivity as the output. J and B values are calculated by the simulator after obtaining potential distribution data from the forward solver.

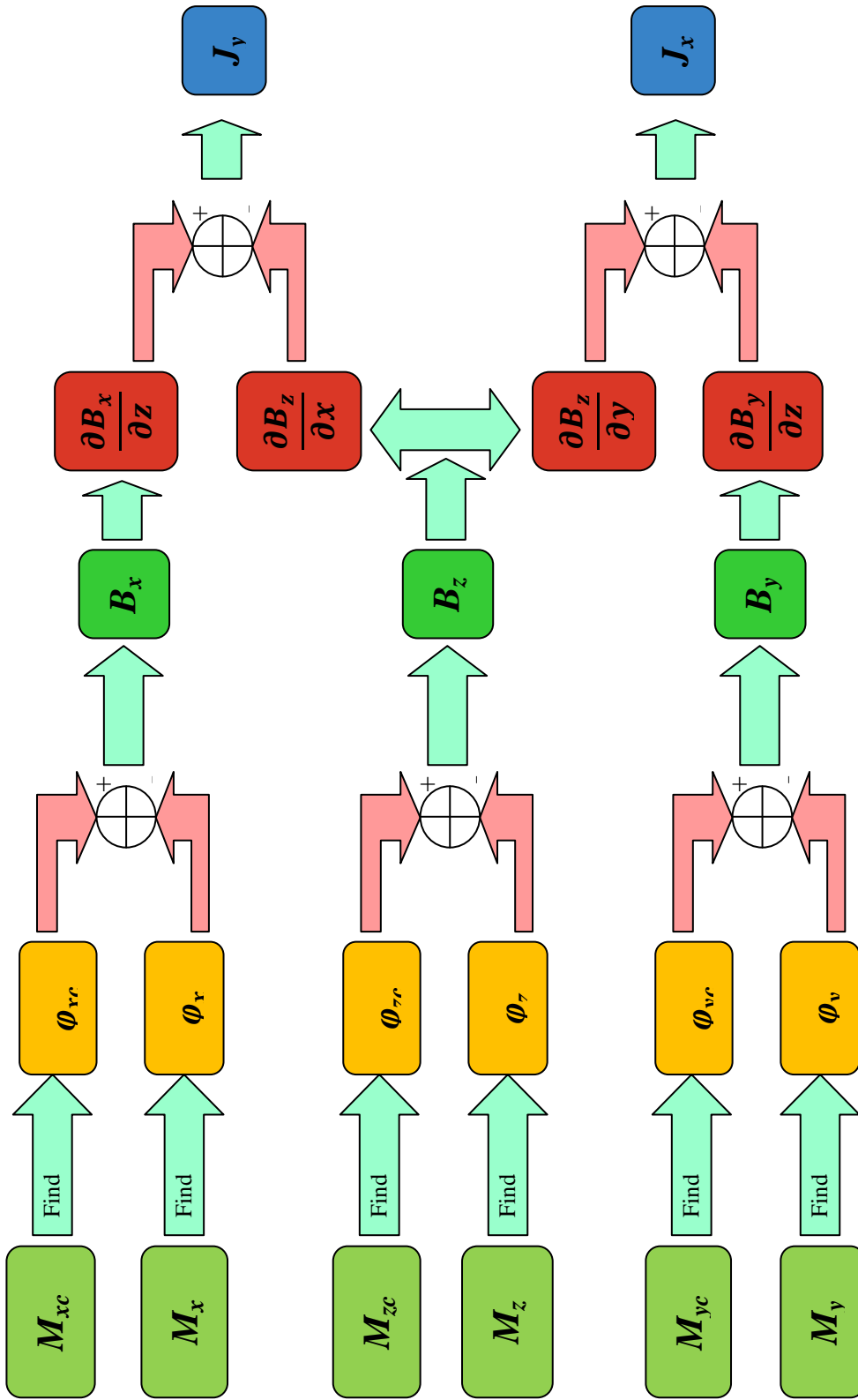


Figure 2.4 - The process block-diagram of obtaining J components from MRI signals.

Phase images of the signals obtained by MRI system are phase wrapped. In other words, since the phase scale is between $-\pi$ and $+\pi$, the boundaries around these values have the contrast of 2π . This condition is shown in Figure 2.5. To eliminate this effect, an unwrapping algorithm is used in the system. This algorithm detects the difference of respective pixels, and if the difference is $2\pi+\delta$, where $\delta>0$, then assigns this value to δ . The comparison of wrapped and unwrapped images can be seen on Figure 2.5.

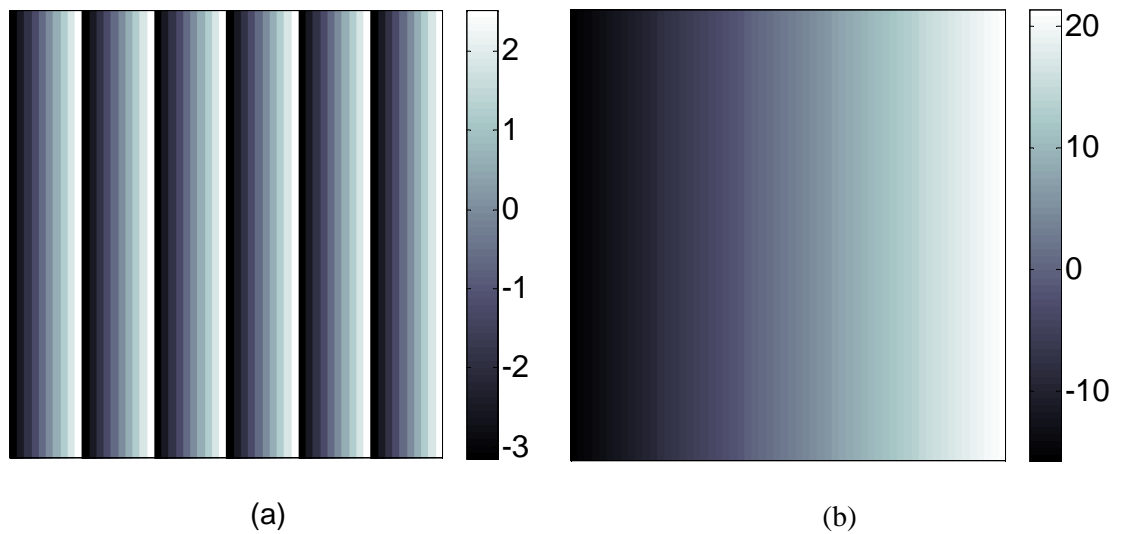


Figure 2.5- An illustration of phase images before and after unwrapping. a) wrapped MRI phase image b) unwrapped phase image.

2.3 Regional Image Reconstruction Using Optimum Currents

In regional image reconstruction (RIR), field of view is divided into sub-regions [13]. And in order to reconstruct the conductivity distribution, optimum current patterns are applied corresponding to each region. After finding the conductivity distributions for each region, these regions are merged to gather complete field of view.

Image contrast can be improved by increasing system SNR or using high magnetic field systems. On the other hand, it can also be improved optimizing the current injection patterns.

There are several principles for optimum current injection:

- current should be injected using opposite electrodes,
- current should be injected by using small electrodes,
- opposite current injection electrodes should be placed providing the current paths pass through the center of the inhomogeneity of interest.

According to the statements above, RIR method can be listed as follows:

1. Divide FOV into multiple regions,
2. Choose optimum injection pattern for each region,
3. Perform MREIT measurements using optimum currents for each region and reconstruct the conductivity distribution of the specified region,
4. Combine regional images to form the image of entire FOV.

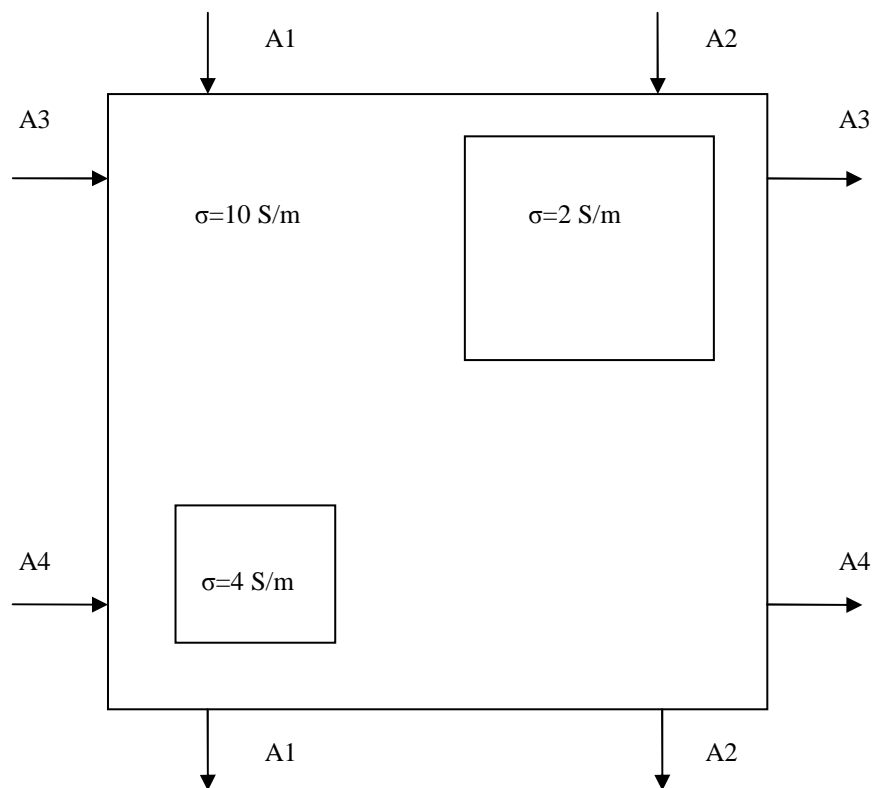


Figure 2.6 - Square model with two conductivity perturbations. Current patterns are shown with arrows numbered from A1 to A4.

Consider that the optimum current injection principles are applied to a model as shown in Figure 2.6. Conductivity values of the inhomogeneities are 10, 4 and 2 S/m. Current patterns from A1 to A4 are used as shown in Figure 2.7 and each current injection pattern is applied individually.

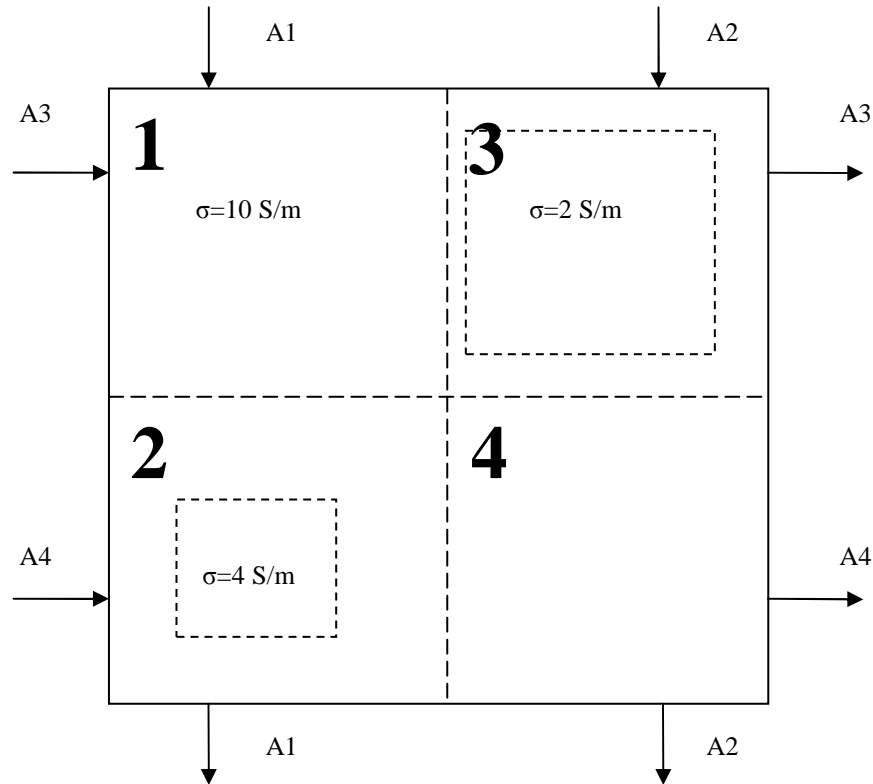


Figure 2.7 - Current injection patterns and regions of FOV

In the previous study by H. Altunel, the errors for conventional reconstruction (CR) and RIR are compared [13]. As a result, it is observed that, errors are very similar for noise-free case. However, when noise is added, RIR provides more accurate conductivity distributions, especially for inhomogeneities in the object. The advantage of this method is that, the reconstruction can be achieved for a specified region without propagation errors arising from other regions. This lowers the error significantly, especially when noise is present. Since there is always an amount of noise for realistic experiments, utilization of RIR provides more accurate conductivity images.

CHAPTER 3

MRI / MREIT SIMULATOR

In this chapter, sub-sections of MRI / MREIT simulator are investigated and designing ideas are explained. These sub-sections can be named as:

- Forward problem solving
- MRI simulator development
- MREIT simulator development
- Application of optimum current injection patterns and regional image reconstruction
- Graphical user interface design

Next, these parts are explained in details.

3.1 Forward Problem Solving

3.1.1 Idea and Implementation of Forward Problem Solving

As it is mentioned in chapter 2, in MREIT, magnetic flux density caused by the applied currents is imaged. These currents are applied using surface electrodes. To

simulate this approach, it is necessary to calculate the potential field distribution in the object depending on conductivity distribution and applied current first.

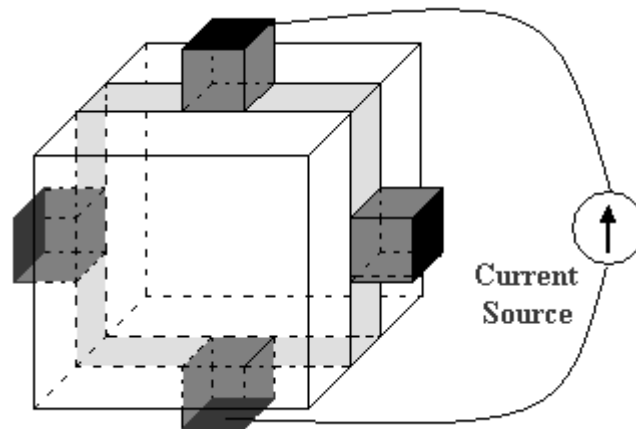


Figure 3.1 - An experimental phantom model showing electrode localization and current injection.

Forward problem solution of MREIT utilizes boundary conditions and previously calculated conductivity distribution. Several electrodes are placed around the surface of the object. In the thesis, models are created with eight electrodes on model surfaces. Two of the electrodes are placed for vertical current injection pattern, two are placed for horizontal current injection pattern and remaining four electrodes are placed for diagonal current injection patterns. Surface electrode localizations can be seen on Figure 3.2.

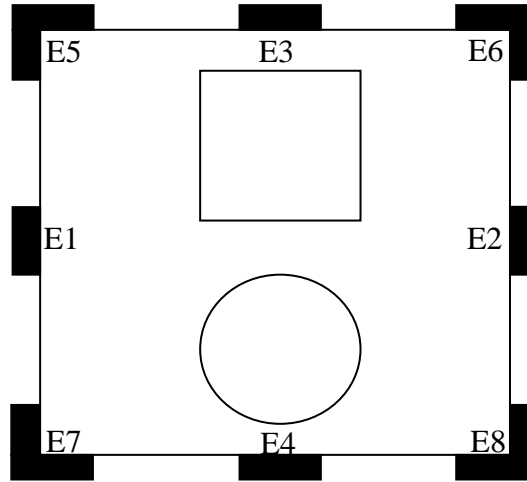


Figure 3.2 - Example simulation model showing surface current injection electrodes.

The equation, that is used to calculate the potential distribution inside the object, is the boundary value problem (BVP) shown in equation (3.1).

$$\sigma \frac{\partial \Phi}{\partial n} = \begin{cases} J & \text{on positive current electrode} \\ -J & \text{on negative current electrode} \\ 0 & \text{elsewhere} \end{cases} \quad (3.1)$$

where,

σ : Conductivity,

Φ : Potential,

n : Outward unit vector on boundary.

The relation between conductivity and potential is as follows:

$$\nabla \cdot (\sigma \nabla \Phi) = 0 \quad \text{in } \Omega \quad (3.2)$$

where,

Ω : Volume of the object.

The problem stated in equation (3.2) is solved using *finite element method* (FEM). Potential is solved on about 3000 nodes for an image of 1600 pixels. However this value can change according to some requirements, namely, if the boundaries inside the object are complex or long, then mesh sizes decrease and conversely solution node number increases. In addition to that, object size also affects the number of solution nodes.

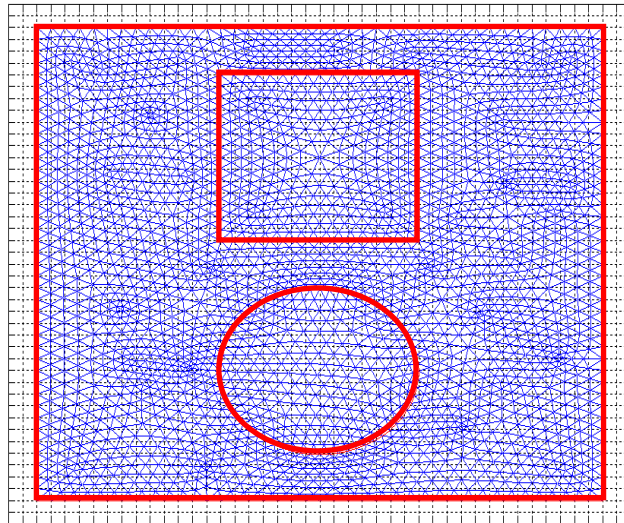


Figure 3.3 - General view of the mesh mode for square-circle model.

In the next step after solving potential distribution, x and y components of current density distribution is calculated using the equations (3.3) and (3.4) where z component of the current density distribution is assumed to be zero.

$$J_x(x, y) = -\sigma(x, y) \frac{\partial \Phi(x, y)}{\partial x} \quad (3.3)$$

$$J_y(x, y) = -\sigma(x, y) \frac{\partial \Phi(x, y)}{\partial y} \quad (3.4)$$

Using the equations above, current density distributions are obtained. However, it is required to go one step further and find magnetic flux density distributions in each direction. Although calculating only B_z is enough when dealing with the magnetic flux density image, it is necessary to calculate B_x and B_y components as well to be used in reconstruction algorithms for conductivity imaging. As it is explained in section 2.2, magnetic flux density distributions can be calculated using Biot-Savart law (shown in equation 2.33). Now, there exist x, y and z components of magnetic flux density generated by injected currents.

All calculations and results those have been obtained till now are for noise-free case. But experimental environments include a noise level. To take it into account for simulator, user can add noise to magnetic flux density data at a desired level to get more realistic results. The resultant magnetic flux density is given into simulator as additive magnetic flux density caused by current injection.

3.1.2 Forward Problem Solving Part on User Interface

The inputs of forward problem solver of the simulator are as follows:

- Model type,
- Image size,
- Injected currents on each electrode (Electrode1, Electrode2 , ... , Electrode8),
- Conductivity values of the inhomogeneities,
- Special geometry descriptions for some models (such as gap length),
- Save directory for saving generated current density distribution,
- Noise level

The functions of these inputs will be explained in details in section 3.5.

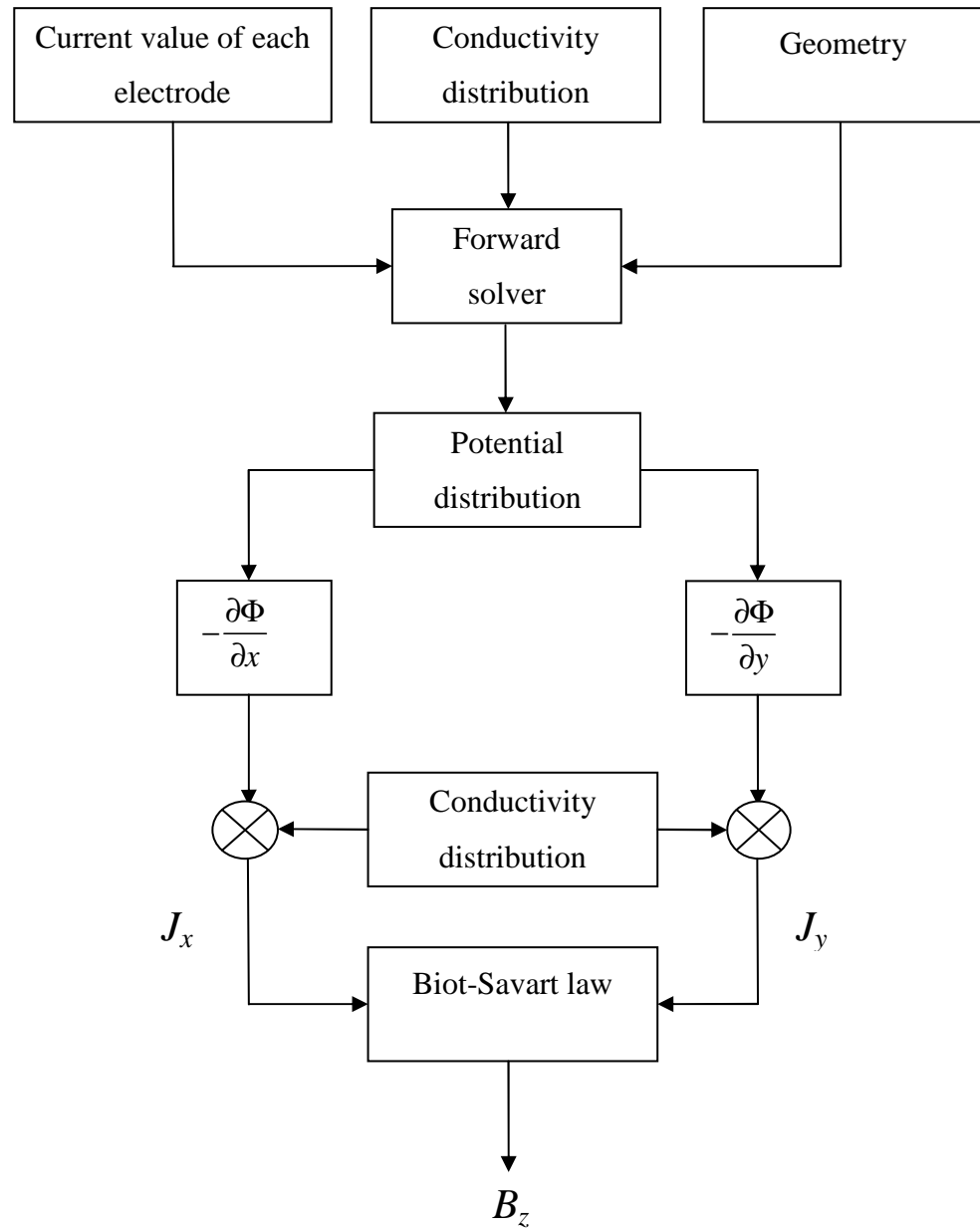


Figure 3.4 - Block diagram showing the steps of forward problem solution.

3.2 MRI Simulator Development

The old version of the MRI simulator is designed by E. Arpinar and H. Yigitler as a part of their thesis [11], [12]. In this study, the simulator is developed for MREIT applications including various models, and control of the system is generalized for

public use. In this part, the developments and the generalization facts will be expressed.

For simulation, first of all, the model geometries must be chosen. According the geometry of the model, spin densities, longitudinal relaxation and transverse relaxation intervals of inhomogeneities are defined. Completing these inputs, all the required parameters about the object are known.

The model geometries available in the simulator are:

- Square-circle model
- Diagonal squares model
- Impulsive squares model
- Shepp-Logan model

These models will be discussed in details in section 3.6.

Models are formed of different inhomogeneities and each inhomogeneity has independent MR parameters. The MR parameters of the models used in the simulator are listed below:

- Longitudinal relaxation time (T_1)
- Transverse relaxation time (T_2)
- Spin density (ρ)

As shown in equation (2.29), these values directly affect the MR signal.

There exist text boxes corresponding to each parameter on the user interface. Exceptionally, since there are 10 inhomogeneity regions in Shepp-Logan phantom, and there are three parameters defined for each region, it may cause a crowded scene on the screen. To overcome this issue, Shepp-Logan parameters are loaded from a previously saved matrix. In addition to that, construction of this matrix can be realized and saved as a file using another tab of the simulator.

Next inputs required for simulation are the pulse sequence parameters. Before expressing the process, listing the inputs of pulse sequences will be more illustrative. Thus, the inputs are given below:

- Model type
- Image size
- Step number in the read-direction
- Step number in the phase-direction
- Main magnetic field strength
- RF transmitter magnetic field strength
- RF receiver magnetic field ratio
- T_R
- T_E
- Maximum gradient strength
- Data file save directory
- Number of averages
- System noise
- Current (on/off)

Field of view (FOV) is one of the most crucial concepts in MRI. It is important to note that, in the MRI simulator, field of view is set to cover exact boundaries of the object. This satisfies equation (2.22). Thus, as soon as the object is chosen, FOV is also defined. After that, using the equations (2.25) and (2.26), step sizes on k-space are calculated. In a classical MRI approach, FOV is adjusted using gradient fields. However, if the aim is to cover whole object, the adjustment of gradients according to desired FOV will be more appropriate [12]. Therefore, the gradient fields and durations are calculated according to the object size and FOV. For the inverse case, gradient fields can be obtained using equation (2.23). Since maximum gradient strength, FOV boundaries, T_R and T_E are already known T_{pe} and T_{acq} can be calculated using equation (2.23) and (2.24).

The outputs of the MRI part are magnitude image and phase image in the spatial domain, magnitude image, phase image, real image and imaginary image in the k-space. These can be selected to be imaged on reconstruction window.

3.3 MREIT Simulator Development

The theory of MREIT is explained in section 2.2. According to the stated procedure, a resultant magnetic flux density distribution caused by current injection is calculated and this magnetic field is added on main magnetic field. The process done in the simulator is basically the same.

In the first section of this chapter, the methods for forward problem solving are expressed. The aim of forward problem solving is to find the magnetic flux density. The thing here done is to take the solution from the forward problem solver part of the simulator and add it to the main magnetic flux density.

$$B_r = B_m + B_j \quad (3.5)$$

where,

B_m : Main magnetic flux density

B_j : Magnetic flux density caused by applied currents

B_r : Resultant magnetic flux density

Then, two MRI data are obtained using B_m and B_r . The difference of phase images for these two data involves magnetic flux density information caused by the injected currents as shown in the equation (2.30) and (2.31). Duration of current injection (T_c) is entered by the user using the interface. Therefore, B_j is calculated easily.

As mentioned in section 2.2, there are basically two approaches for conductivity reconstruction in MREIT. These are B-based algorithms and J-based algorithms. B-based algorithms directly utilize each component of magnetic flux density measurements (B_x , B_y and B_z) in order to reconstruct conductivity [19]. However, since only z-component of \vec{B} can be measured by an MRI system, it is necessary to rotate object to obtain x and y components of \vec{B} . This rotation is also available in the MREIT part of the simulator, in other words each component is calculated. J-based algorithms utilize current density distributions. To achieve this, each component of current density (J_x, J_y, J_z) is calculated using magnetic flux density measurements. Equation (2.32) shows the way to find \vec{J} using \vec{B} . Writing this equation for each parameter, equations below are obtained:

$$\begin{aligned}
 J_x &= \frac{1}{\mu_0} \left(\frac{\partial B_z}{\partial y} - \frac{\partial B_y}{\partial z} \right) \\
 J_y &= \frac{1}{\mu_0} \left(\frac{\partial B_x}{\partial z} - \frac{\partial B_z}{\partial x} \right) \\
 J_z &= \frac{1}{\mu_0} \left(\frac{\partial B_y}{\partial x} - \frac{\partial B_x}{\partial y} \right)
 \end{aligned} \tag{3.6}$$

As it can be seen on equation (3.6), derivatives of \vec{B} components are required to find \vec{J} values. In the simulator, each component of \vec{J} is calculated using these derivatives. The process can be seen in Figure 2.4 clearly.

3.4 Image Reconstruction

3.4.1 Conventional Image Reconstruction

It is expressed that, there are several algorithms developed for MREIT reconstruction. Since all components of magnetic flux density are known and the

derivatives are calculated, the required parameters for any MREIT reconstruction algorithm can be assumed as prepared.

In this study, EPP algorithm is chosen as the reconstruction algorithm [20].

The inputs of the algorithm are:

- x component of current density distribution ($J_x(x,y)$),
- y component of current density distribution ($J_y(x,y)$),
- Potential distribution ($\Phi(x,y)$).

Although the potential distribution covering whole object is inserted, only the surface potential values are used.

EPP algorithm can be utilized applying either one current injection pattern or multiple current injection patterns. If more than one current injection pattern is used, the conductivity distribution is reconstructed for each pattern individually, and then final conductivity is found by averaging these distributions.

3.4.2 Regional Image Reconstruction

In the theory section, an explanation of the idea and principles of regional image reconstruction is given. Now, the application of this approach in the simulator will be expressed in details.

In this study, the reconstruction algorithm used for this approach is also EPP algorithm. The idea of reconstruction technique is almost the same with conventional image reconstruction. The difference is that, the object is divided into several sub-regions, and appropriate current injection patterns are applied to reconstruct each region. Finally, these regions are combined together and the complete image is obtained.

For any MREIT application for this simulator, user can apply currents in any electrode shown in Figure 3.2. Hence, the current patterns can be selected by the user easily. The data which is acquired after each current injection pattern must be saved

before starting a new one. That is because the reconstruction algorithm needs the data to select the region to be reconstructed.

In the previous studies, object is divided into four sub-regions for a square model [13]. Different from those, square models are divided into nine sub-regions. The reason lays behind is to provide similarity of electrode configuration with the models designed for conventional MREIT applications. For any square model in the simulator, the current injection patterns are shown in Figure 3.5. V1, V2 and V3 represent vertical patterns; H1, H2 and H3 represent horizontal patterns; and D1 and D2 represent diagonal current injection patterns.

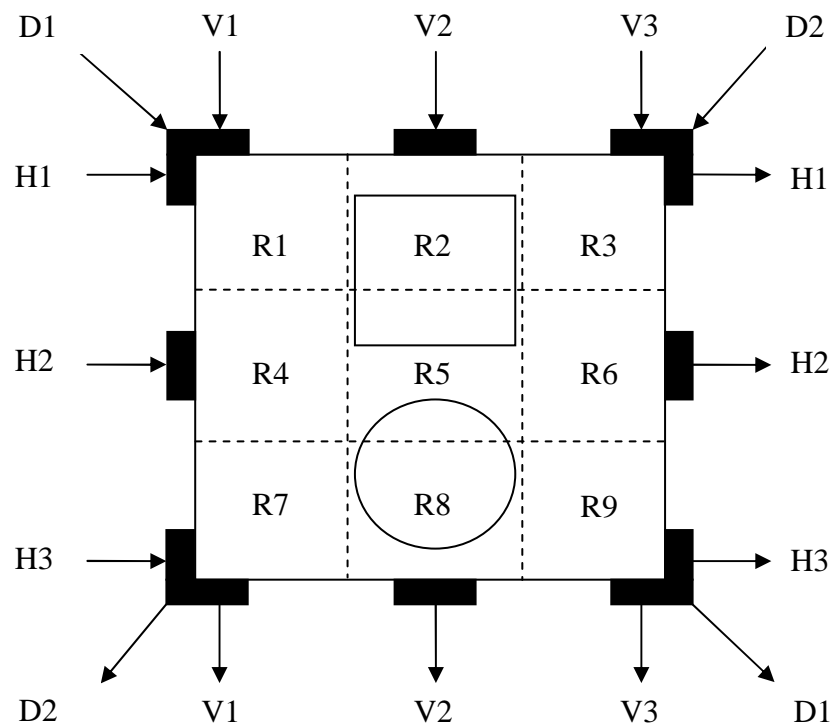


Figure 3.5 - Current injection patterns and region divisions for regional image reconstruction

The table showing the current injection patterns with respect to the reconstructed regions is given below.

Table 3.1 - Injection patterns utilized for each sub-regions.

Region	Utilized Current Injection Patterns			
Region 1 (R1)	V1	H1	D1	-
Region 2 (R2)	V2	H1	-	-
Region 3 (R3)	V3	H1	D2	-
Region 4 (R4)	V1	H2	-	-
Region 5 (R5)	V2	H2	D1	D2
Region 6 (R6)	V3	H2	-	-
Region 7 (R7)	V1	H3	D2	-
Region 8 (R8)	V2	H3	-	-
Region 9 (R9)	V3	H3	D1	-

In the procedure of RIR, reconstruction is done for whole object utilizing each current injection pattern as shown above. Each region's conductivity is calculated averaging the two corresponding patterns.

Another model type that can be used in regional reconstruction algorithm is Shepp-Logan phantom. Since Shepp-Logan is an elliptical phantom, regional division and current injection patterns are different from square models.

Shepp-Logan phantom used in the simulator and the current injection patterns is given on Figure 3.6. Since the outer boundary of the object is square shaped, the current is carried towards the Shepp-Logan phantom by created current paths (white paths on Figure 3.6). The conductivity values of these regions are assigned as the conductivity value of the outer region of Shepp-Logan phantom. On the other hand, the black regions, which are not desired to be conductive, have zero conductivity. Hence, current cannot pass through these regions.

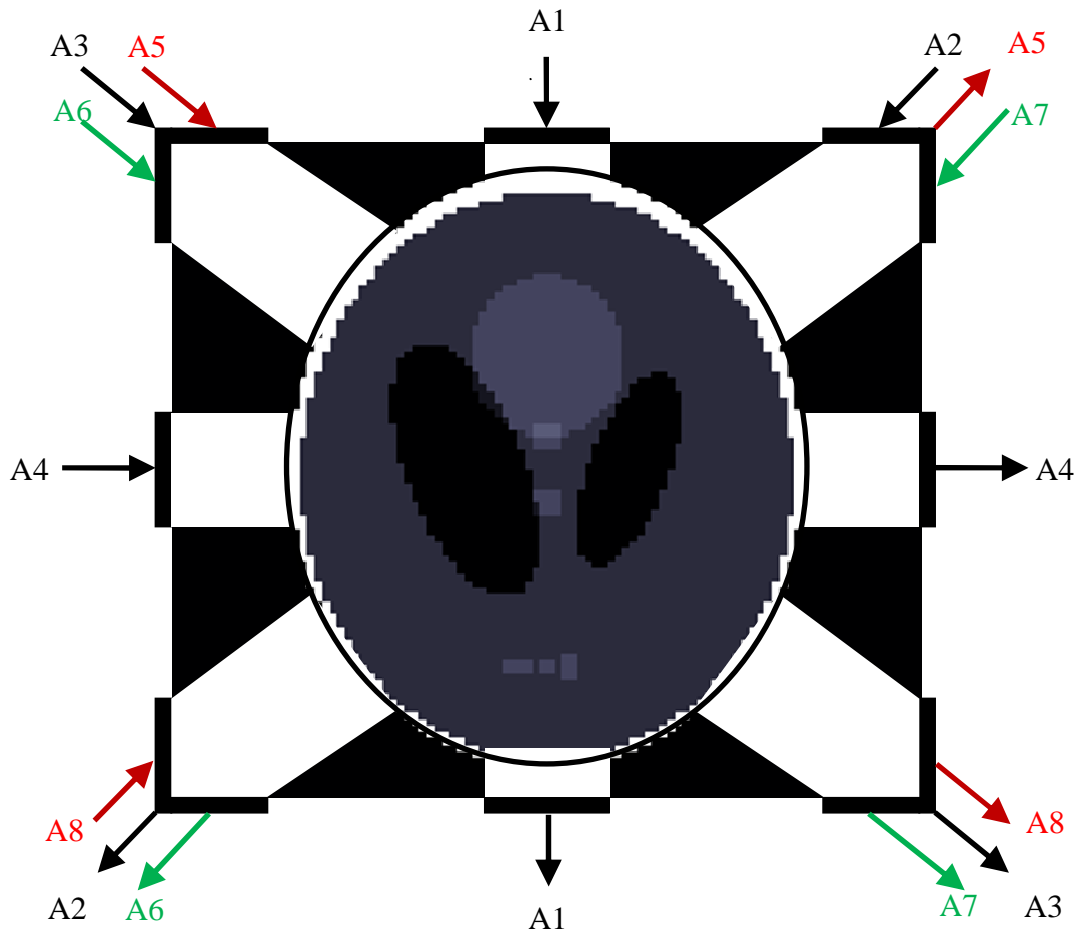


Figure 3.6 - Current injection and sink electrode placements for each current injection pattern.

Similar with the square model case, this model should be divided into sub-regions. Below, on Figure 3.7, there is an illustration showing how the regions are separated.

Table 3.2 states the utilized current injection patterns with respect to the sub- regions of FOV. These patterns are chosen in order to maximize the image contrast.

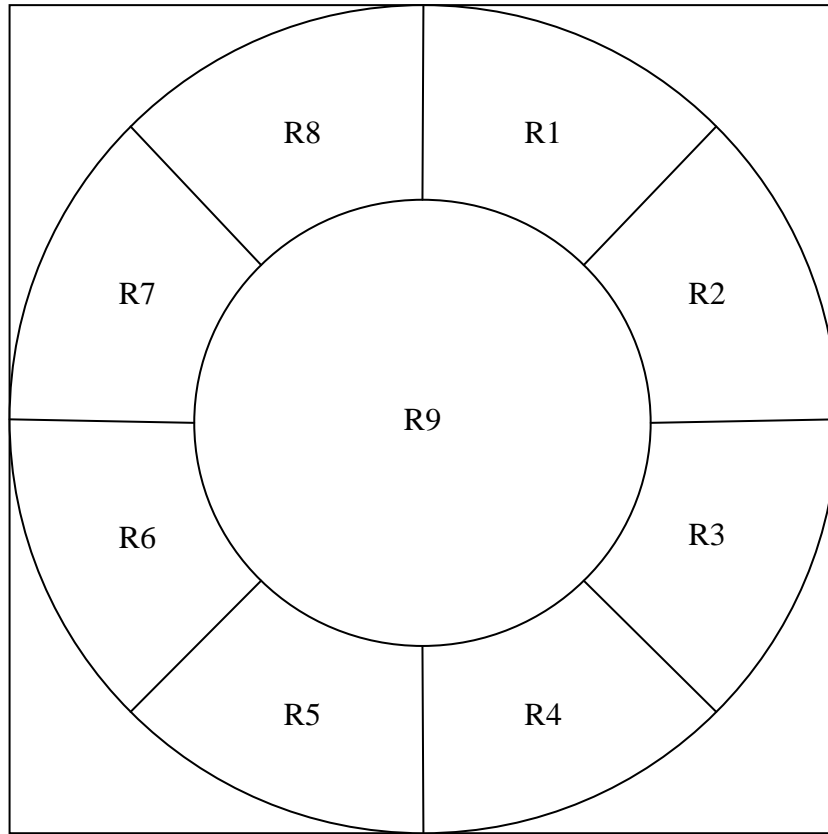


Figure 3.7 - The regions of FOV for RIR using Shepp-Logan phantom.

Table 3.2 - Sub-regions of Shepp-Logan phantom and corresponding current injection patterns utilized for each region.

Current Patterns	Regions of the Phantom								
	R1	R2	R3	R4	R5	R6	R7	R8	R9
A1	√			√	√			√	√
A2	√	√			√	√			√
A3			√	√			√	√	√
A4		√	√			√	√		√
A5	√	√					√	√	√
A6					√	√	√	√	√
A7	√	√	√	√					√
A8			√	√	√	√			√

The results obtained using the given model will be discussed in the results section.

3.5 User Interface Design Using LabVIEW

3.5.1 Introduction to LabVIEW

LabVIEW is the abbreviation stands for **L**aboratory **V**irtual **I**nstrument **E**ngineering **W**orkbench. It is one of the leading tools for acquiring, analyzing and visualizing data. LabVIEW is an open environment interfacing with any kind of measurement hardware. It includes more than 450 built in functions specifically designed for data acquisition, signal processing and measurement analysis. LabVIEW also provides tools for user interface design, web publishing, software connection, data management and visualization. The software suit implemented for METU MRI system involves the abilities mentioned above [1].

LabVIEW is a graphical programming environment combining the abilities of conventional programming languages with a rapid development environment. While designing software on LabVIEW, icons are used for function representations. Therefore, the complexity of software code syntax and the required time decrease whereas the productivity increases. Each virtual instrument (VI), namely each program in LabVIEW, has two main parts called front panel and the block diagram.

The front panel is the visual part of the interface. In other words it is the window that the user faces. This window contains controls, indicators, text boxes, plotting figures, tables, etc.

The block diagram is the software in graphical design. Every item on front panel has a corresponding icon on block diagram. All of the items on the front panel are controlled by these icons on block diagram. By wiring the icons and changing the variables appropriately, programs are designed.

LabVIEW is a dataflow programming language. Using this dataflow structure, differently from text-based languages, it can execute multiple operations in parallel and synchrony.

Since this thesis includes only software design, any card of National Instruments (NI) is not utilized and controlled.

3.5.2 LabVIEW Part of the MRI/MREIT Simulator

3.5.2.1 Data Acquisition Panel

MRI/MREIT simulator is controlled by an interface. Therefore, all of the necessary inputs for executing the simulator are entered on the front panel. In this section, the recently added parts of this interface corresponding to different affairs are going to be explained. But first, the general view of the previous version of the data acquisition part (designed by M. Ozsut) is shown in order to notice the additional parts.



Figure 3.8 - Screenshot of the data acquisition front panel while spin echo pulse sequence is being applied.

In Figure 3.8, general view of the previous version is shown. The new sections on data acquisition window are added on the tab window which is seen right bottom part of Figure 3.9.

The new tabs can be listed as follows:

- Acquisition Parameters
- Model Parameters
- Create Current Distribution
- Create Shepp-Logan Phantom

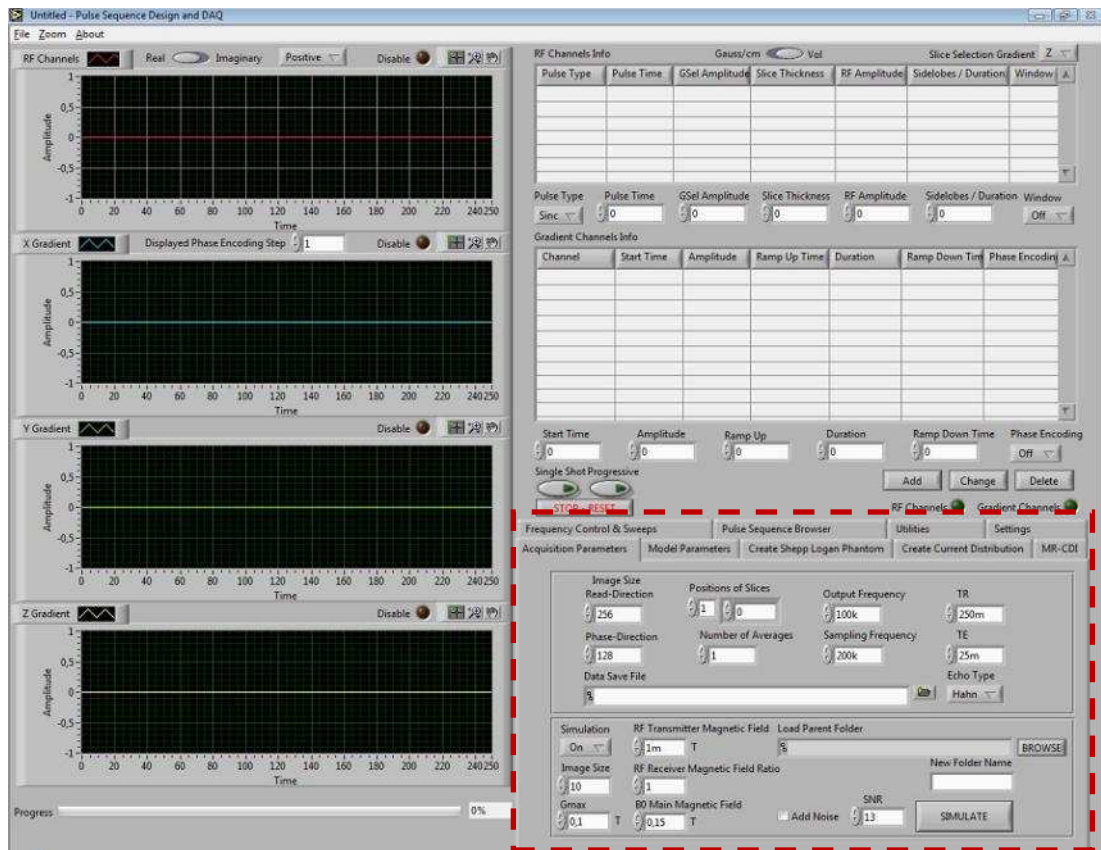


Figure 3.9 - New vision of the data acquisition window after the additional parts

"Acquisition Parameters" tab is not newly designed, but several new input boxes for simulator are added on this tab.

These inputs and their functions are expressed below:

- Image Size: Pixel number of a square image in one direction,
- B0 Main Magnetic Field: The value of the main magnetic field,
- RF Transmitter Magnetic Field: The magnetic field strength of the RF transmitter,
- RF Receiver Magnetic Field Ratio: The strength ratio between the RF transmitter and the receiver,
- Load Parent Folder/New Folder Name: Determine the path to save the simulation directory,

- Gmax : Maximum gradient strength,
- Add Noise/SNR: The noise level in the system.

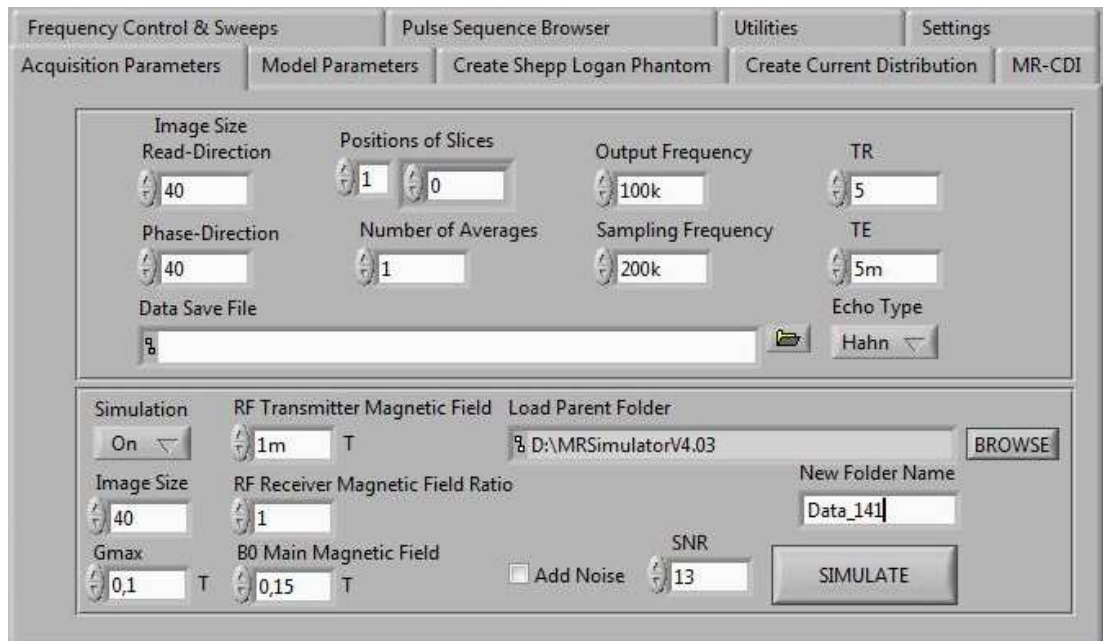


Figure 3.10 - "Acquisition Parameters" tab.

In addition to those above, following inputs that are used in METU-MRI system are also combined with the simulator:

- TR,
- TE,
- Image Size Read Direction (as frequency encoding step number),
- Image Size Phase Direction (as phase encoding step number).

"Model Parameters" tab includes the inputs to create the object to be imaged in the simulator. The inputs are as follows:

- Model Type: The type of the model,
- T1, T2 and spin density values: MR parameters of each inhomogeneity,
- Load Shepp-Logan Phantom: Only visible if Shepp-Logan model is chosen and loads the file including the MR parameters for Shepp Logan phantom,
- Current: The button to turn on or off the current. If the current is turned on, following inputs become active.
 - Browse Current Density: Path loader that is used to load the file including pre-created current density distribution for the model,
 - Current Duration: The total amount of time that the current is applied,
 - B component: The button to select the B component which is wanted to add to the main magnetic field.

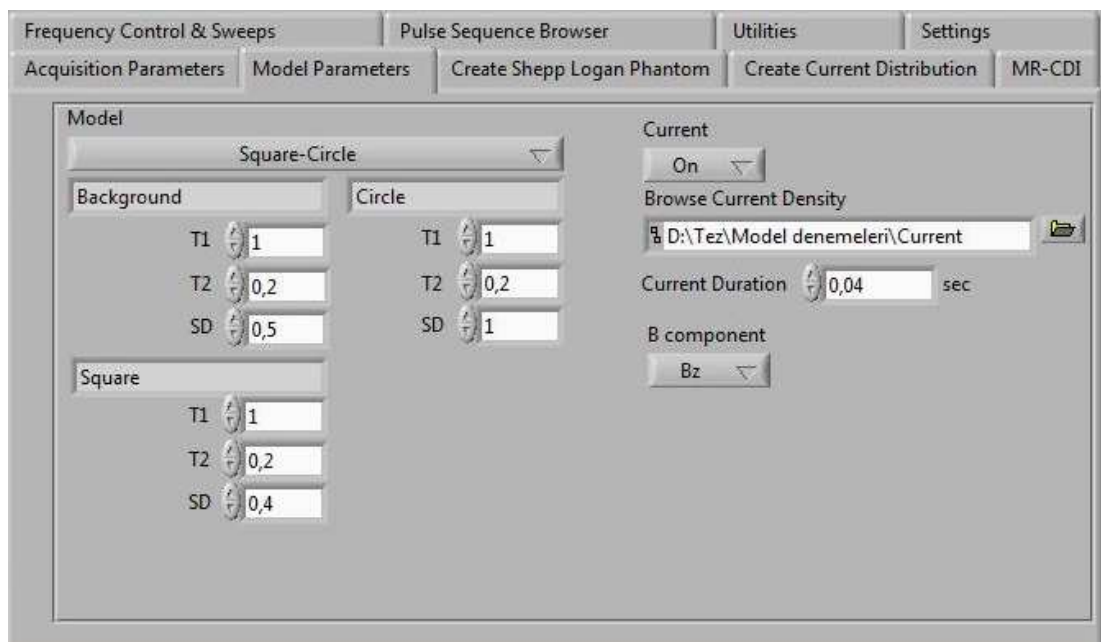


Figure 3.11 - "Model Parameters" tab.

"Create Current Distribution" tab is designed in order to obtain current density distribution and magnetic flux density components by injecting current to a specified model.

The inputs of this part are:

- Current Model: Current injected model is chosen,
- Image Size: The size of the object in pixels,
- Conductivity values: Conductivity of each inhomogeneity,
- Current values: Amplitude of currents injected on each electrode,
- Square Gap Number (Available only for impulsive square model): The pixel number between two impulsive squares,
- Save Model: File path to save the created model,
- Load Shepp - Logan Conductivity Vector: Conductivity values of the Shepp-Logan phantom,
- Add Noise/SNR: Noise level of the current injection system.

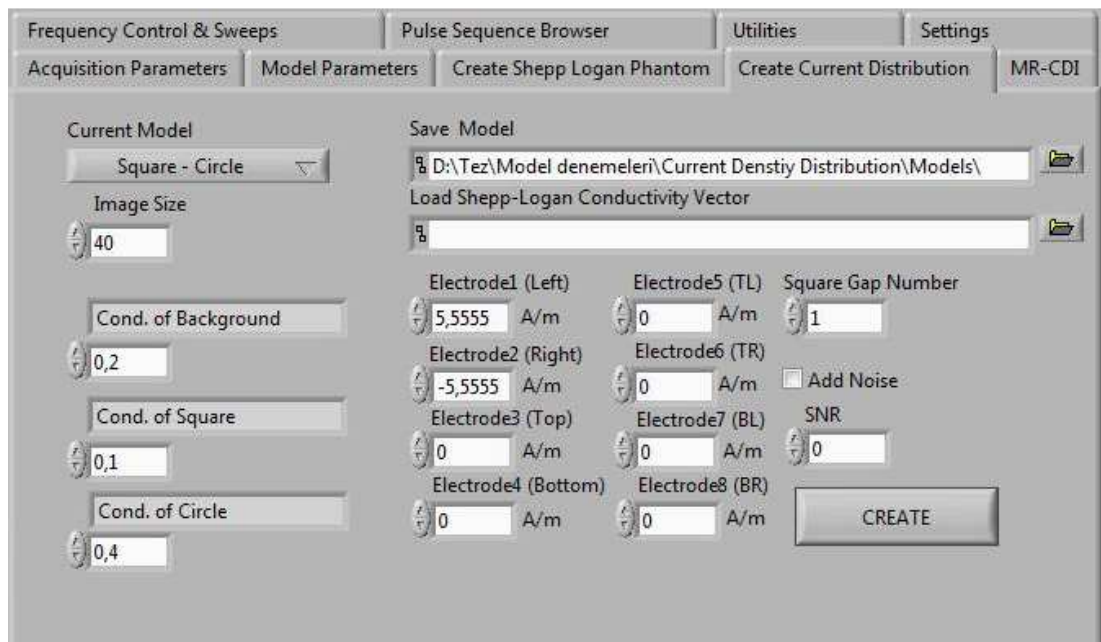


Figure 3.12 - "Create Current Distribution" tab.

The next tab is "Create Shepp-Logan Phantom". On this tab T1, T2, spin density and conductivity values of each section are determined for Shepp-Logan phantom. This tab is seen as matrix structure. The inputs are:

- T1, T2, spin density and conductivity values of each section,
- Save MR parameters: Create a file to save the MR parameters of the model,
- Save Cond. Parameters: Create a file to save the conductivity parameters.

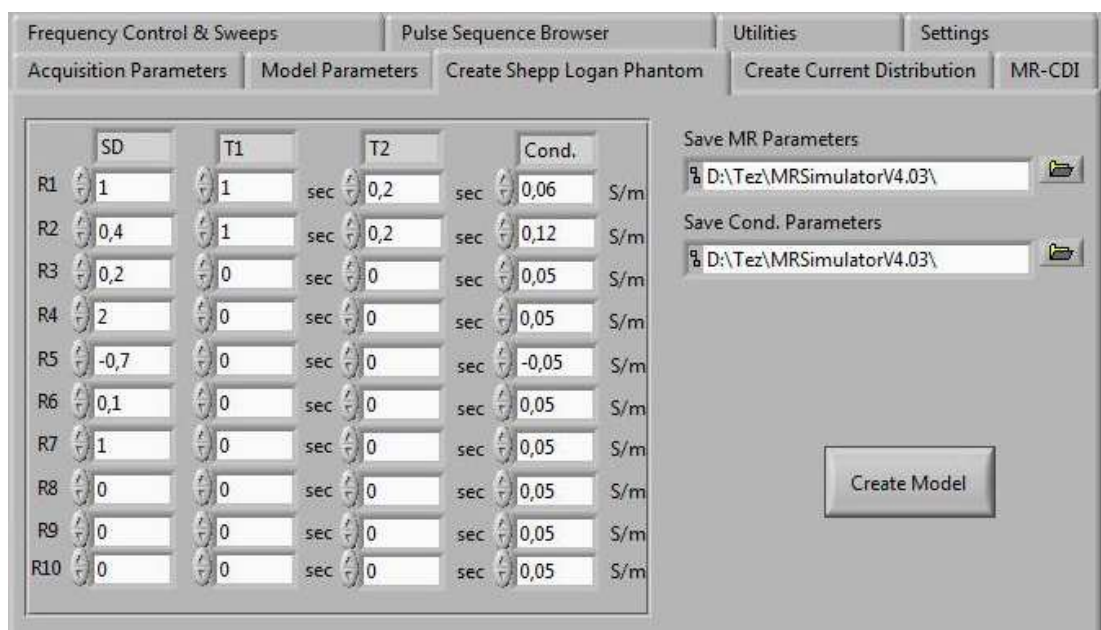


Figure 3.13 - "Create Shepp - Logan Phantom" tab.

3.5.2.2 Image Reconstruction Panel

Image reconstruction panel is the window where previously acquired data are imaged and processed. Same as the data acquisition panel, the additions are made on the tab window of this panel as well. To compare with the new one, the old version of the program is shown in Figure 3.14.

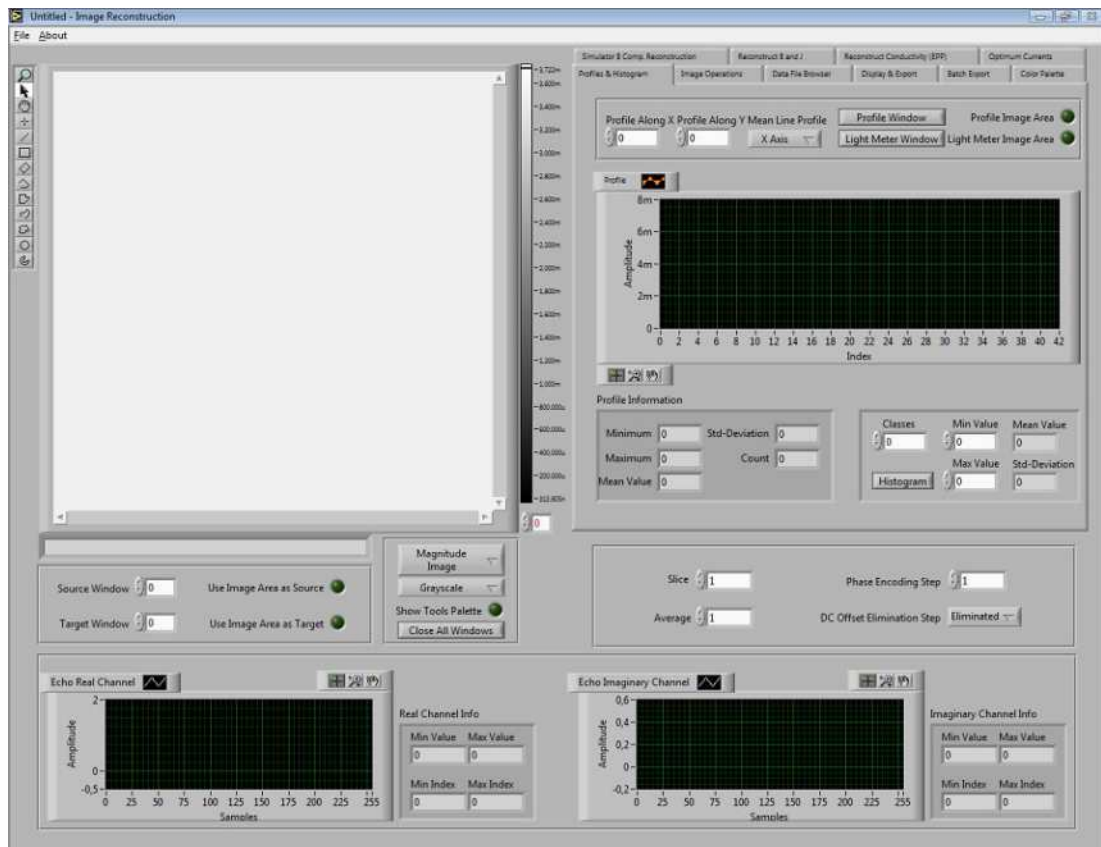


Figure 3.14 - Old version of the image reconstruction panel.

The new tabs designed for the simulator are as follows:

- B Component Reconstruction
- Reconstruct B and J
- Reconstruct Conductivity
- Optimum Currents

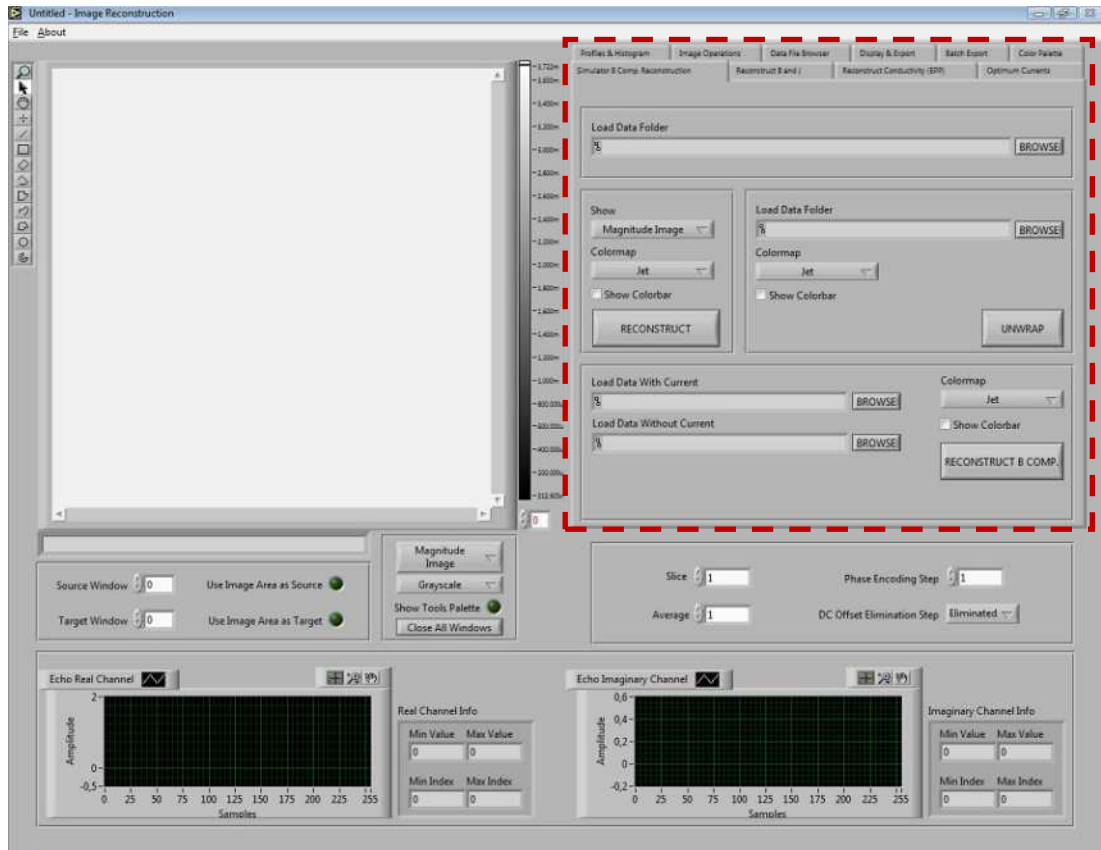


Figure 3.15 - New version of the image reconstruction panel.

"B Component Reconstruction" tab is used for several purposes. One of them is reconstructing the MR data and imaging parameters of the signal. In addition to that one can unwrap a wrapped phase image on this tab and see it. In the end, the B component is obtained by loading the data with and without injected currents.

The inputs of this tab are listed below:

- Load Data Folder (for reconstruction): Loads the folder containing acquired data to be reconstructed,
- Show: Parameter to be imaged is chosen,
- Colormap (available in each part of the tab) : The colormap to image the reconstructed signal is chosen,

- Show Colorbar (available in each part of the tab): Shows the colorbar if activated,
- Load Data Folder (for unwrap) : Loads the folder containing acquired data to be unwrapped,
- Load Data With Current : Loads the data folder which includes the signal acquired by injecting current,
- Load Data Without Current : Loads the data folder which includes the signal acquired without injecting current.

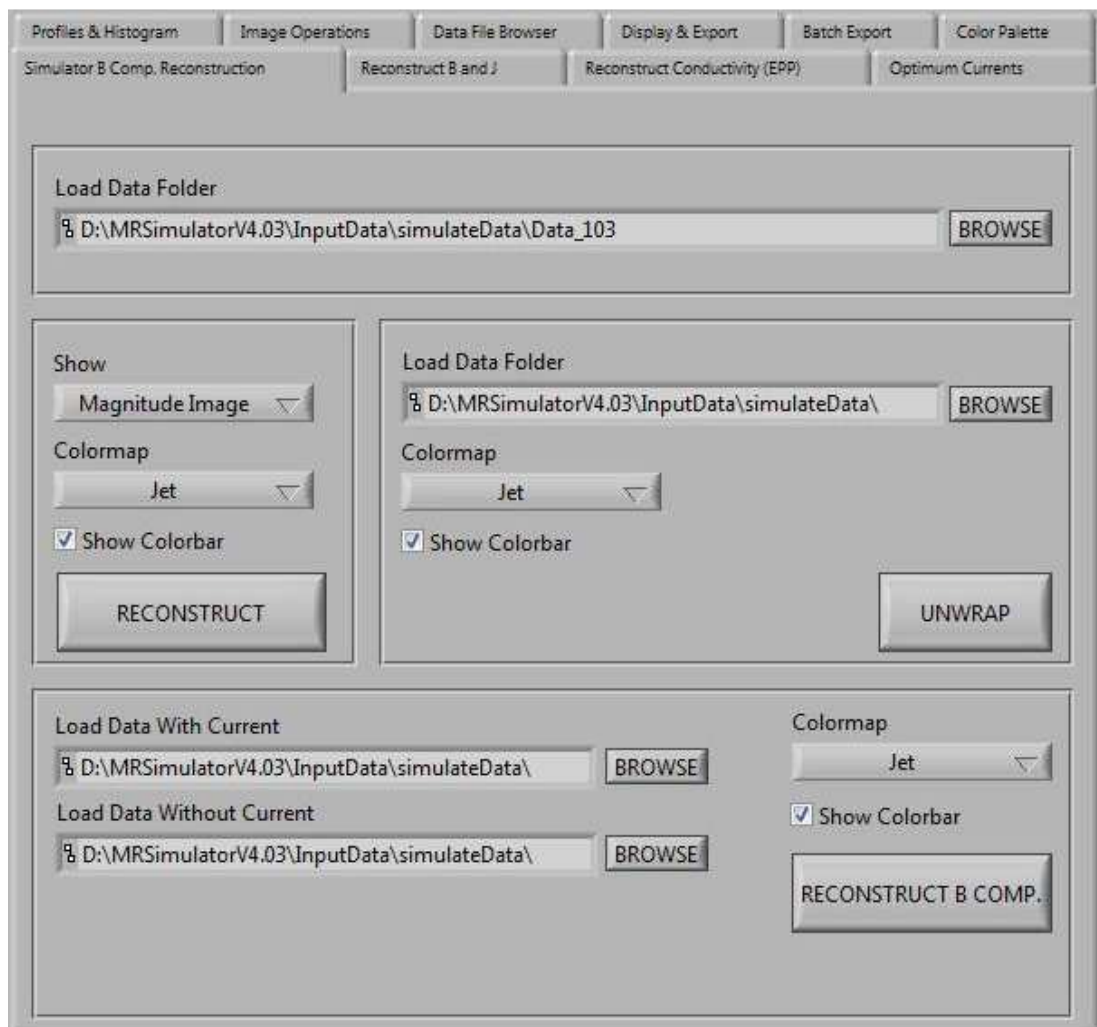


Figure 3.16 - "Simulator B Comp. Reconstruction" tab.

The next tab on this panel is "Reconstruct B and J". In this section x, y and z components of \vec{B} and \vec{J} are obtained. To achieve this, MREIT data for each component must be collected. In other words, created B_x , B_y and B_z images must be given to simulator as magnetic flux density distribution caused by injected currents, and phase images must be obtained before. When the current-free phase image is subtracted from phase images, each component of \vec{B} can be calculated.

The inputs of this tab are:

- Load Data With Current For Bx: Loads the folder including B_x distribution as the additive magnetic field,
- Load Data With Current For By: Loads the folder including B_y distribution as the additive magnetic field,
- Load Data With Current For Bz: Loads the folder including B_z distribution as the additive magnetic field,
- Load Data Without Current : Loads the folder including current free data,
- Save B and J: Saves reconstructed components of \vec{B} and \vec{J} and the derivatives of \vec{B} with respect to each component to be used in various reconstruction algorithms in the future,
- Load B and J Files: Loads the previously calculated and saved \vec{B} and \vec{J} parameters. In this part each parameter can be shown in desired colormap and with colorbar.

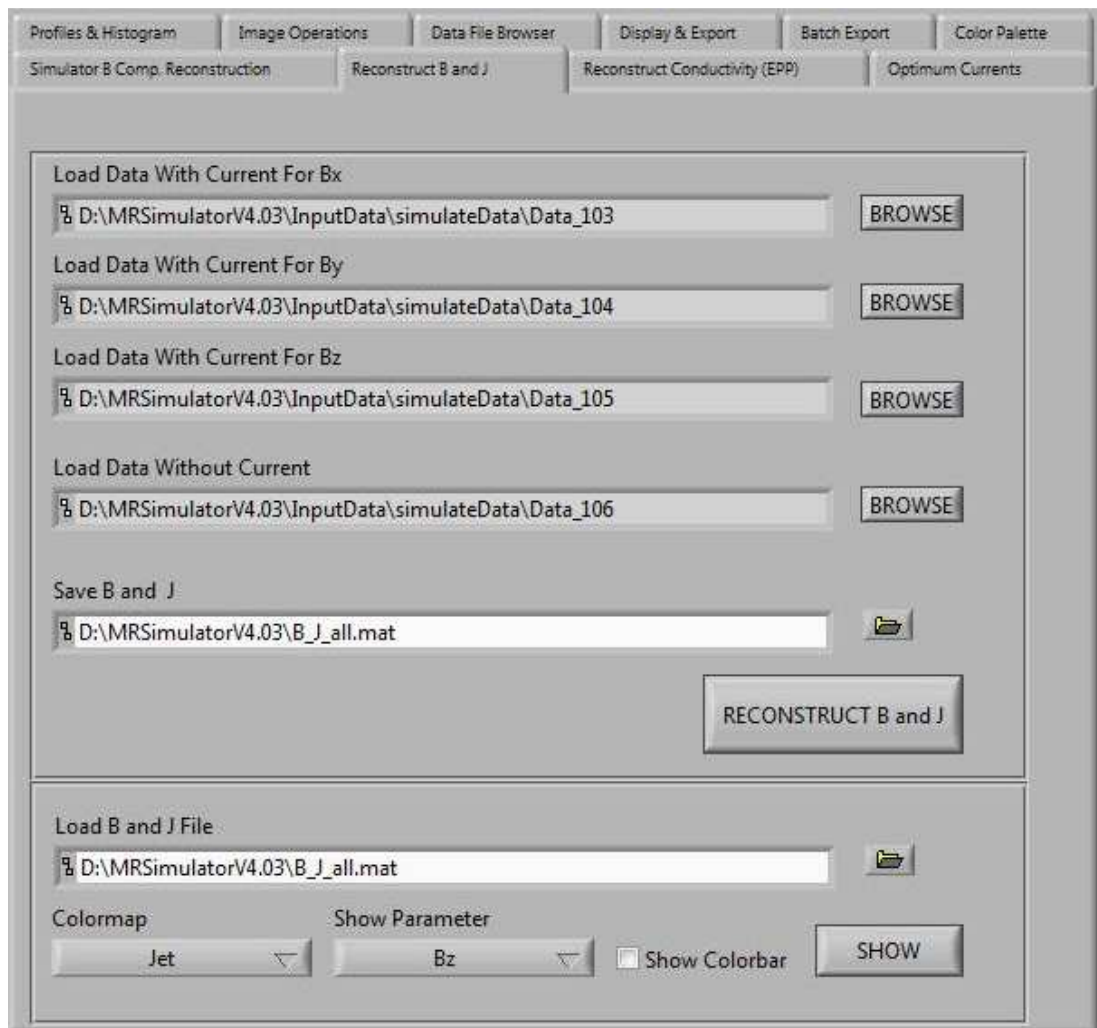


Figure 3.17 - "Reconstruct B and J" tab.

In "Reconstruct Conductivity (EPP)" tab, necessary inputs (J_x , J_y and potential distribution) for EPP algorithm are loaded. EPP algorithm can be run by using different current patterns such as horizontal, vertical or diagonal. In this part, user is allowed to load at most four different current patterns to reconstruct conductivity. The inputs to achieve these are:

- Load File For J_x , J_y , Potential 1 : Loads J_x , J_y and potential distribution obtained by "Reconstruct B and J" tab for the first current injection pattern,

- Load File For J_x , J_y , Potential 2 : Loads J_x , J_y and potential distribution obtained by "Reconstruct B and J" tab for the second current injection pattern,
- Load File For J_x , J_y , Potential 3 : Loads J_x , J_y and potential distribution obtained by "Reconstruct B and J" tab for the third current injection pattern,
- Load File For J_x , J_y , Potential 4 : Loads J_x , J_y and potential distribution obtained by "Reconstruct B and J" tab for the fourth current injection pattern,
- Save Reconstructed Conductivity : Saves the conductivity distribution that is reconstructed in this tab.

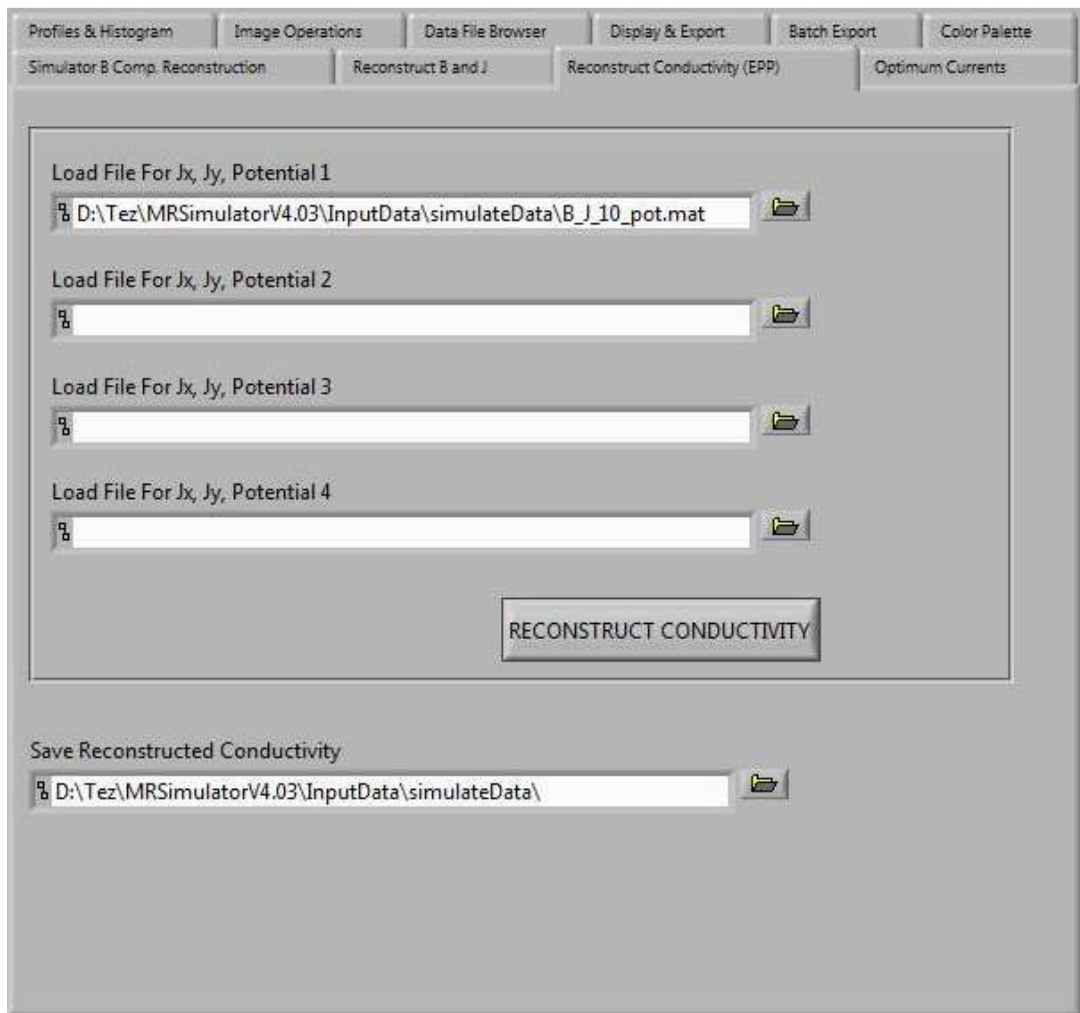


Figure 3.18 - "Reconstruct Conductivity (EPP)" tab.

"Optimum Currents" is the tab where the regional MREIT reconstruction is realized. The model parameters are inserted by the user and software applies proper current injections for the model and reconstructs conductivity distribution using regional reconstruction approach.

The inputs of "Optimum Currents" tab are listed and expressed below:

- Model : Model type to be reconstructed,
- Image Size: Pixel number of a square image in one direction,
- Conductivity Values: Conductivity of each inhomogeneity,
- Add Noise/SNR: Noise level of the system.
- Simulation Type: determines simulation type. If "direct" is chosen, conductivity is reconstructed using only current information obtained in forward solver part. If "MREIT" is chosen, conductivity is reconstructed using MREIT procedure,
- Colormap : The colormap to image the reconstructed signal is chosen,
- Show Colorbar : Shows the colorbar if activated,
- Save Conductivity Distribution: Saves the obtained conductivity distribution to a file,
- Load Shepp -Logan Conductivity: Loads the conductivity information of Shepp-Logan model if the model is chosen as Shepp-Logan.

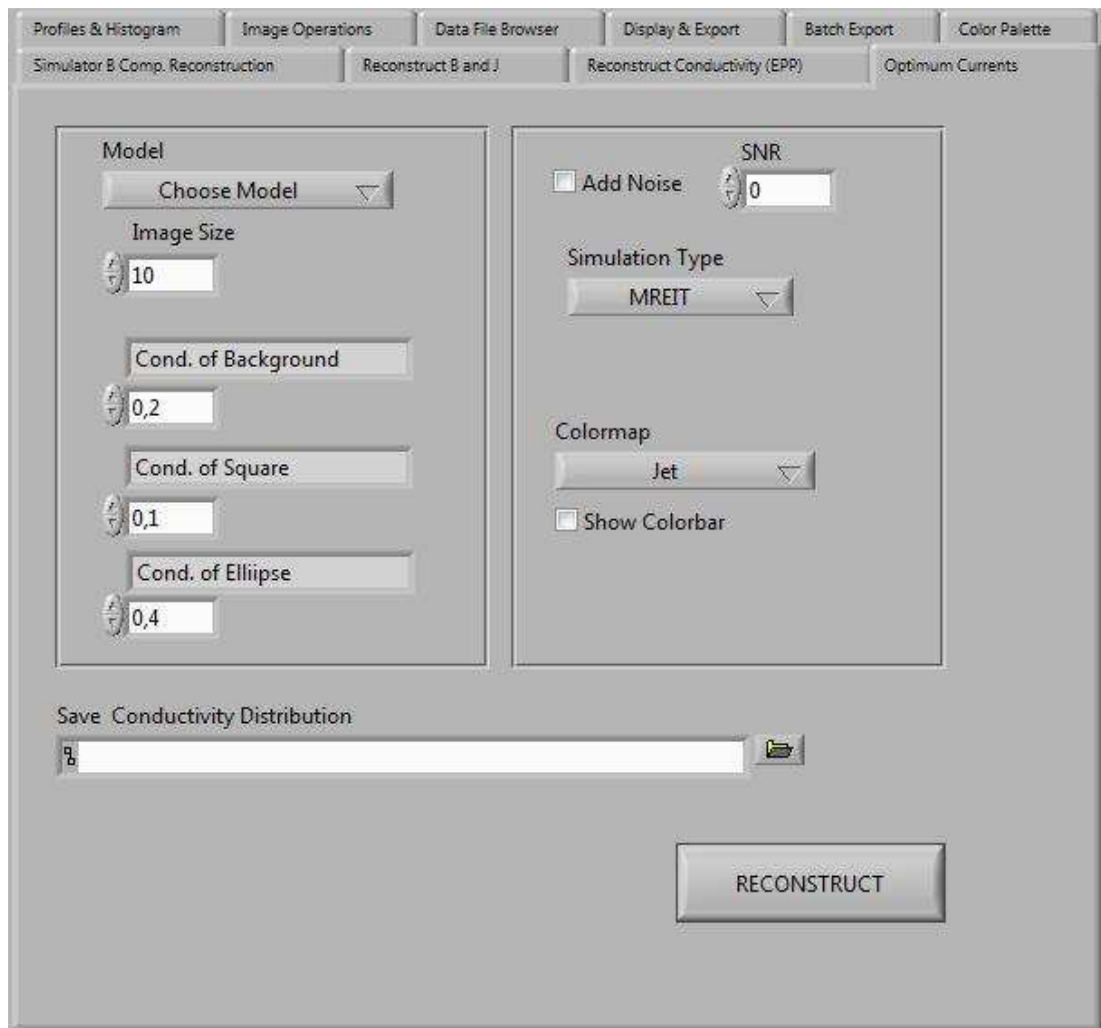


Figure 3.19 - "Optimum Currents" tab.

3.6 Models Designed For the Simulator

3.6.1 Square - Circle Model

Square - circle model is composed of two inhomogeneities inside a background. These are a square above and a circle below the square. The shape of the model can be seen on Figure 3.20.

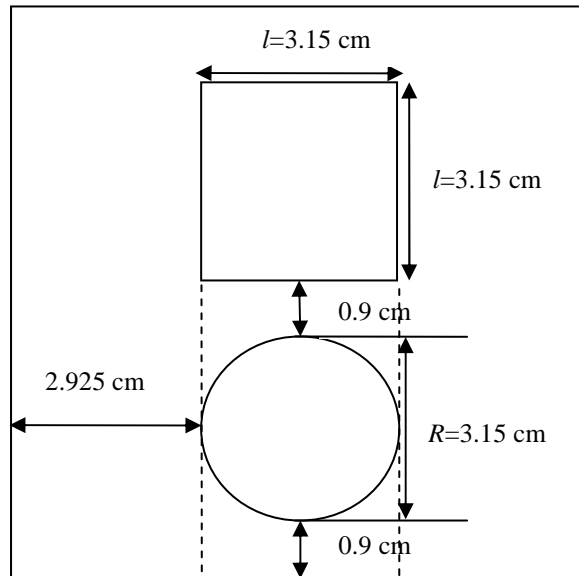


Figure 3.20 - Square -circle model.

Conductivity, T_1 , T_2 and spin density of each inhomogeneity is assigned by the user. The length of all sides at the outer region is 9 cm. This value is chosen to be consistent with the previous studies.

Each edge of the square inside the background has a length of 3.15 cm. Circle has a diameter of 3.15 cm. The centers of both square and circle are in the same vertical line which is passing through the center of the model.

3.6.2 Diagonal Squares Model

Diagonal squares model includes diagonally placed nine small squares. Each square has an edge length of 0.45 cm. The distance between two sequential squares is 0.45 cm along both horizontal and vertical axis. The model is shown on Figure 3.21.

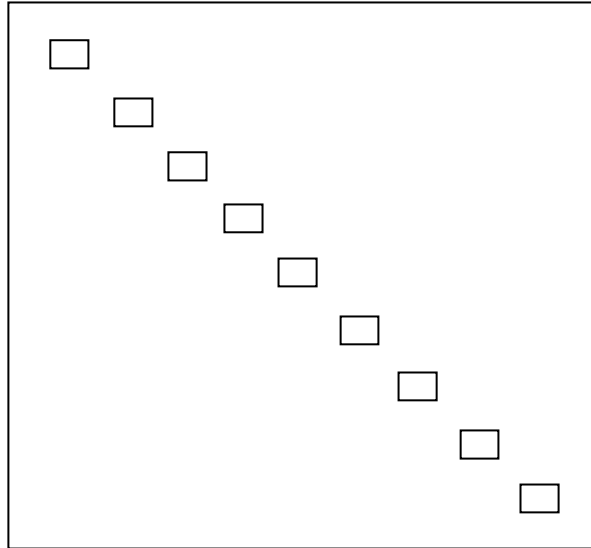


Figure 3.21 - Diagonal squares model

The conductivity, T_1 , T_2 and spin density values of all squares are the same. Each parameter of the squares and the background is assigned by the user. In order to use this model, image size should be at least 40x40 pixels. Otherwise the geometry of the squares is distorted.

3.6.3 Impulsive Squares Model

Impulsive squares model is used to observe the output of the system for an impulsive inhomogeneity. The inhomogeneity is composed of background and two squares having a size of 0.225x0.225 cm. These symmetrically placed squares can be separated from each other in horizontal axis according to the user assignment.

This model can be seen on Figure 3.22.

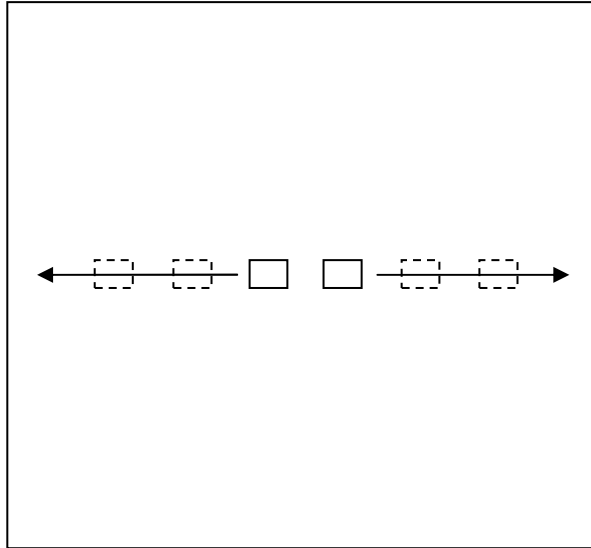


Figure 3.22 - Impulsive squares model.

The difference between the squares is in terms of square size. User can select gap length starting from 1 to 37 squares.

3.6.4 Shepp - Logan Model

The Shepp - Logan phantom is also included in the simulator. Although Shepp - Logan phantom is widely used in tomographic imaging, the parameters can be adjusted suitably for MRI and MREIT simulations. Different from the previous models, Shepp- Logan is an elliptic phantom. In the simulator, current is carried from the electrodes on the image boundary to the Shepp- Logan model using current canals as shown in Figure 3.22. These canals have the same conductivity value with the first (outer) region of the model.

Shepp - Logan has ten regions in itself. Each has an independent value of conductivity, T_1 , T_2 and spin density. User assigns the parameters of each region.

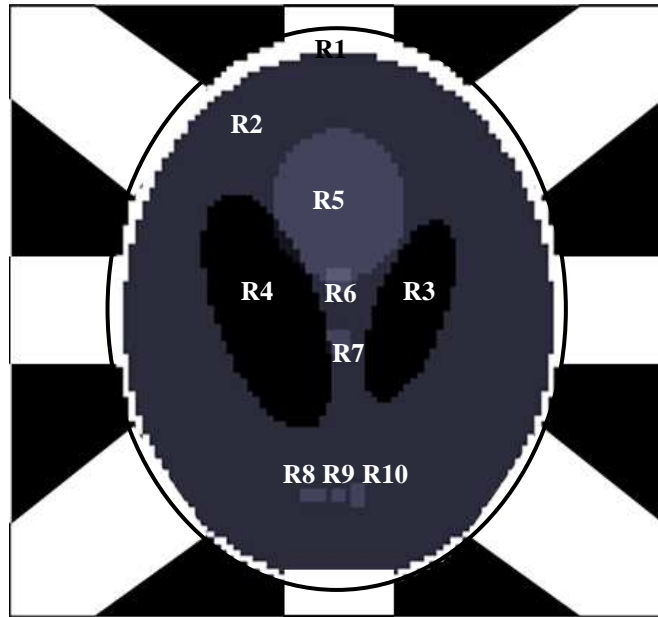


Figure 3.23 - Shepp-Logan model.

Conductivity value and MR parameters of a Shepp-Logan model are saved as matrices in different files. These data can be loaded on the user window when needed. Region division of Shepp-Logan is as shown in Figure 3.23, the matrix including the MR parameters has the size of 10x3 and the conductivity vector has the size of 10x1.

Conductivity value of each region is the summation of the previous regions lying below that region. For example, if the user assigns the conductivity vector as shown in equation (3.7), then the region values are constructed as shown in Table 3.3.

$$\sigma = \begin{bmatrix} 0.06 \\ 0.12 \\ 0.05 \\ 0.05 \\ -0.05 \\ 0.05 \\ 0.05 \\ 0.05 \\ 0.1 \\ -0.05 \end{bmatrix} \quad (3.7)$$

Table 3.3 - Conductivity values created using the conductivity vector shown in equation (3.7)

	R1	R2	R3	R4	R5	R6	R7	R8	R9	R10
$\sigma(\text{S/m})$	0.06	0.18	0.23	0.23	0.13	0.23	0.23	0.23	0.28	0.13

3.6.5 Electrode Configurations of the Models

There are eight electrodes on the surface of each model. Two of them are on the vertical edges, two are on horizontal edges and remaining four electrodes are on the corners. The configuration of the electrodes is shown in Figure 3.24. Any current density value can be assigned by the user to any of these electrodes.

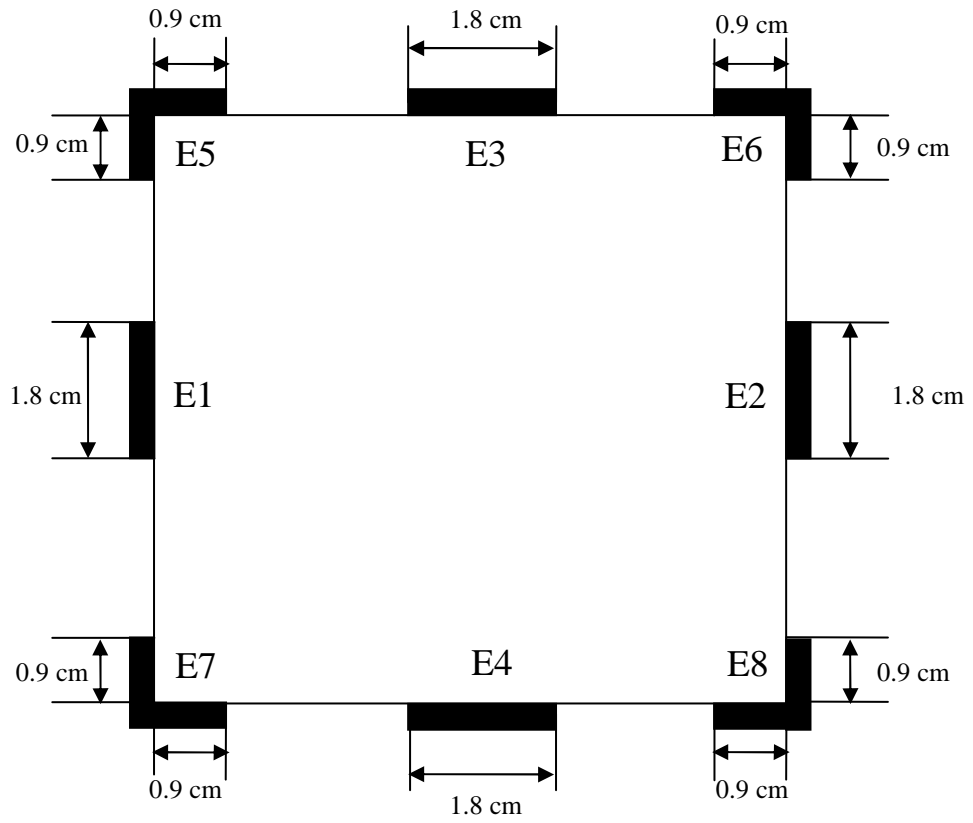


Figure 3.24 - Electrode configuration with their names and sizes.

CHAPTER 4

RESULTS

4.1 Forward Problem Solution Results

In this section, the results obtained while solving the forward problem of MREIT will be given. First, all of the models will be introduced and then the results acquired using these models will be shown.

4.1.1 Models Created by the Simulator

The four models expressed in chapter 3 are generated by the simulator having the sizes of 40-by-40. The results are obtained using these models.

As explained in chapter 3, conductivity, T_1 , T_2 and spin density values of each inhomogeneity can be assigned by the user independently.

The four models which are used in the simulator are given in Figure 4.1.

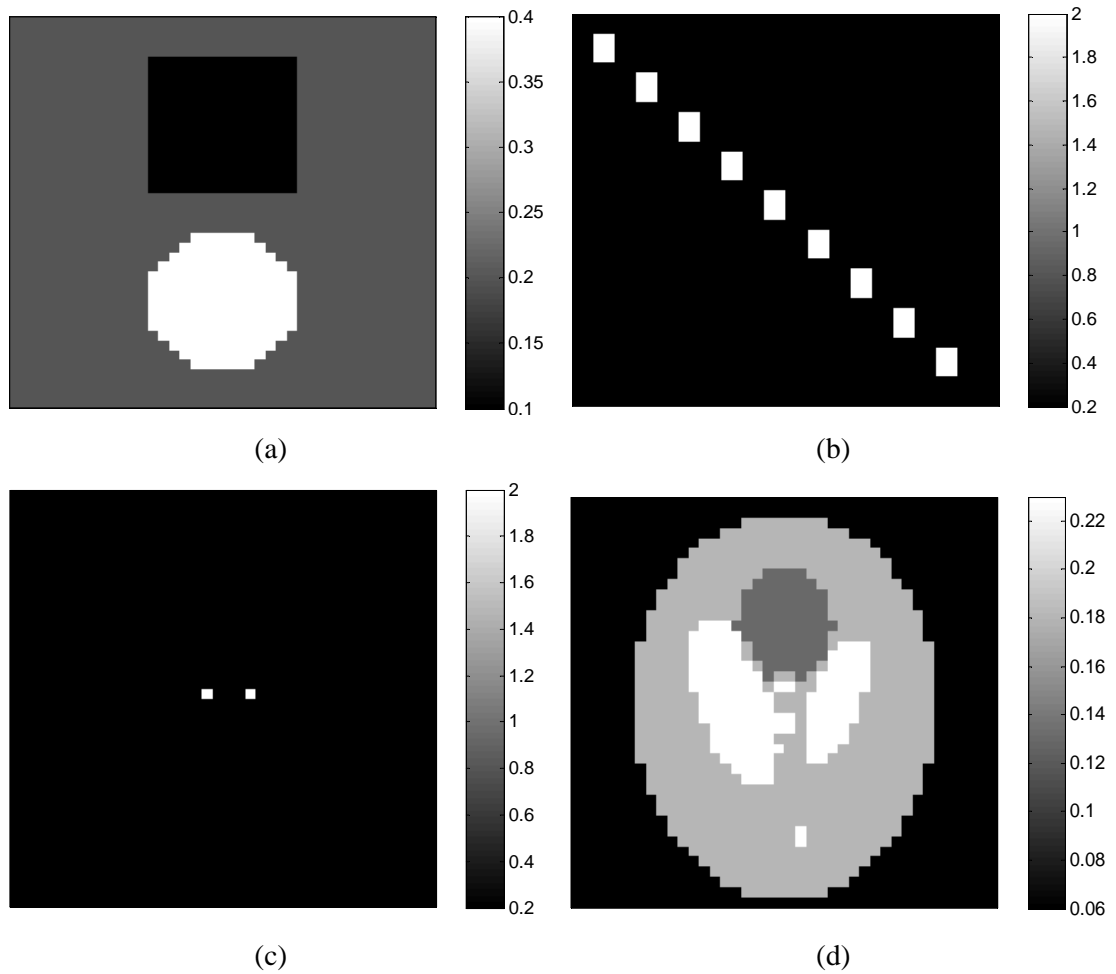


Figure 4.1 - Models used in the simulator. (a) Square - circle model, (b) diagonal squares model, (c) impulsive squares model, (d) Shepp-Logan model.

4.1.2 Potential, Current Density and Magnetic Flux Density Results

Potential distribution of an object is extracted from a forward solver in the same size with the object, and the current density components are calculated using equations (3.3) and (3.4). After obtaining current density components, magnetic flux density distributions are found using Biot-Savart law as shown in equation (2.33). Conversely, the current density distributions are calculated by using the derivatives of magnetic flux density in equation (2.32). Comparison of current density distribution calculated using equations (3.3), (3.4) and (2.33) shows the accuracy of forward problem solution part.

The results of forward problem solutions for square ellipse model and noise free case are given in this section.

Potential distribution and current density distribution for square circle model are shown in, where the conductivity of background is 0.2 S/m, conductivity of square is 0.1 S/m, and conductivity of circle is 0.4 S/m. The results are obtained using horizontal current injection pattern with the amplitude of 20mA.

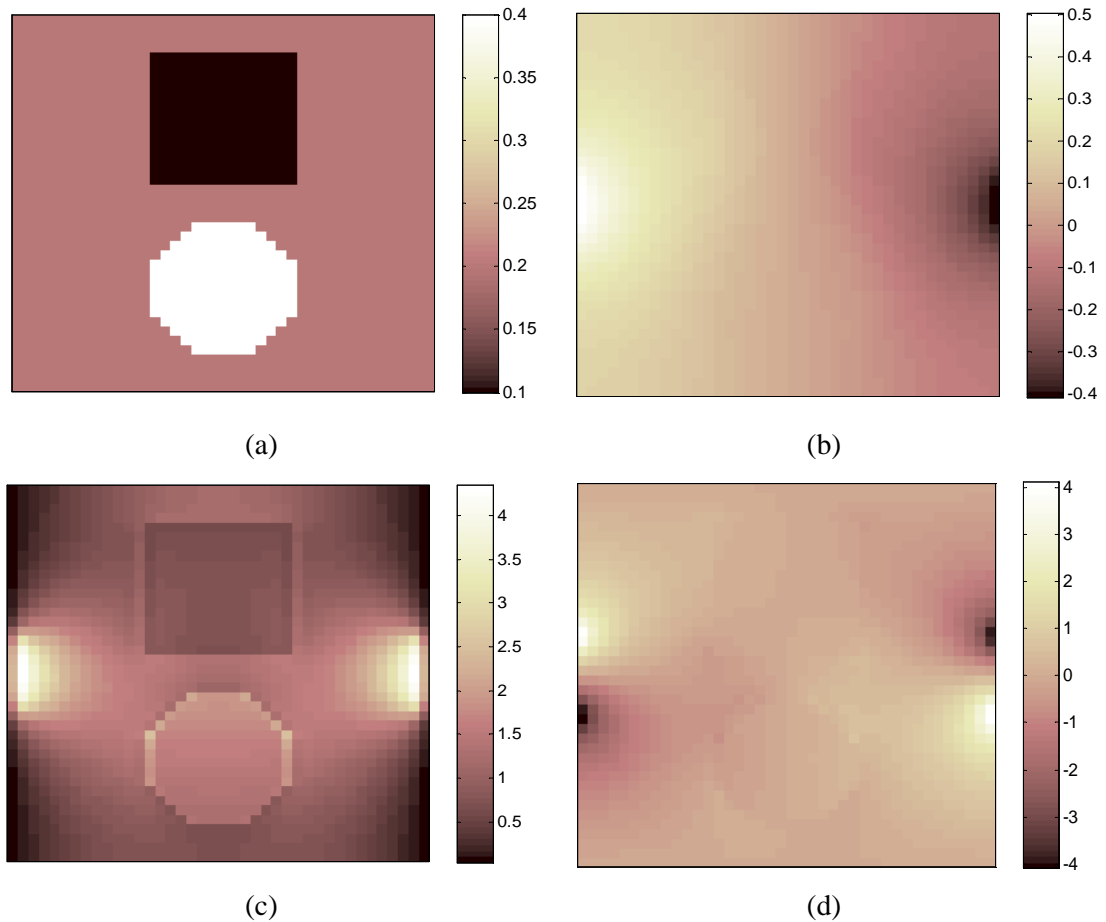


Figure 4.2 -Conductivity, potential and current density distributions of square circle model for 20mA current injection in horizontal axis and noise free case (a) conductivity distribution (S/m), (b) potential distribution (V), (c) x-component of J (J_x) (A/m^2), (d) y-component of J (J_y) (A/m^2).

As it is shown on Figure 4.2, potential and current density distributions are calculated as expected.

Using the current density distributions on Figure 4.2, magnetic flux density distributions are calculated using equation 2.33. The results of the calculations are shown in Figure 4.3.

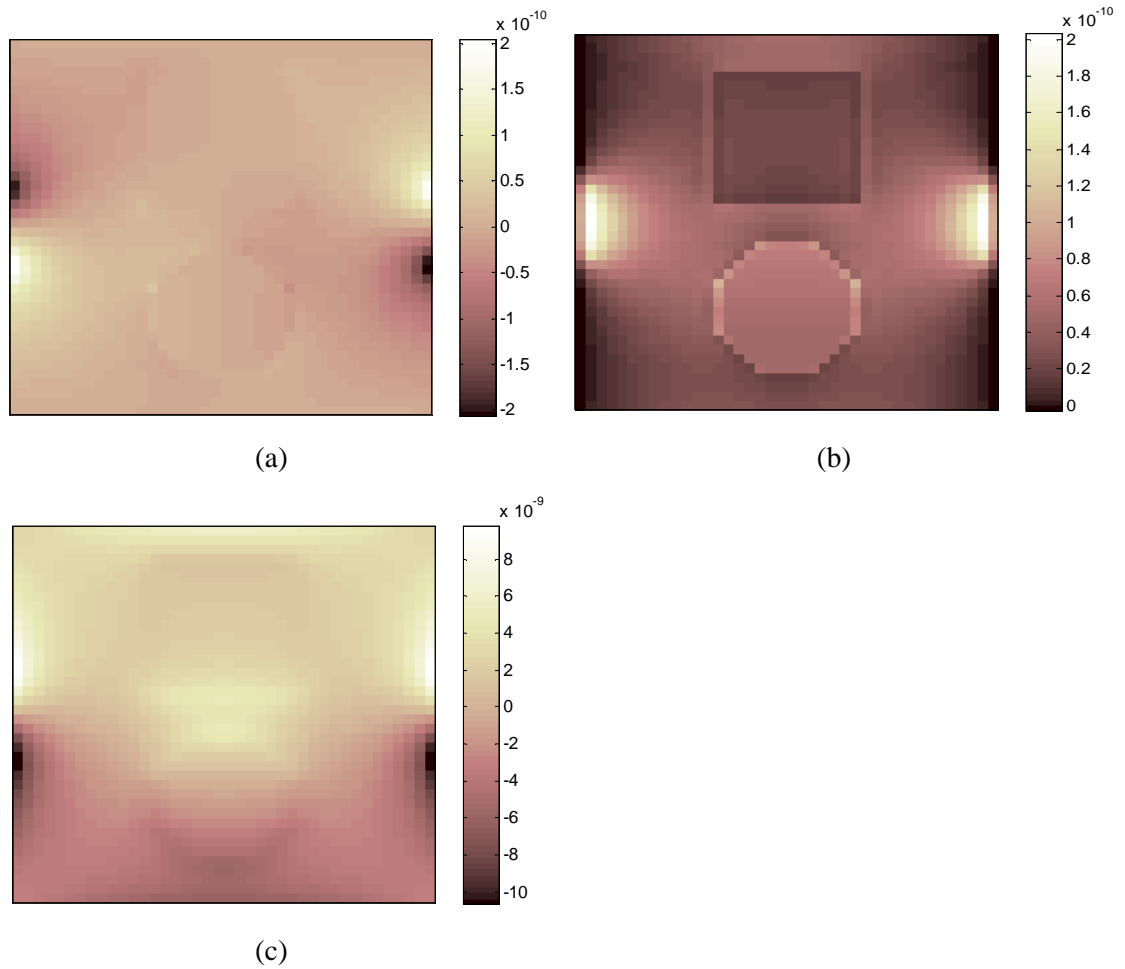


Figure 4.3 - x, y, z components of the magnetic flux density distribution for square circle model and noise free case. (a) B_x (T), (b) B_y (T), (c) B_z (T).

Derivatives of magnetic flux density components with respect to their orthogonal directions are calculated for square ellipse model are given in Figure 4.5.

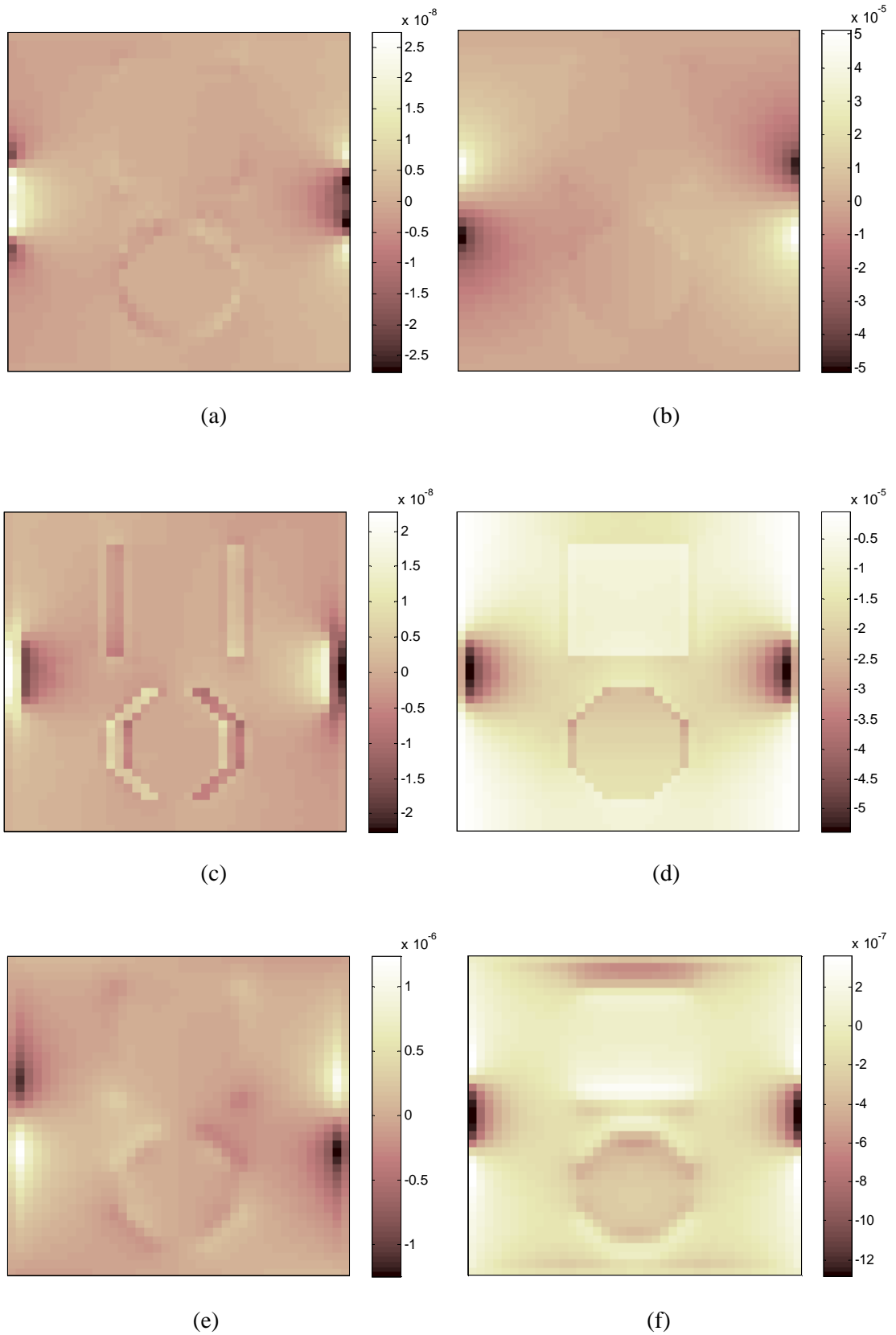


Figure 4.4 - Derivatives of B components shown in Figure 4.3 with respect to their orthogonal directions for square circle model and noise free case. (a) dB_x/d_y (T/m), (b) dB_x/d_z (T/m), (c) dB_y/d_x (T/m), (d) dB_y/d_z (T/m), (e) dB_z/d_x (T/m), (f) dB_z/d_y (T/m).

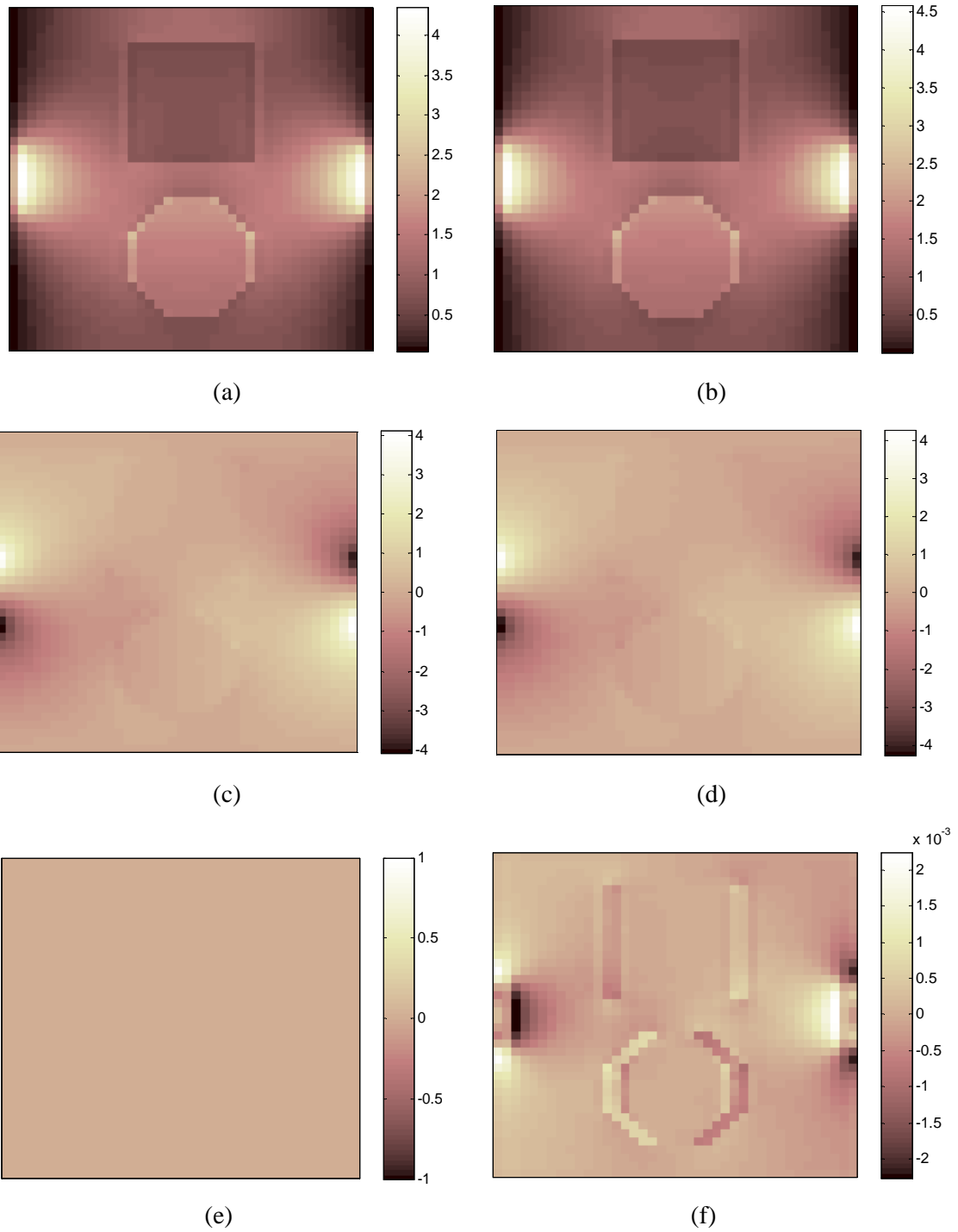


Figure 4.5 - Comparison of J components for square circle model obtained using equation (3.3), (3.4) and (3.6) for noise free case. (a) J_x (A/m^2) distribution obtained by using equation (3.3), (b) J_x (A/m^2) distribution obtained by using equation (3.6), (c) J_y (A/m^2) distribution obtained by using equation (3.4), (d) J_y (A/m^2) distribution obtained by using equation (3.6), (e) J_z (A/m^2) distribution which is equal to zero, (f) J_z (A/m^2) distribution obtained by using equation (3.6).

J_x , J_y and J_z can also be obtained using the derivatives shown in Figure 4.4. This inverse way indicates the accuracy of the calculation. As it is shown on Figure 4.5, the difference between J components calculated using equation (3.3) and equation (3.6) is perceptually low. The errors of J_x and J_y using equation (3.6) are 6.31% and 2.16% respectively.

These results show that the forward problem solution gives accurate results. Magnetic flux density distributions and current density distributions are obtained correctly to be used in the simulator.

4.2 Magnetic Resonance Imaging Results

In this section the results taken by the MRI part of the simulator will be given. The results will be shown using square circle model. T_1 values of square, circle and background are 1 s, T_2 values of square, circle and background are 0.2 s and spin density values of square, circle and background are 0.4, 1 and 0.5. T_R is chosen as 5 s and T_E is chosen as 5 ms. Thus, the reconstructed image is expected to be spin density weighted. Phase encoding and frequency encoding is made by 40 steps. Magnetic field strength is assigned as 0.15 T.

Spin density distribution of the model is shown in Figure 4.6.

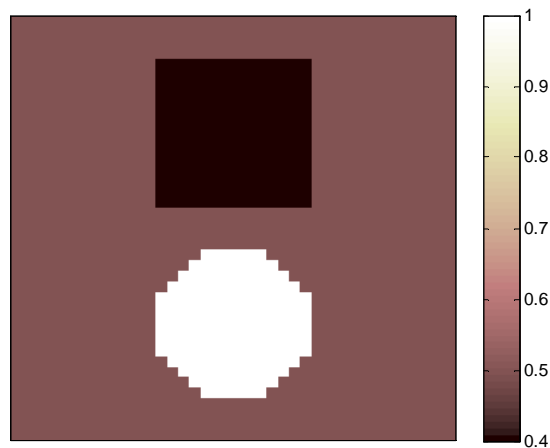


Figure 4.6 - Spin density distribution for square circle model (S/m).

Magnitude and phase images of acquired and reconstructed data are shown in Figure 4.7.

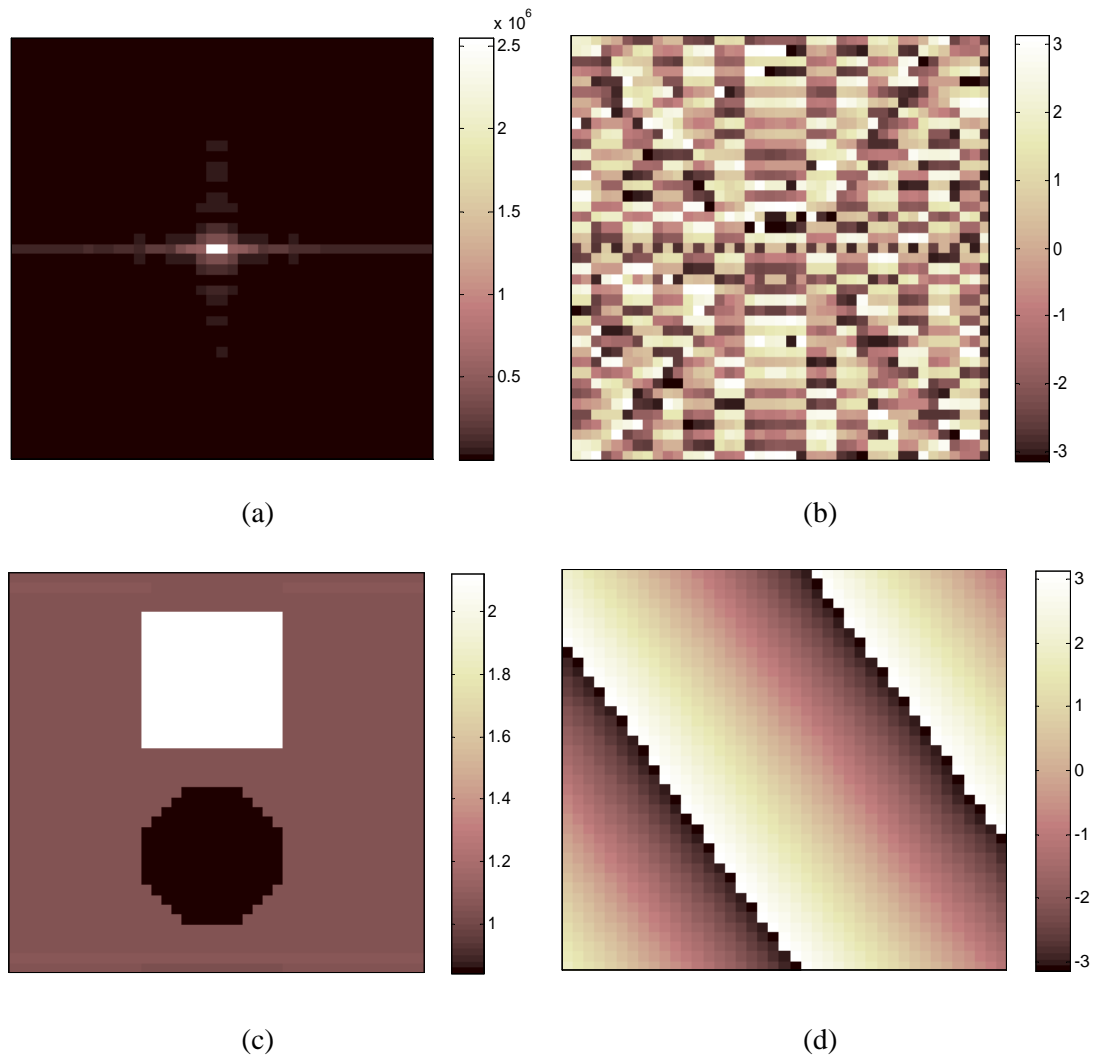


Figure 4.7 - Magnitude and phase images of acquired k-space data and reconstructed data for the model given in Figure 4.6. (a) Magnitude image of k-space data (cycles/m), (b) phase image of k-space data (rad), (c) magnitude image of the reconstructed data, (d) unwrapped phase image of the reconstructed image (rad).

The results are obtained as expected. Accuracy of phase image is crucial for MREIT. The results for MREIT application are shown in section 4.3.

4.3 Magnetic Resonance Electrical Impedance Tomography Results

Magnetic resonance electrical impedance tomography utilizes difference of MRI phase images with and without current injection. Scaling this difference with gyro magnetic constant and current injection duration gives the magnetic flux density component as shown in equation (2.31).

The effect of current is realized in the simulator by adding the magnetic flux density obtained in forward problem solution part to the main magnetic flux density. First data is acquired for constant main magnetic flux density component and the second one is acquired with additional magnetic flux density.

Unwrapped phase images obtained with and without current injection for the model shown in Figure 4.6 are given in

Figure 4.8.

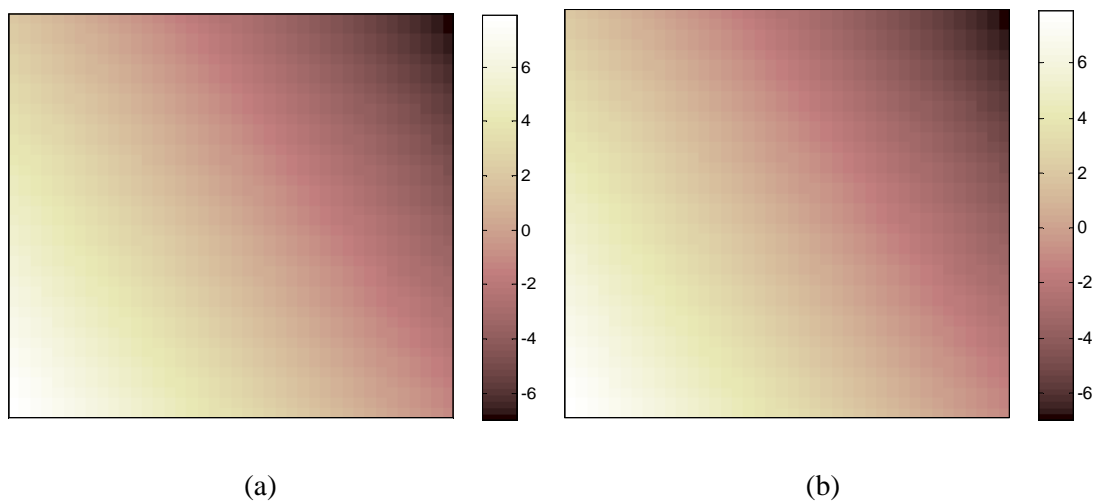


Figure 4.8 - Phase images for model in Figure 4.6 obtained using and without using 20 mA horizontal current injection. (a) Phase image for current-free case, (b) phase image with current application.

The magnetic flux density for current injection, which is given to MREIT simulator as input, and resultant magnetic flux density distribution which is obtained by subtracting phase images, are given in Figure 4.9. The percentage error is calculated as 0.80 %.

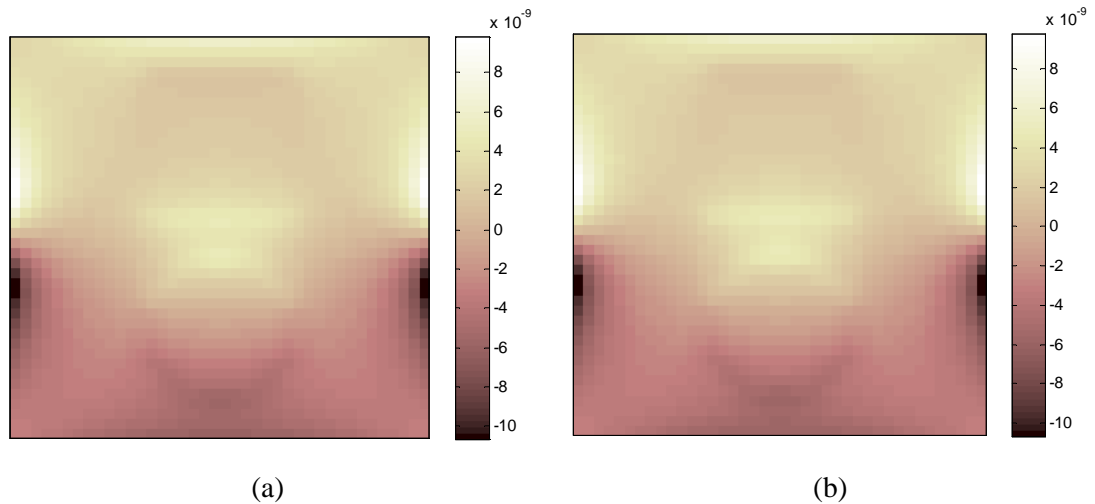


Figure 4.9 - Magnetic flux density obtained by forward solver and obtained by subtracting and scaling phase images with and without current. (a) Magnetic flux density (T) which is given as input to MREIT simulator, (b) magnetic flux density (T) taken as output of the MREIT simulator.

In the MREIT part of the simulator, all magnetic flux density and current density components and potential distribution can be saved by the user. Components of magnetic flux density are obtained as expressed, and current density information is calculated using equation (3.6). Resultant magnetic flux density and current density information is prepared for various reconstruction algorithms. EPP algorithm is embedded into simulator.

4.4 MREIT Reconstruction Results

In this part of the simulator, EPP algorithm is used. This algorithm utilizes the potential distribution, x and y components of current density. The inputs for noise free case are given in Figure 4.10.

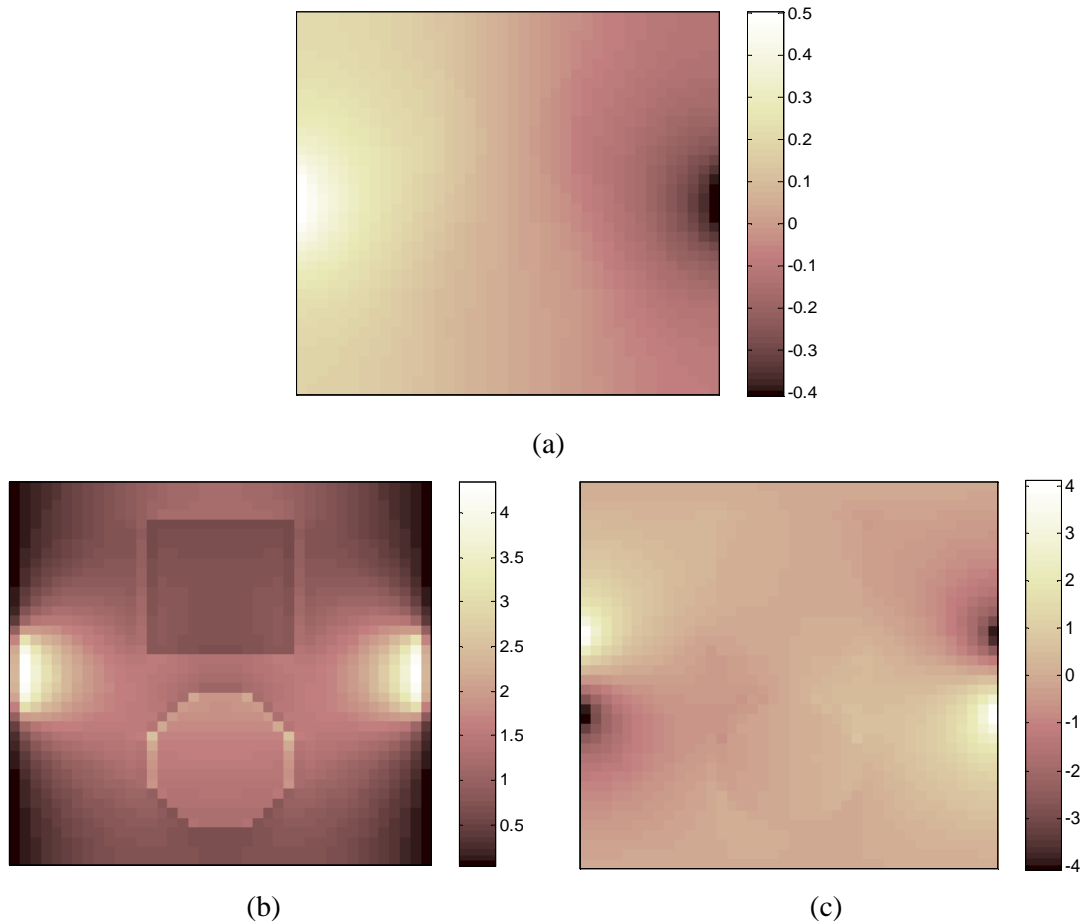


Figure 4.10 - Potential, J_x and J_y distributions given into reconstruction part of the simulator as input for horizontal current injection having the amplitude of 20mA. (a) Potential distribution (V), (b) J_x distribution (A/m^2), (c), J_y distribution (A/m^2).

The comparison of true conductivity and obtained conductivity is shown in Figure 4.11

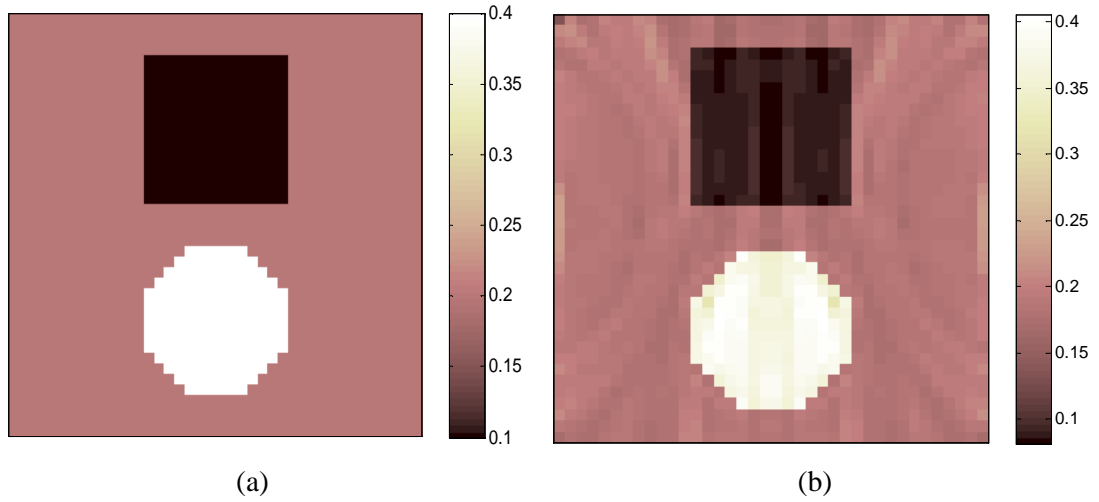


Figure 4.11 - True conductivity and reconstructed conductivity using EPP algorithm for horizontal current injection pattern. (a) True conductivity (S/m), (b) reconstructed conductivity (S/m) using EPP algorithm.

Conductivities obtained by EPP algorithm for SNR 30 and SNR 13 are shown in Figure 4.12.

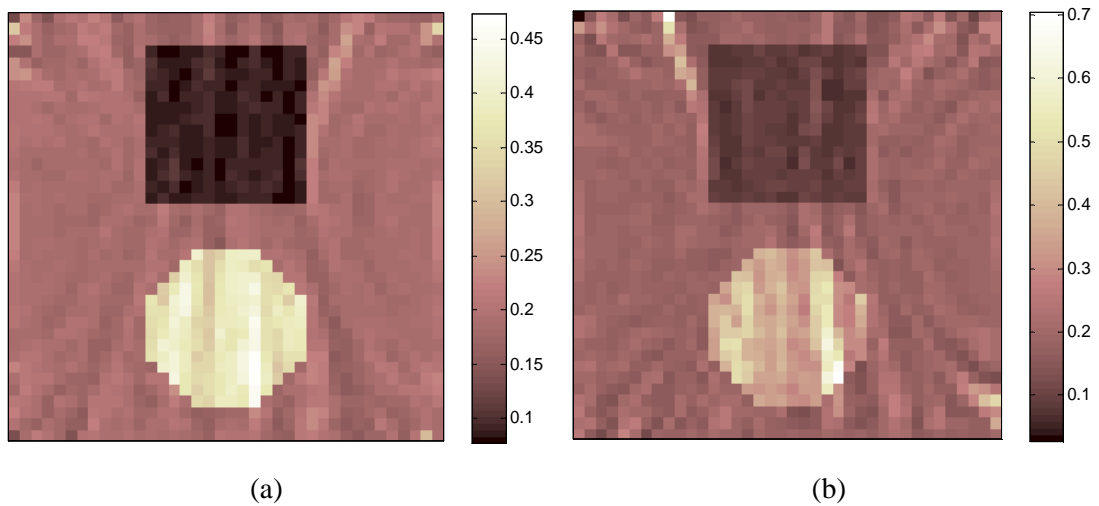


Figure 4.12 - Reconstruction results obtained using horizontal current injection pattern for SNR 30 and SNR 13. (a) Conductivity distribution (S/m) for SNR 30, (b) conductivity distribution for SNR 13 (S/m).

The results for square circle model with different current injection patterns for noise free case are given in Figure 4.13.

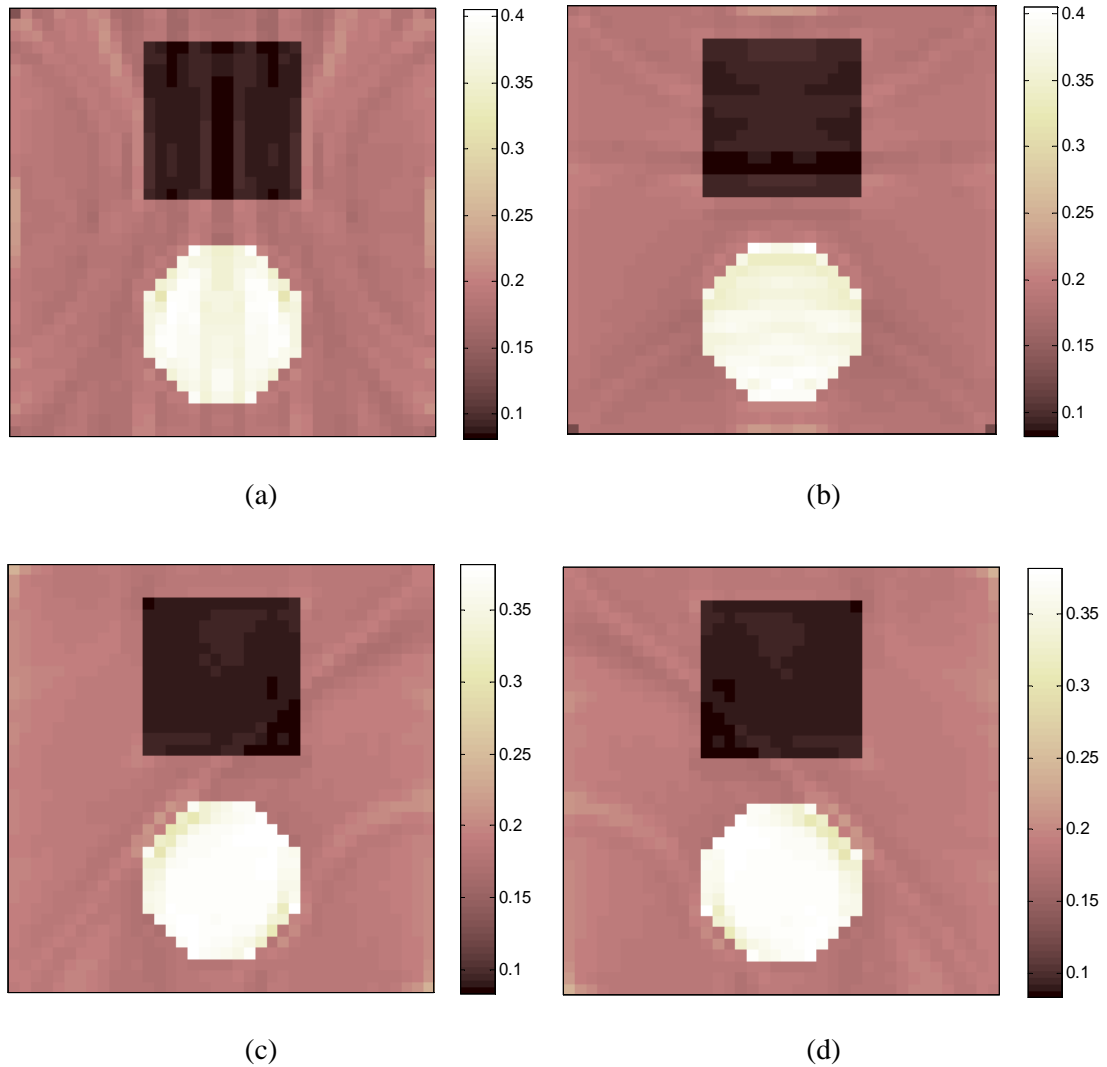
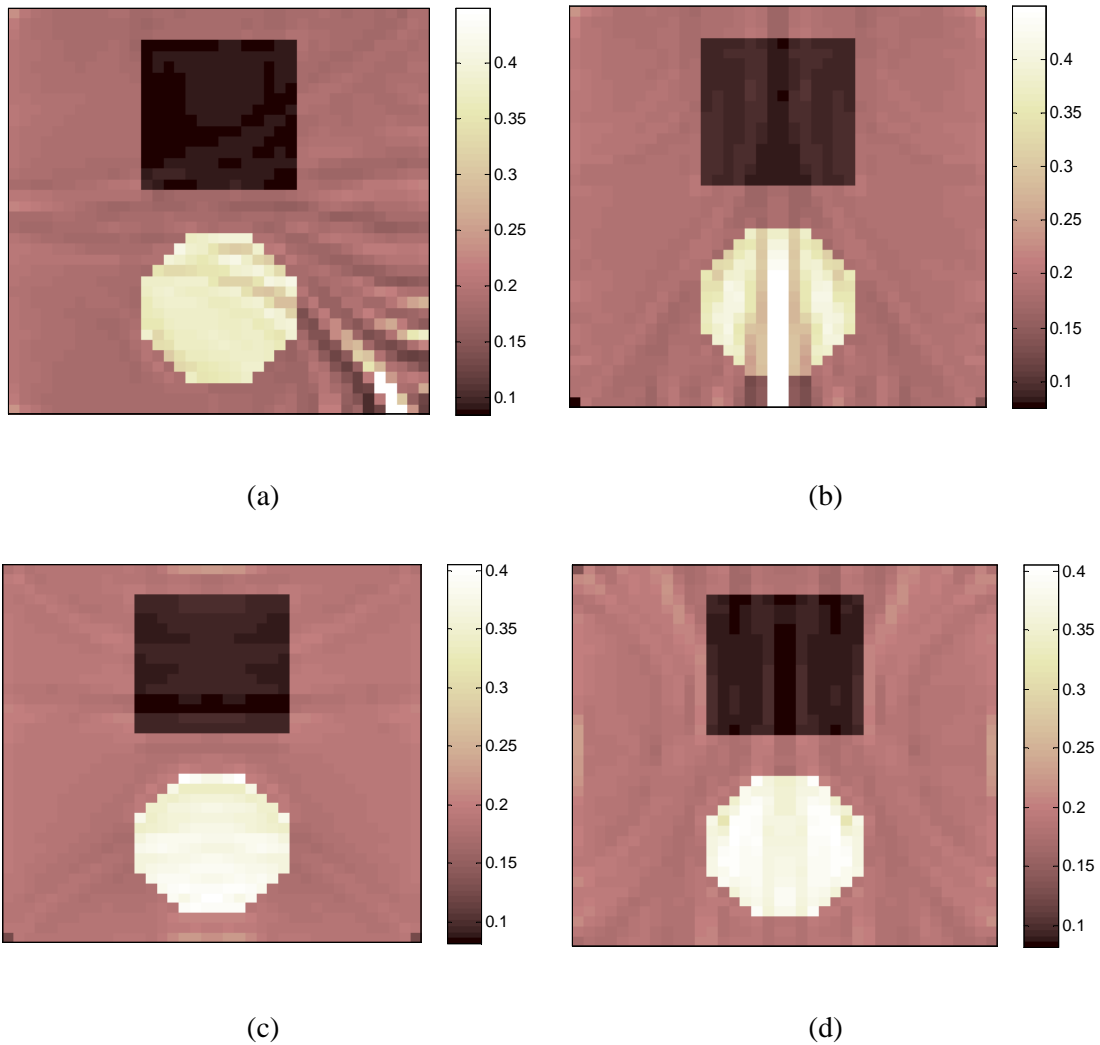


Figure 4.13 - Reconstructed conductivity results for various current injection patterns having the amplitude of 20mA and for noise free case. (a) Reconstructed conductivity (S/m) distribution for horizontal current injection pattern, (b) reconstructed conductivity (S/m) distribution for vertical current injection pattern, (c) reconstructed conductivity (S/m) distribution for diagonal (from top-left to bottom-right) current injection pattern, (d) reconstructed conductivity (S/m) distribution for diagonal (from top-right to bottom-left) current injection pattern.

4.5 Regional Magnetic Resonance Electrical Impedance Tomography Reconstruction

As explained in section 3.4.2, regional reconstruction is the approach that divides the field of view into sub-regions and utilizes the current injection patterns maximizing the accuracy of each region.

The current injection patterns for square models used in regional reconstruction are given in Figure 3.5. The results obtained by the simulator for each current injection pattern are given in Figure 4.14, where the conductivities of square, circle and background are 0.1 S/m, 0.4 S/m, and 0.2 S/m respectively.



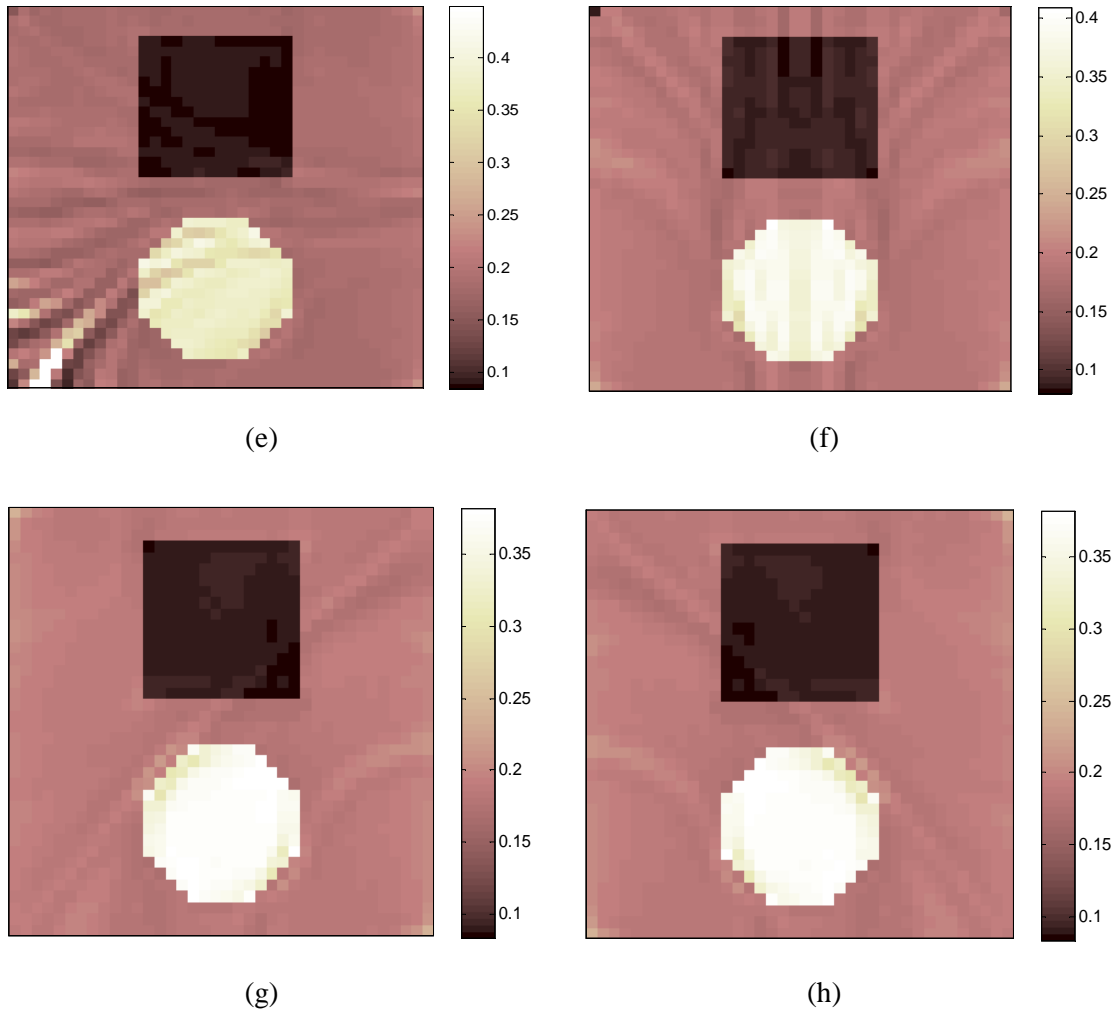


Figure 4.14 - Conductivity distributions for regional MREIT reconstruction part obtained by applying individual current patterns shown in Figure 3.5, where conductivities of square, circle and background are 0.1 S/m, 0.4 S/m, and 0.2 S/m respectively. (a) Reconstructed conductivity distribution (S/m) for Vertical 1 (V1) current pattern, (b) reconstructed conductivity distribution (S/m) for Horizontal 1 (H1) current pattern, (c) reconstructed conductivity distribution (S/m) for Vertical 2 (V2) current pattern, (d) reconstructed conductivity distribution (S/m) for Horizontal 2 (H2) current pattern, (e) reconstructed conductivity distribution (S/m) for Vertical 3 (V3) current pattern, (f) reconstructed conductivity distribution (S/m) for Horizontal 3 (H3) current pattern, (g) reconstructed conductivity distribution (S/m) for Diagonal 1 (D1) current pattern, (h) reconstructed conductivity distribution (S/m) for Diagonal 2 (D2) current pattern.

As it can be seen on Figure 4.14, if the current passing through a region is weak, the reconstruction for that region becomes inaccurate. The distortions on reconstructed images can be clearly seen on Figure 4.14 (a), (b) and (e). The regions further from electrodes are highly distorted. In addition to that, comparing (b) and (f)

perceptually, it can be said that, if the conductivity of the further region is high, it is much more affected from distortions.

In regional reconstruction algorithms these deformations are tried to be minimized.

Conductivity distribution obtained by using regional MREIT reconstruction for the current patterns and model shown in Figure 4.14 is given in Figure 4.15.

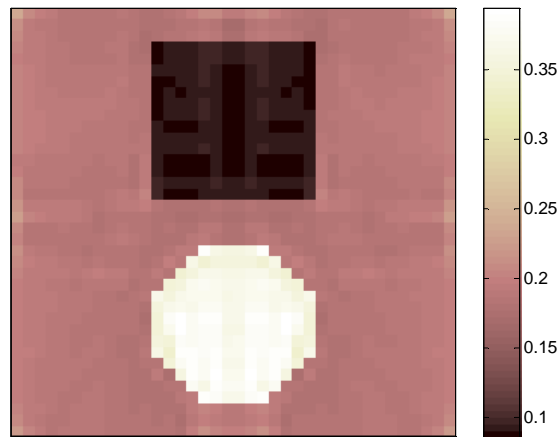


Figure 4.15 - Conductivity distribution obtained by regional MREIT reconstruction where conductivities of square, circle and background are 0.1 S/m, 0.4 S/m, and 0.2 S/m respectively.

Error comparison of conventional MREIT current patterns and regional MREIT reconstruction current patterns for square circle model shown in Figure 4.6 are given in Table 2.1. For multiple current injections, the average of individual reconstructed conductivities for given patterns is used.

Table 4.1 - Reconstruction errors calculated using various current injection pattern combinations shown in Figure 3.5 for square circle model and noise-free case.

Current Injection Pattern	Overall	Square	Circle	Background
H2	7.36 %	10.59 %	7.08 %	7.34 %
V2	7.39 %	7.97 %	8.03 %	6.97 %
D1	8.02 %	8.93 %	9.61 %	6.91 %
D2	8.03 %	8.93 %	9.59 %	6.90 %
H2, V2	6.87 %	8.70 %	7.12 %	6.62 %
D1, D2	7.57 %	8.80 %	9.05 %	6.51 %
H2, V2, D1	6.95 %	8.65 %	7.72 %	6.39 %
H2, V2, D2	6.96 %	8.65 %	7.70 %	6.40 %
H2, V2, D1, D2	6.99 %	8.64 %	7.94 %	6.30 %
Regional Recons.	7.06 %	8.15 %	8.02 %	6.39 %

Table 4.2 - Reconstruction errors calculated using various current injection pattern combinations shown in Figure 3.5 for square circle model and SNR 30.

Current Injection Pattern	Overall	Square	Circle	Background
H2	10.33 %	11.72 %	10.53 %	10.14 %
V2	8.83 %	8.65 %	8.99 %	8.75 %
D1	8.33 %	9.24 %	9.92 %	7.21 %
D2	8.23 %	9.12 %	9.74 %	7.18 %
H2, V2	8.10 %	9.28 %	8.50 %	7.81 %
D1, D2	7.65 %	8.96 %	9.05 %	6.65 %
H2, V2, D1	7.49 %	9.01 %	8.37 %	6.85 %
H2, V2, D2	7.51 %	8.97 %	8.27 %	6.92 %
H2, V2, D1, D2	7.26 %	8.88 %	8.26 %	6.54 %
Regional Recons.	7.22 %	8.31 %	8.29 %	6.48 %

Table 4.3 - Reconstruction errors calculated using various current injection pattern combinations shown in Figure 3.5 for square circle model and SNR 13.

Current Injection Pattern	Overall	Square	Circle	Background
H2	20.14 %	17.21 %	21.31 %	19.57 %
V2	23.92 %	11.98 %	11.20 %	29.10 %
D1	9.55 %	10.18 %	10.71 %	8.79 %
D2	9.69 %	10.23 %	10.49 %	9.21 %
H2, V2	16.33 %	11.70 %	12.80 %	18.21 %
D1, D2	8.44 %	9.53 %	9.54 %	7.69 %
H2, V2, D1	12.01 %	10.08 %	10.43 %	12.91 %
H2, V2, D2	12.09 %	10.29 %	10.30 %	13.07 %
H2, V2, D1, D2	10.15 %	9.60 %	9.42 %	10.56 %
Regional Recons.	7.57 %	8.67 %	8.34 %	7.03 %

The error tables show that, for noise free case some current injection patterns may give better results for each inhomogeneity compared to regional reconstruction. But even for this case the errors are very close to regional reconstruction application. Looking at Table 4.2 and Table 4.3, it is seen that regional reconstruction gives more accurate results for each inhomogeneity as noise level increases. Reconstruction errors for diagonal current injection patterns are relatively low. That occurs depending on the model geometry. For diagonal current patterns, large amount of current passes through background instead of circle and square. Since the number of background pixels (1092 pixels) are much more than square and circle pixels (196 and 156 pixels respectively), overall and background errors are lower compared to other current injection patterns. In addition to those, conventional reconstruction for overall and each inhomogeneity is much affected by the noise whereas regional reconstruction is slightly affected.

The conductivity distributions for Shepp-Logan model are also obtained by using regional reconstruction algorithm for different noise levels. These results are compared to the conductivity distributions which are calculated by using individual current injection patterns. The utilized current injection patterns are the same with the case that is shown in Figure 4.14. The Shepp-Logan model used in this study is given in Figure 4.16, and the results for each individual current injection pattern are shown in Figure 4.17. The results are similar with the square – circle model case. Same with the square – circle case, in addition to regional reconstruction, errors for different current injection combinations are calculated and given in Table 4.4 for different noise levels.

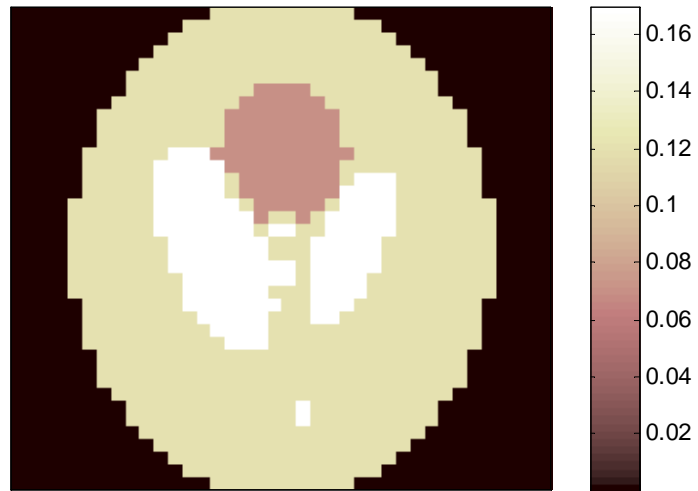
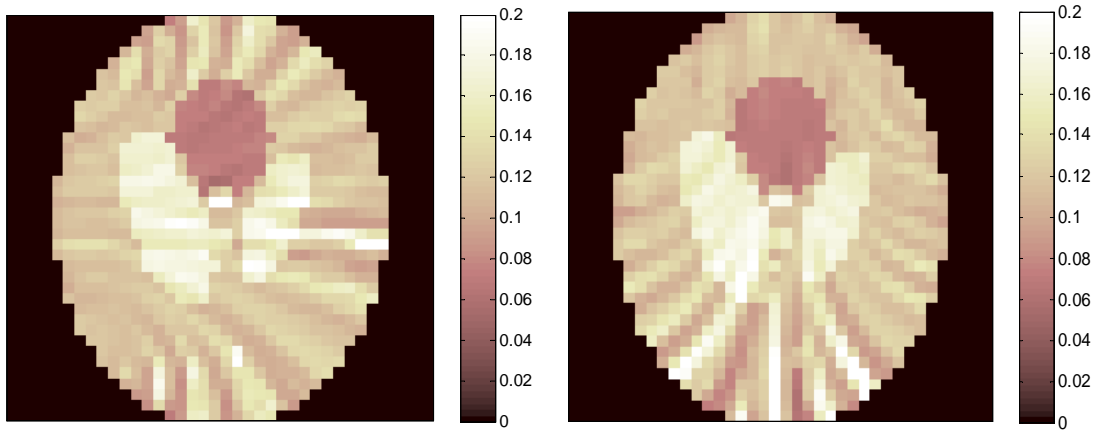
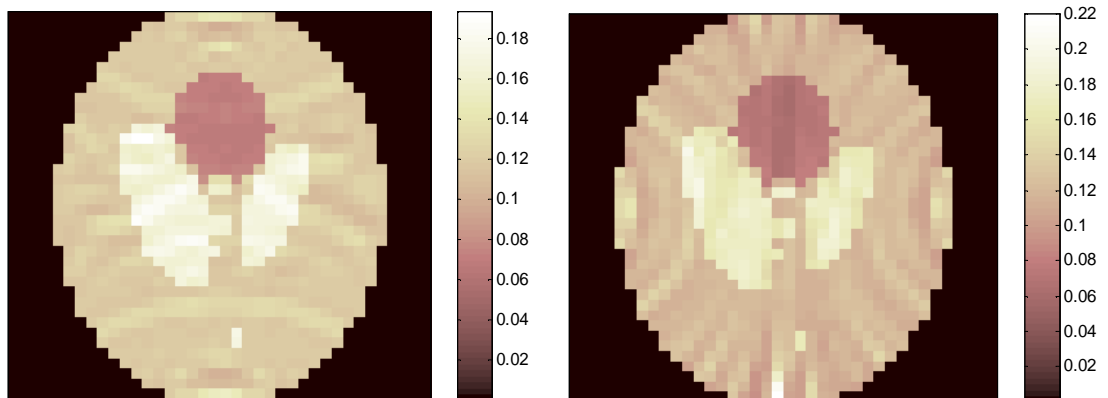


Figure 4.16 - Shepp - Logan model used for comparison of regional reconstruction and conventional reconstruction techniques.



(a)

(b)



(c)

(d)

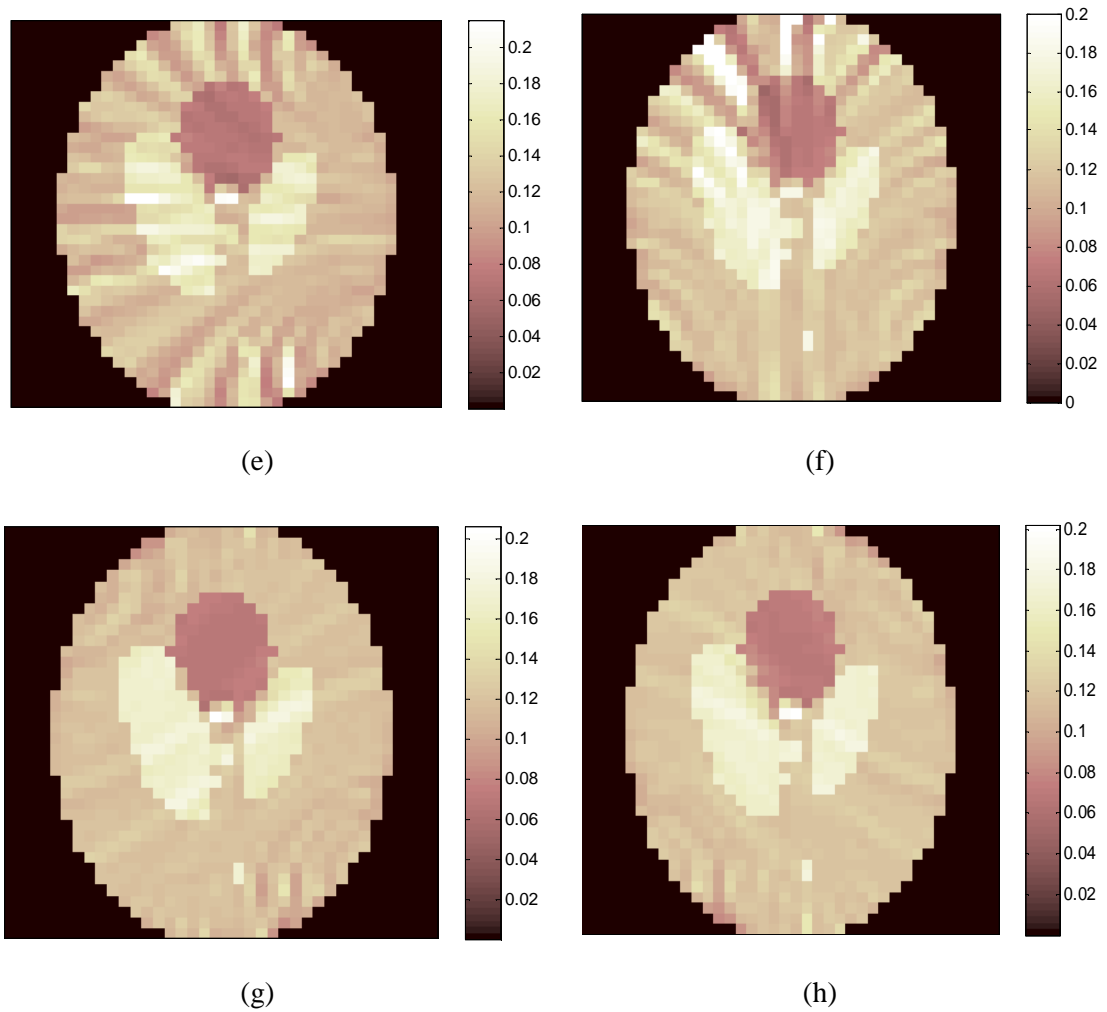


Figure 4.17 - Conductivity distributions for regional MREIT reconstruction part obtained by applying individual current patterns shown in Figure 3.5, where conductivity distribution of the model is as shown in Figure 4.16. (a) Reconstructed conductivity distribution (S/m) for Vertical 1 (V1) current pattern, (b) reconstructed conductivity distribution (S/m) for Horizontal 1 (H1) current pattern, (c) reconstructed conductivity distribution (S/m) for Vertical 2 (V2) current pattern, (d) reconstructed conductivity distribution (S/m) for Horizontal 2 (H2) current pattern, (e) reconstructed conductivity distribution (S/m) for Vertical 3 (V3) current pattern, (f) reconstructed conductivity distribution (S/m) for Horizontal 3 (H3) current pattern, (g) reconstructed conductivity distribution (S/m) for Diagonal 1 (D1) current pattern, (h) reconstructed conductivity distribution (S/m) for Diagonal 2 (D2) current pattern.

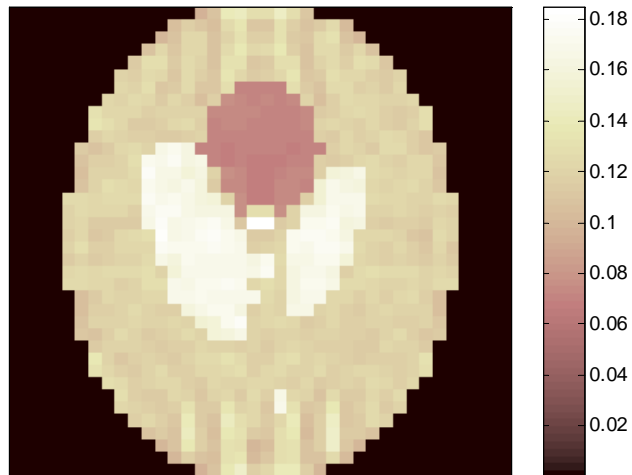


Figure 4.18 - Conductivity distribution obtained by regional MREIT reconstruction where conductivity distribution of the Shepp - Logan phantom is as shown in Figure 4.16.

Table 4.4 - Reconstruction errors calculated using various current injection pattern combinations shown in Figure 3.5 for Shepp - Logan model.

Current Injection Pattern	Noise-free	SNR 30	SNR 13
H2	8.34 %	17.22 %	46.67 %
V2	5.29 %	13.71 %	29.03 %
D1	5.52 %	14.38 %	37.25 %
D2	5.53%	14.37 %	40.91 %
H2, V2	4.99 %	10.69 %	30.03 %
D1, D2	4.07 %	7.45 %	29.65 %
H2, V2, D1	3.93 %	6.38 %	13.18 %
H2, V2, D2	3.85 %	6.33 %	20.70 %
H2, V2, D1, D2	3.34 %	5.00 %	17.36 %
Regional Recons.	6.24 %	7.02 %	9.30 %

As it is shown in Table 4.4, regional reconstruction technique gives better results as the noise level increases for Shepp - Logan model as well. The results are similar with the square - circle model examinations.

CHAPTER 5

CONCLUSIONS AND FUTURE WORK

5.1 Conclusions

In this thesis, a user friendly MREIT simulator is designed on LabVIEW environment, which is a graphical programming workbench. A software code had been implemented on LABVIEW for Middle East Technical University (METU) Electrical and Electronics Engineering Department MRI system control unit by M. Ozsut as his MSc thesis [1]. In addition to that, in this study, an MRI/MREIT simulator is integrated on this MRI control unit software, thus user is provided to use either MRI system or the designed simulator on the same panel.

Previously, an MRI simulator had been designed by E. Arpinar and H. Yigitler as parts of their PhD and MSc thesis respectively [11], [12]. Although the simulator was working properly, it was designed for restricted cases, providing the results for their thesis study. Namely, it was capable of simulating for fixed model geometry, fixed object size, fixed phase and frequency steps. In this thesis, that simulator is generalized for specific model geometries; user assigned object size, phase and frequency encoding steps. The simulator is also improved for solution of MREIT applications (data acquisition and reconstruction).

For MREIT applications, forward problem solver is implemented for the simulator. By this addition, user has the ability of creating desired current density distribution to be added to the simulator. After both MRI and current data is provided, magnetic

flux density and current density data are calculated. These data can be saved by the user for later studies.

As the last step of the MREIT procedure, conductivity is reconstructed using equipotential projection algorithm [20]. In addition to conventional reconstruction algorithm, regional reconstruction algorithm is also integrated into the simulator as well. All these steps for MREIT are combined on the graphical software designed on LabVIEW environment. The results for each part of the simulator are investigated individually. The results of the simulator are consistent with the expected results. Forward problem solution part is working with an average accuracy of 5%. That is crucial for providing current data to MREIT simulator correctly. In the MREIT part, magnetic flux density distribution taken from the forward solver part is added to the main magnetic flux density used in the MRI part. Consistency of the magnetic flux density distribution given to the simulator as input and the output taken from the MREIT part of the simulator indicates the accuracy of the MREIT part. The results show that, input and the output magnetic flux density distributions of this part are 99% consistent.

Using each component of magnetic flux density distributions, current density distributions are obtained and given to equipotential projection algorithm. Results are obtained for various current drives. Performances of current injection patterns vary depending on the model geometry and conductivity distribution. Averaging multiple current injection patterns improves the accuracy of the reconstruction. On the other hand, regional MREIT reconstruction procedure is also implemented and the results are obtained. These results show that, regional reconstruction approach gives better results than most of the current injection patterns for noise free case. When the noise is increased the benefit of the regional reconstruction becomes clearer. Using four different current drives for conventional reconstruction of Shepp – Logan model, the error of the reconstructed image is calculated as 17.36% for SNR 13. However, using regional image reconstruction algorithm, the error percentage is decreased to a value of 9.30%. Naturally regional reconstruction approach is not affected by the noise as much as conventional approach. Hence, for noisy cases this method gives the best results.

5.2 Future Works

In this thesis an MREIT simulator is designed for some model geometries. In the future it would be beneficial to add new model types the simulator for further studies. Regional reconstruction algorithm can be tested for various model types and different system parameters. Experimental data is very important to observe the performance of an algorithm; therefore it would be a good study if regional reconstruction algorithm is applied experimentally. Since the simulator is designed, the comparison of simulation data and experimental data will be easier.

REFERENCES

- [1] M. Özsüt, "Design and Implementation of Labview Based Data Acquisition and Image Reconstruction Environment for Metu MRI System," 2005.
- [2] F. Bloch, "Nuclear Induction," *Physical Review*, no. 70., pp. 460-474, 1946.
- [3] F. Bloch, W. W. Hansen, and M. Packard, "The Nuclear Induction Experiment," *Physical Review*, no. 70, pp. 474-485, 1946.
- [4] E. M. Purcell, E. C. Torrey, and R. V. Pound, "Resonance Absorbtion by Nuclear Magnetic Moments in a Solid," *Physical Review*, no. 69, pp. 37-38, 1946.
- [5] R. Damadian, M. Goldsmith, and L. Minkoff, "NMR in cancer: XVI. Fonar image of the live human body," *Physiological Chemistry and Physics*, no. 9, pp. 97-100, 1977.
- [6] Z. P. Liang and Lauterbur P. C., *Principles of Magnetic Resonance Imaging.*, 2000.
- [7] E. J. Woo and J. K. Seo, "Magnetic Resonance Electrical Impedance Tomography for High Resolution Conductivity Imaging," *Physiological Measurement* , no. 29, pp. R1-R26, 2008.
- [8] N. Zhang, "Electrical Impedance Tomography Based on Current Density Imaging," University of Toronto, Toronto, CANADA, M S Thesis 1992.
- [9] E. J. Woo, S. Y. Lee, and C. W. Mun, "Impedance Tomography Using Internal Current Density Distribution Measured by Nuclear Magnetic Resonance," *Proc.*

SPIE, no. 2299, pp. 377-85, 1994.

- [10] O. Birgul and Y. Z. Ider, "Use of Magnetic Field Generated by The Internal Distribution of Injected Currents for Electrical Impedance Tomography," in *Proc. 9th Int. Conf. Elec. Bio-Impedance*, Heidelberg, GERMANY, 1995, pp. 418-9.
- [11] H. Yigitler, "Permanent magnet design and image reconstruction algorithm for magnetic resonance imaging in inhomogeneous magnetic fields," METU, Ankara, TURKEY, M.S. Thesis 2006.
- [12] V. E. Arpinar, "Analysis of magnetic resonance imaging in inhomogenous main magnetic field," METU, Ankara, TURKEY, Ph.D. Thesis 2009.
- [13] H. Altunel, "Optimum current injection strategy for magnetic resonance electrical impedance tomography ," METU, Ankara, TURKEY, Ph.D. Thesis 2008.
- [14] M. Eyuboglu, A. Koksall, and H. Altunel, "Regional Image Reconstruction with Optimum Currents for MREIT — Evaluation on Shepp-Logan Conductivity Phantom," in *4th European Conference of the International Federation for Medical and Biological Engineering*, Antwerp, BELGIUM, 2008, pp. 756-759.
- [15] M. Eyuboglu and E. Degirmenci, "Equipotential projection based MREIT reconstruction without potential measurements," in *13th International Conference on Electrical Bioimpedance and the 8th Conference on Electrical Impedance Tomography*, Graz, AUSTRIA, 2007, pp. 516-519.
- [16] P. Gould. (2010, March 15th)
<http://www.diagnosticimaging.com/mri/content/article/113619/1533291>.
- [17] O. Birgul, Y.Z. Ider B.M. Eyuboglu, "A Dual Modality System for High Resolution - True Conductivity Imaging," in *Proceedings of XIth International Conference on Electrical Bio-impedance*, Oslo, NORWAY, 2001, pp. 409-413.

- [18] R. Boyacioglu, "Performance evaluation of current density based magnetic resonance electrical impedance tomography reconstruction algorithms," METU Electrical and Electronics Engineering Department, Ankara, TURKEY, M.S. Thesis 2009.
- [19] G. Eker, "Performance evaluation of magnetic flux density based magnetic resonance electrical impedance tomography reconstruction algorithms," METU Electrical Electronics Engineering Department, Ankara, TURKEY, M.S. Thesis 2009.
- [20] B. M. Eyuboglu, O. Ozbek M.S. Ozdemir, "Equipotential projection based magnetic resonance - electrical impedance tomography and experimental realisation," *Physics in Medicine and Biology*, vol. 20, no. 49, pp. 4765-4783, 2004.

APPENDIX

MANUSCRIPTS PUBLISHED DURING THE THESIS

- Tankut Topal, Evren Değirmenci, Rasim Boyacıođlu, V. Emre Arpınar, B. Murat Eyübođlu, “Current Source Design for MREIT Technique and Its Experimental Application”, 15th National Biomedical Engineering Meeting (BIYOMUT), Antalya-Turkey,2010.